Development and Characterization of New Molecular Conductors Based on the Multi-Chalcogen π-Molecules

Akane Sato

Doctor of Science

Department of Functional Molecular Science,
School of Mathematical and Physical Science,
The Graduate University for Advanced Studies

1998

Acknowledgments

The present work has been carried out under the supervision of Professor Hayao Kobayashi (Institute for Molecular Science and the Graduate University for Advanced Studies) and alsc under the instruction of Professor Akiko Kobayashi (The University of Tokyo) with assistance of all of members of the laboratory. The author is thankful to all the following names for many precious advice and discussions.

Firstly, the author would like to express her sincere thanks to Professor Hayao Kobayashi, who has provided the chance and place for the study, and encouraged and guided the author in any time. The author is deeply thankful to Professor Akiko Kobayashi, who offered the instruction in the X-ray structure analyses, the extended Hückel tight binding calculation and creating the papers, and has given many precious advice in various things as a female scientist. The author's appreciation goes to Dr. Toshio Naito (Hokkaido University), who had given the author the instruction of the synthesis operation mainly at Toho University for the author's master's thesis research, which is a basis of the present work. Dr. Hiroki Akutsu (Osaka University) kindly advised and had many discussions with the author which offered her important considerations on the λ-BETS system. The author is grateful to Dr. Fujiwara (Institute for Molecular Science), who gave valuable advice on the synthesis and offered great help to improve the manuscript. Valuable discussions were held with Dr. Fujiwara, Dr. Takafumi Adachi, Dr. Bakhyt Zh. Narymbetov and Miss Emiko Ojima (all at Institute for Molecular Science), who always encouraged and assisted the author, especially the author huge indebted to Miss Ojima for her kindly supplement and instruction on synthesis of BETS molecule. The author express her heartfelt thanks to Dr. Yasuhiro Nakazawa (Institute for Molecular Science), who has given the author the precious opinions for the study of λ-BETS system. Dr. Yuko Hosokoshi (Institute for Molecular Science) is greatly appreciated for her acquaintance with the study in the magnetic field. The author thanks to Dr. Hisashi Tanaka (The University of Tokyo) who hold many discussions on the study of BETS system. Regarding technical supports for the experimental operations at low temperature, the author appreciates all stuffs of the low temperature center of Institute for Molecular Science. The

author is grateful to Secretary Haruna Sato and all members of Miyajima Laboratory (Institute for Molecular Science), who kindly encouraged the author. The author enjoyed the life of Institute for Molecular Science because of her colleagues and friends who amused and encouraged for all the time. Finally, the author would like to conclude this acknowledgment with expression of her thanks to all these, including my family, who have continuously supported and encouraged me throughout my student life. The author wishes dedicate this thesis to all of them.

Contents

Chapter 3 Enhancement of the dimensionality of molecular conductors by the selone substitution of $M(dmit)_2$: $M(dmise)_2$ system (M= Ni, Pd)

Chapter 1

General introduction

1.1 Historical survey on the conductors based on the planar π-molecules

The research of the organic conductor started in late of 1940s, when the semiconducting properties of phtalocyanines and condensed aromatic hydrocarbons were discovered [1]. Since the discovery of the first organic metal, (TTF)(TCNQ) (TTF= tetrathiafulvalene; TCNQ= 7,7,8,8-tetracyanoquinodimethane) in 1973 [2], scientists have made attempts to develop the higher conductive materials, and have synthesized the molecular conductors and superconductors, successfully (Table 1.1). The molecular conductors which shows the metallic behavior (i.e. the resistivity decreases with reducing temperature) are called the "synthetic metals".

In order to give the electron conductivity to the organic material which is usually regarded as the electrical insulator, synthesis of the charge-transfer complex is effective. The charge-transfer complexes are generally consisted of the planar π-conjugated donor and/or acceptor molecules. In the crystal structures of the conducting charge-transfer complexes such as (TTF)(TCNQ), the donor and acceptor molecules are stacked separately to form the segregated columns (Fig.1.1). Then the highest occupied molecular orbitals (HOMO's) of donor molecules and the lowest unoccupied molecular orbitals (LUMO's) of acceptor molecules overlap between the neighboring molecules along the stacks to form one-dimensional (1D) electron bands. When the interaction between columns cannot be neglected, the band structure will become quasi-1D or 2D. By the partial charge transfer between donor and acceptor

molecules, the metal electrons are produced in the electron bands.

As mentioned above, (TTF)(TCNQ) is the first synthetic metal, which keeps the metallic behavior down to 53 K. Below 53 K, this salt transforms into an insulator. This metal-insulator (MI) transition is characteristic of 1D metal system and is called as "Peierls transition" or "charge density wave (CDW) transition".

As easily imagined, owing to the anisotropy of HOMO and LUMO, the molecular conductors has a strong tendency to take the low dimensional electronic structures. However, the low dimensional conductors have a serious weak point that it has difficulty in keeping the stable metallic state, because 1D metal band tend to be destabilized by the development of CDW or "spin density wave (SDW)", which open a gap in the 1D metal band. Therefore synthesis of the stable metallic molecular conductors or superconductors requires increasing the dimensionality of electron band, in other words, getting more strong interaction among the neighboring molecular stacking columns. Expansion of π-conjugated system of TTF molecule and introduction of selenium atoms in TTF skeleton are effective strategies for this aim.

$(TMTSF)_2PF_6$ (TMTSF = tetramethyltetraselenafulvalene) is the first organic superconductor reported in 1980 (T_c= 0.9 K, 12 kbar) [3]. TMTSF is a TTF-like donor molecule with four selenium atoms. In this compound, TMTSF molecules stack to make one dimensional column, and intermolecular short Se···Se contacts exist along the columnar direction as well as along the transverse direction. Unlike plane Fermi surface of (TTF)(TCNQ), Fermi surface of $(TMTSF)_2PF_6$ shapes warped (quasi-one dimensional), suggesting the transverse intermolecular interactions. BEDT-TTF [= bis(ethylenedithio)tetra-thiafulvalene], an expanded π-conjugated system, succeeds to form many 2D metals and superconductors. $(BEDT\text{-}TTF)_2ClO_4\bullet(TCE)_{0.5}$ (TCE= 1,1,2-trichloroethane) is the first 2D BEDT-TTF conductor with metallic state down to 20 K [4]. Calculated electronic structure of $(BEDT\text{-}TTF)_2ClO_4\bullet(TCE)_{0.5}$ is two dimensional [5]. The BEDT-TTF system has produced numbers of metallic conductors and more than 30 of superconductors.

On the other hand, the intensive studies of the conductors based on the transition metal complexes such as $K_2[Pt(CN)_4]Br_{0.3}\bullet 3H_2O$ (called as "KCP") and its homologues were started around 1968 [6]. KCP is the typical 1D metal complexes whose conduction paths are

formed from the d_{z^2} orbitals of Pt atoms. The existence of the metal-complex conductors with the π-conduction bands was noticed in the course of the studies on the molecular conductors based on the metal-bis(dithiolene) complexes. $Li_{0.8}(H_3O)_{0.33}[Pt(mnt)_2]\cdot 1.7H_2O$ [mnt = bis(dicyanoethylenedithiolate) = maleonitriledithiolate] reported in 1981 is the first metallic bis(dithiolene) complex conductor [7]. Thereafter, many metallic conductors of the metal-bis(dithiolene) complex systems were developed by using $M(dmit)_2$ complexes (dmit = 1,3-dithiol-2-thioxo-4,5-dithiolate = dimercaptoisotrithione) [8]. As BEDT-TTF is an improved molecule of TTF, $M(dmit)_2$ is an improved complex of the simple metal dithiolene complex like $M(mnt)_2$. The $M(dmit)_2$ system has played an important role for the development of the π acceptor metals and superconductors.

While the studies of the molecular conductors had made a progress toward the developments of higher T_c superconductors, the trials of the constructions of new types of conductors with π-d interaction also have been started. $(DCNQI)_2Cu$ system was the key material of the study of the π-d interaction where Cu ions are in the mixed-valence state. In recent years, it is not any exaggeration at all that one of the most active studies is the attempt to prepare the molecular metals where π-d interaction plays a crucial role.

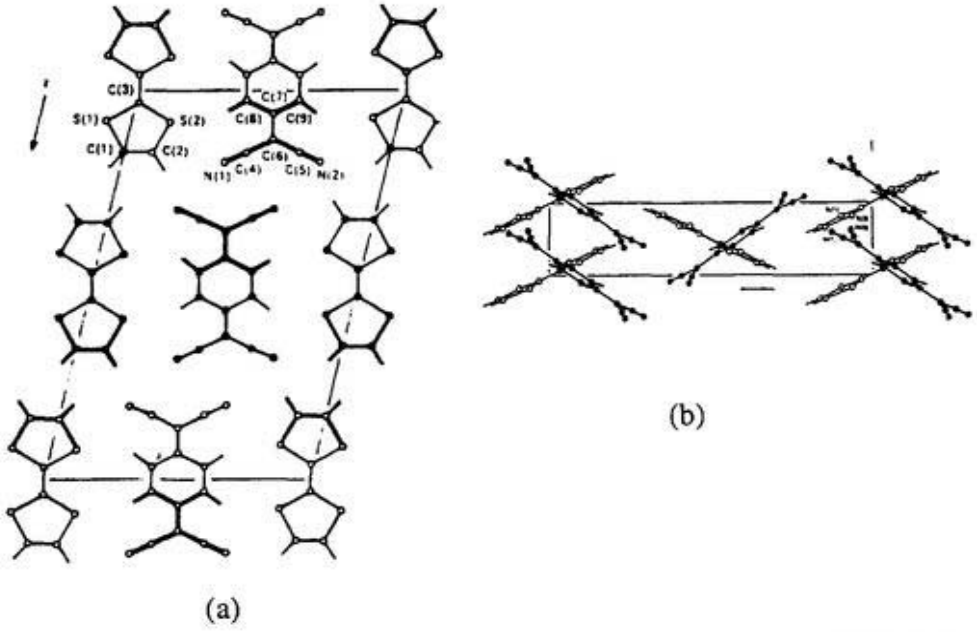

Fig.1.1 (a) Top- and (b) side-views of the crystal structure of (TTF)(TCNQ) [2(c)].

1.1.1 Low dimensional conductors

In 1979, the family of quasi-one dimensional organic conductors $(TMTSF)_2X$ (X= inorganic monoanion) were reported. The $(TMTSF)_2X$ family, called the "Bechgaard salts", are isostructural to each other. As mentioned above, the first organic superconductor of $(TMTSF)_2PF_6$ was reported in 1980. Successively, superconductivity were also observed with five $(TMTSF)_2X$ salts (X= AsF_6^-, SbF_6^-, TaF_6^-, ReO_4^-, FSO_3^-) under the high pressure [9-12]. A short time later, $(TMTSF)_2ClO_4$ was reported to be the first superconductor at the atmospheric pressure (T_c= 1.4 K) [13]. Salts of X= PF_6^-, AsF_6^-, SbF_6^-, TaF_6^-, ReO_4^-, FSO_3^-, NO_3^- and ReO_4^- with high conductivities of 10^5 S cm^{-1} at room temperature show the metal-insulator (MI) transition at the ambient pressure [14-16] (Fig.1.2).

Though $(TMTSF)_2X$ is isostructural, the different counter anions make a variety of the physical properties. Centrosymmetrical anion salts (X= PF_6^-, AsF_6^-, SbF_6^- and TaF_6^-) show the MI transitions in the temperature region of (12-17) K at the ambient pressure. The anisotropy of the magnetic susceptibilities of these salts below T_{MI} shows the MI transition to be antiferromagnetic (AF) transition originated from SDW instability of the quasi-1D metal band [17] (Fig.1.3).

Behaviors of non-centrosymmetrical anion salts differ from those of centrosymmetrical hexafluorophosphate anion salts. The salt containing ReO_4^- anion exhibits the MI transition at 180 K. The anion ordering is responsible for the MI transition. Owing to the ordering of anions, superlattice appears and the system transforms into an insulator. On the other hand, ClO_4^- salt whose anions are also tetrahedral transforms to a superconductor when slow-cooling. However, ClO_4^- salt exhibits a MI transition at 1.3 K on rapid-cooling where SDW develops below T_{MI} [18-19].

The family of $(TMTTF)_2X$ (TMTTF= tetramethyltetrathiafulvalene) is isostructural to that of $(TMTSF)_2X$. Nevertheless, $(TMTTF)_2PF_6$ is a semiconductor below room temperature due to the small intermolecular overlap integral of HOMO (or band width) and strong correlation effect of π conduction electrons. The system transforms to a spin-Peierls non-magnetic insulating ground state around 20 K. The $(TMTTF)_2X$ and $(TMTSF)_2X$ (so-called "TMs family") are considered to be the most important organic conductors not only because

they afforded the first organic superconductor but also because their pressure-temperature (*P-T*) phase diagram contains the general aspect commonly observed in the organic superconductors discovered thereafter [20] (Fig.1.4).

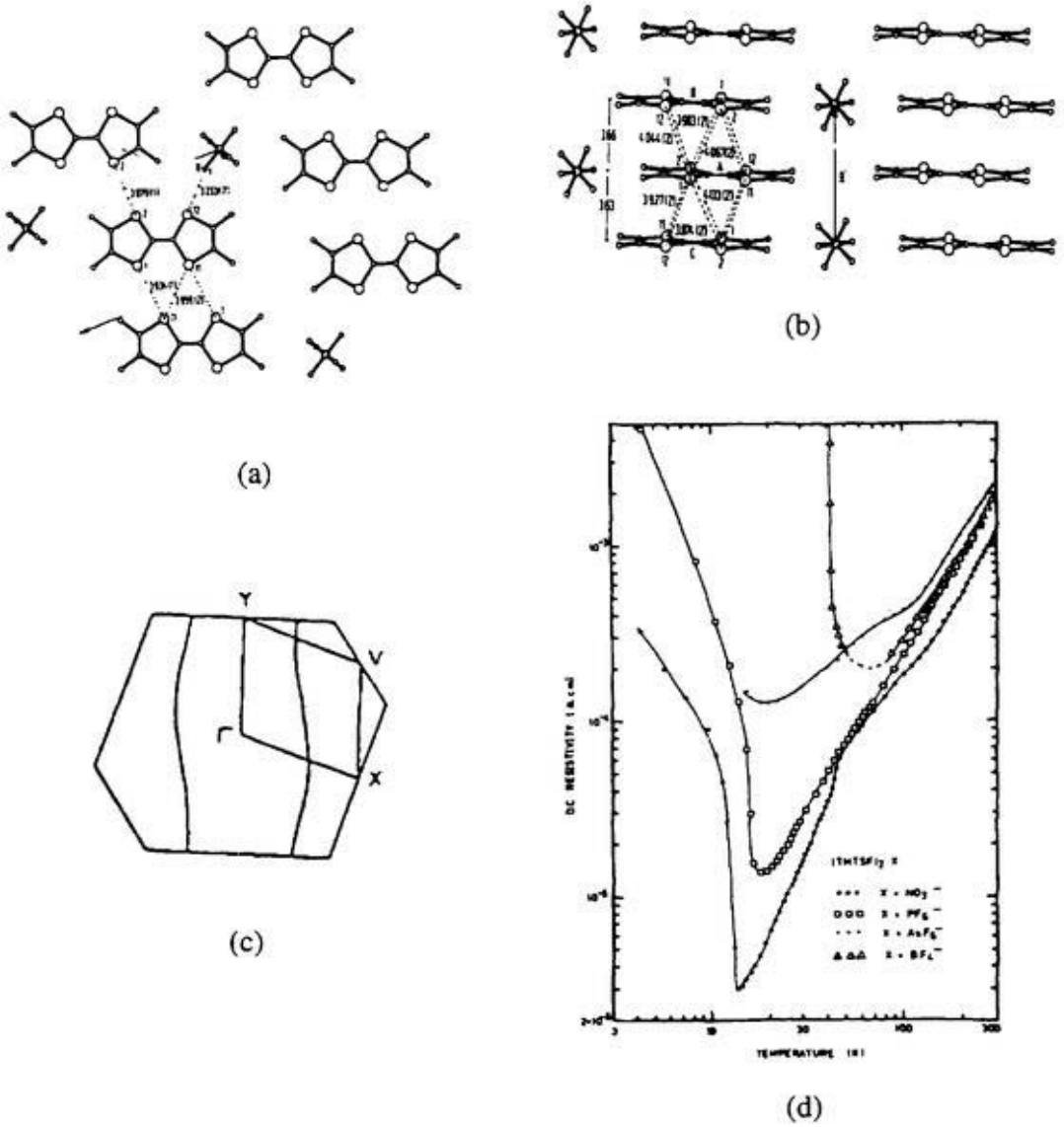

Fig.1.2 (a) Top- and side-views of the crystal structure [15], (c) Fermi surface and (d) the electric resistivity of $(TMTSF)_2X$ [14]

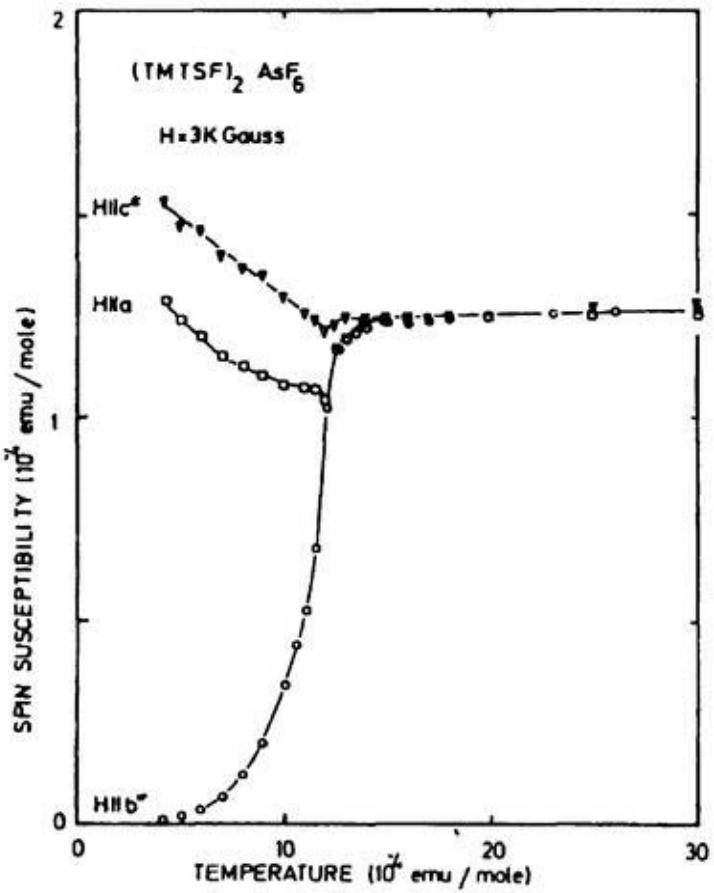

Fig.1.3 The magnetic suscepyibility of single crystal of $(TMTSF)_2AsF_6$ [17].

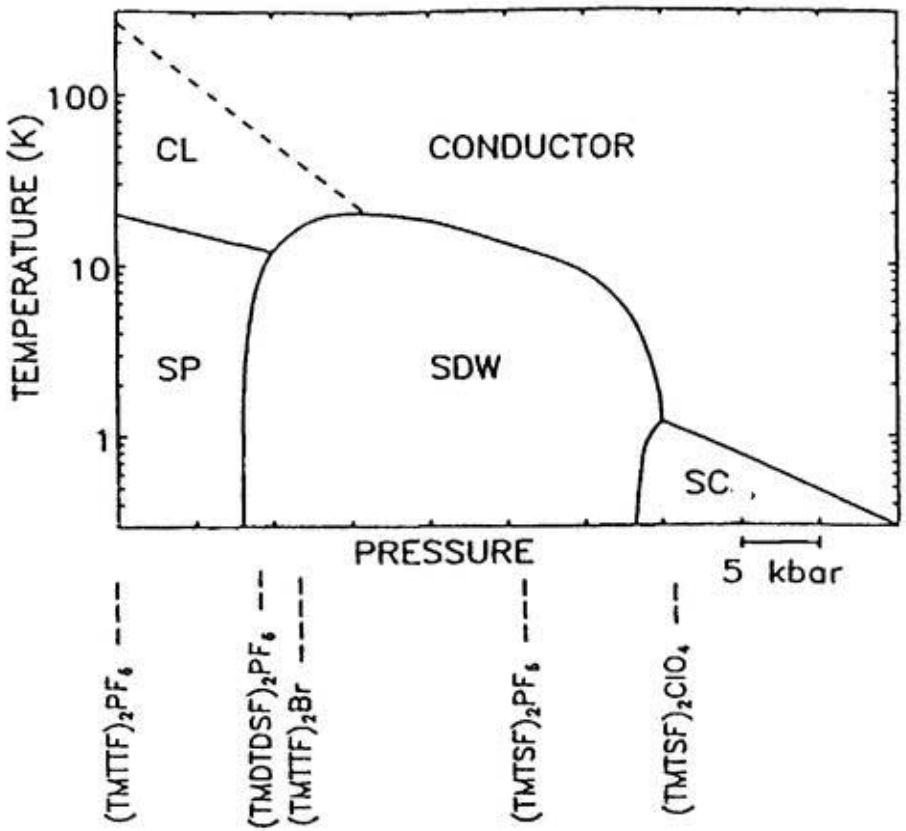

Fig.1.4. General phase diagram of TM_2X serieis. Notations of SP, SDW and SC refer to spin-Peierls, spin density wave and superconducting ground states, respectively. The dashed line denotes the limit between the metal-like and the charge localized (CL) behavior [20(b)].

1.1.2 BEDT-TTF and BETS systems

BEDT-TTF system is said to be the second family of organic conductors which provided the metallic conductors and the superconductors. Numbers of superconductors based on BEDT-TTF system have been discovered. The critical temperatures of superconductivity of the BEDT-TTF system are higher as compared with those of $(TMTSF)_2X$.

A numerous number of BEDT-TTF salts formed with various anions are reported, but most of salts are classified into several types (α-, β-, θ-, κ-, etc.) of molecular arrangements. The molecular arrangement types correlates largely with the physical properties. For example, most of superconductors belong to the β-, θ- and κ-type arrangements and the system with κ-type arrangement is believed to have possibility to be superconductors. The molecular arrangements of β-, θ- and κ-type will be described as follows.

In the crystal structure of β-$(BEDT\text{-}TTF)_2I_3$ [T_c= 1.4 K (1 bar) and 8.0 K (0.3 kbar)] [21], BEDT-TTF molecules are stacked in face-to-face like the donors in a typical low dimensional crystal. Sheets formed by BEDT-TTF stacks are parallel to the *ab*-plane with separated by the insulating layer of the I_3^- (Fig.1.5). In θ-$(BEDT\text{-}TTF)_2I_3$ (T_c= 3.6 K) [22], BEDT-TTF columns, in which donor molecules incline to the right and the left, are arranged alternatively in the transverse direction (Fig.1.6). κ-$(BEDT\text{-}TTF)_2I_3$ (T_c= 3.6 K) has a quite different structure from usual molecular conductors [23]. κ-type arrangement is now regarded as the ultimate arrangement for creating the two dimensional electronic structure and considered to be the most suitable arrangement to find a new organic superconductors. Pairs of BEDT-TTF molecules are in contact with face-to-face, but the adjacent pairs are aligned almost orthogonal (Fig.1.7). κ-type is the most advantageous to the superconductivity. Molecular superconductors having the "high T_c" ($T_c \geq 10$ K) also have the κ-type molecular arrangements. They are κ-$(BEDT\text{-}TTF)_2Cu[N(CN)_2]Cl$, κ-$(BEDT\text{-}TTF)_2Cu[N(CN)_2]Br$, κ-$(BEDT\text{-}TTF)_2Cu(NCS)_2$ [24-26].

BETS molecule (BETS= bis(ethylenedithio)tetraselenafulvalene) is a selenium-substituted derivatives of BEDT-TTF molecule. In the BETS system, number of metallic conductors were synthesized such as $(BETS)_2SbF_6$, $(BETS)_2TaF_6$, $(BETS)_4HgBr_4 \cdot (C_6H_5Cl)_x$, $(BETS)_2I_3$ and so on. These molecular arrangements are classified into α-, κ- or

θ-type [27]. In 1993, λ-type salt with $GaCl_4^-$ were found to be a superconductor at relatively higher temperature (T_c= 8 K, 1 bar) [28] (Fig.1.8). On the other hand, λ-type salt with $FeCl_4^-$ transforms into an insulator (T_{MI}= 8.5 K) around the similar temperature as of the T_c of $GaCl_4$ salt [29]. λ-BETS system is worthy to direct an attention, because it has very interesting physical property due to a strong correlation of π-system and/or characteristic π-d interaction.

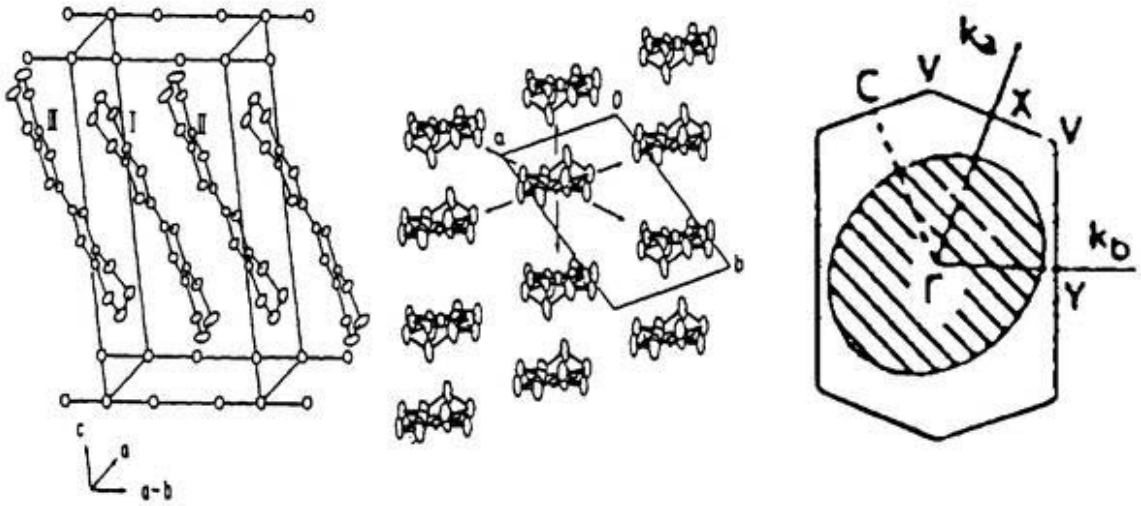

(a) (b) (c)

Fig.1.5. (a) Crystal structure, (b) stacking arrangement of BEDT-TTF molecules viewed along the long molecular axis [21(e-f)] and (c) Fermi surface [20(a)] of β-$(BEDT\text{-}TTF)_2I_3$.

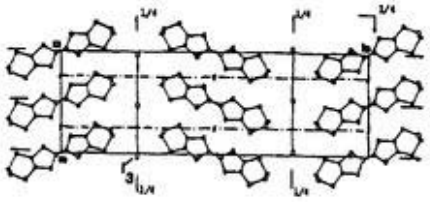

(a)

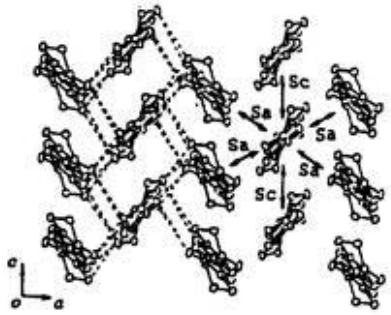

(b)

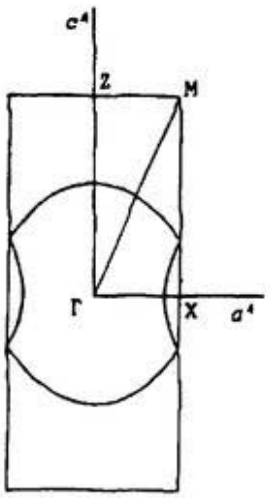

(c)

Fig.1.6. (a) Crystal structure, (b) stacking arrangement of BEDT-TTF molecules viewed along the long molecular axis and (c) Fermi surface of θ-(BEDT-TTF)$_2$I$_3$ [22(a)].

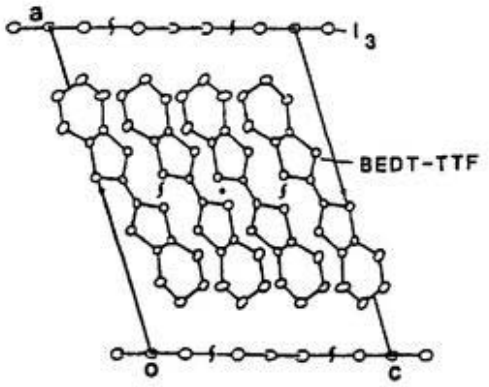

(a)

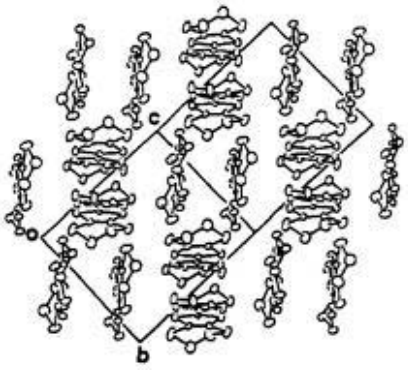

(b)

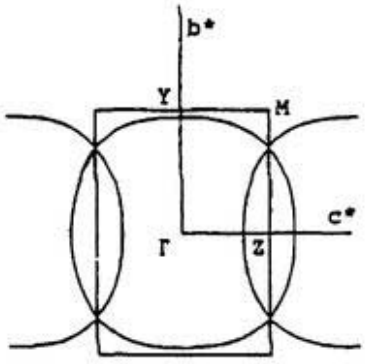

(c)

Fig.1.7. (a) Crystal structure, (b) stacking arrangement of BEDT-TTF molecules viewed along the long molecular axis and (c) Fermi surface of κ-(BEDT-TTF)$_2$I$_3$ [23(a)].

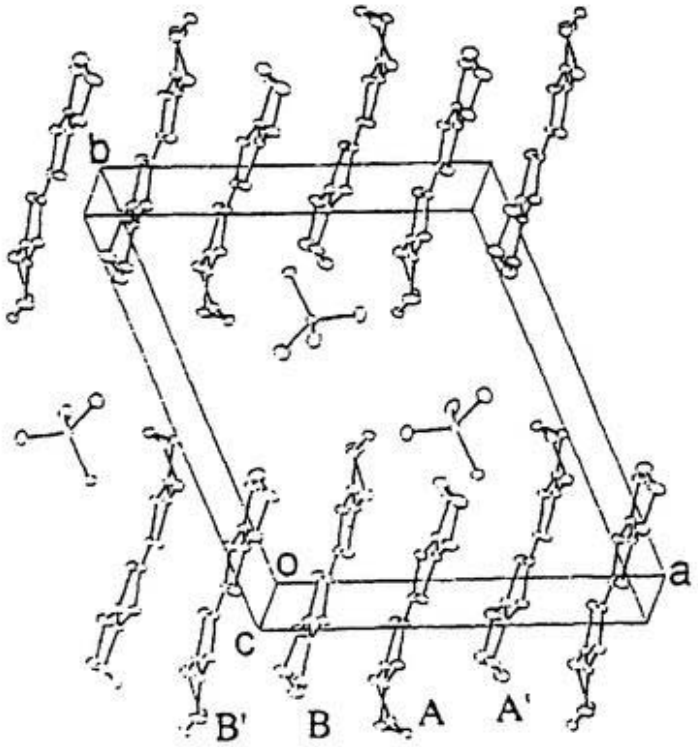

(a)

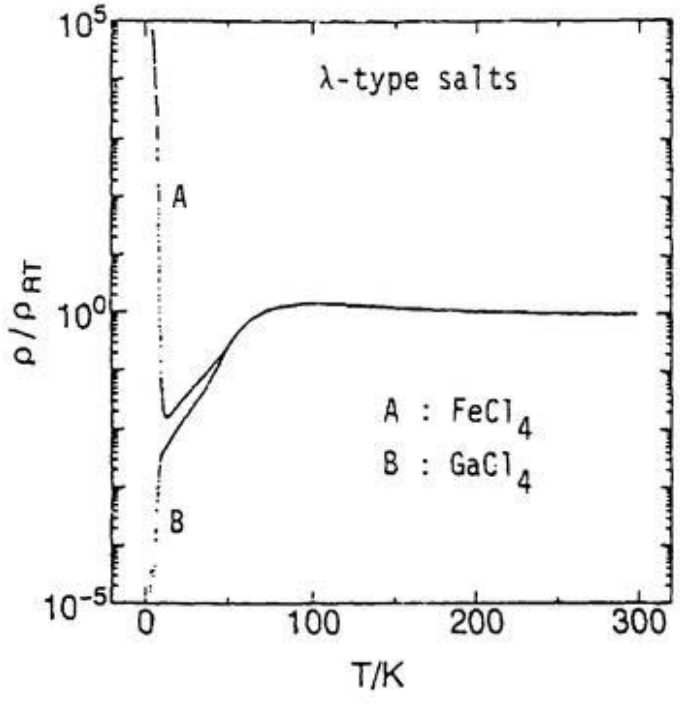

(b)

Fig.1.8. (a) Crystal structure and (b) electronic resistivity of λ-$(BETS)_2MCl_4$ (M= Ga and Fe) [29].

1.1.3 M(dmit)$_2$ (M= Ni, Pd, Pt, ...) system

The synthesis of the dmit ligand was firstly reported in 1975 [30] and some Ni(dmit)$_2$ complexes with tetraalkylammonium cations were prepared in 1979 [31]. The M(dmit)$_2$ species exist as $[M(dmit)_2]^{2-}$, $[M(dmit)_2]^{-}$ or $[M(dmit)_2]^{0}$. Although the central metals are not directly relevant to forming the conduction band, the existence of the central metal makes the properties of M(dmit)$_2$ system to be complex and interesting. Conduction band of usual acceptor consists of LUMO (the lowest unoccupied molecular orbital) [32]. LUMO of Ni(dmit)$_2$ molecule has a nodal plane on the central Ni atom (Fig.1.9), so the transverse intermolecular interactions are not so strong in the Ni(dmit)$_2$ conductor. Therefore the M(dmit)$_2$ system tends to be low dimensional. On the other hand, the energy gap is very small between HOMO (the highest occupied molecular orbital) and LUMO in the M(dmit)$_2$ system. Because the Pd(dmit)$_2$ or Pt(dmit)$_2$ molecules tend to dimmerize in their crystal, the inversion of the band component from LUMO into HOMO occurs [33]. But metallic nature of the Pd(dmit)$_2$ or Pt(dmit)$_2$ conductor tends to be faded by the existence of the large mid gap, which makes the effective band width narrow.

Some M(dmit)$_2$ conductors keep the stable metallic state either by (1) the two-level crossed column crystal structure or by (2) the molecular arrangement that one molecule bridges to the neighboring molecules. Eight superconductors [34-41] and three stable metallic conductors [42-44] are discovered in the M(dmit)$_2$ system. Fermi surfaces of the type (1) crystal structure do not nested (i.e. vanished) by a single wave number vector. α-, γ-$[(CH_3)_2(C_2H_5)_2N][Ni(dmit)_2]_2$ and α-(N,N-dimethylpiperidinium)$[Ni(dmit)_2]_2$ which are in the stable metallic state take the type (2) molecular arrangements. Type (2) arrangement is called "spanning overlap mode". Three stable metallic Ni(dmit)$_2$ conductors are two dimensional owing to "spanning overlap mode".

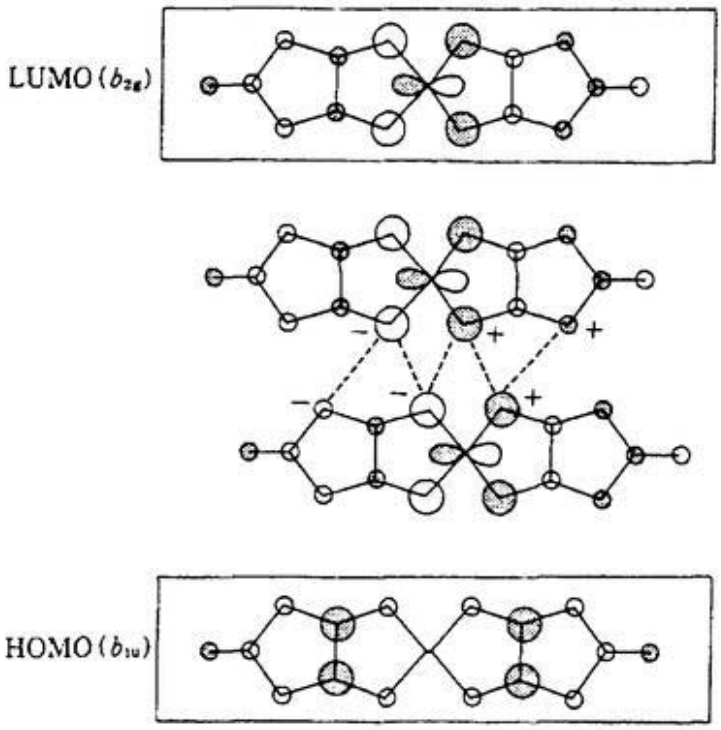

Fig.1.9. LUMO and HOMO of $M(dmit)_2$ and the illustration to explain the small LUMO...LUMO interaction.

1.2 Scope of this thesis

Development of the new material and the characterization are the most important works in the field of molecular conductors. View points of the present study is the developments of the new materials which covers from low dimensional to quasi-three dimensional ones. These systems were investigated through the structural, electric and magnetic studies.

This thesis is composed of five chapters : the general introduction (Chapter 1), the experimental (Chapter 2), discussions (Chapter 3-5) and the concluding remarks.

[Chapter 2]

Outlines of the synthesis and the experimental apparatus are mentioned. Single crystals were prepared electrochemically. Investigation of the physical property was made in the temperature range from room temperature down to low temperature. Electrical resistivity and magnetic susceptibility were measured on the instrument in general use. X-Ray measurements at low temperature were performed on a diffractometer equipped with a helium refrigerator. The structure of the low temperature X-ray system is explained.

[Chapter 3]

New system of $M(dmise)_2$, a derivative of $M(dmit)_2$, is described. Charge transfer complexes were prepared with an expectation that $M(dmise)_2$ system might have a lager dimensionality than the $M(dmit)_2$ system. The crystal and electronic structure and the electrical property are mainly discussed.

[Chapter 4]

Ground states of several low dimensional conductors based on the EDT-TTF and its selenium derivatives system : $(EDT\text{-}TTF)_2MCl_4$, $(EDST)_2MCl_4$ and $(EDTS)_2MCl_4$ (M= Ga^{3+} and Fe^{3+}), are examined. The electrical resistivity, the magnetic susceptibility and the crystal structures are summarized on each salt. Discussion is made by comparison with the phase diagram of TM systems .

[Chapter 5]

λ-$(BETS)_2(Fe_xGa_{1-x})Cl_4$ is an organic alloy system having mixed magnetic and non-magnetic (Ga^{3+} and Fe^{3+}) anions. In present study, the influences of various concentrations of magnetic moment of Fe^{3+} upon the physical property in λ-BETS system were investigated. Magnetic property and electrical resistivity were mainly examined. Temperature *versus* composition phase diagram of λ-$(BETS)_2(Fe_xGa_{1-x})Cl_4$ is discussed.

Table 1.1 Molecular superconductors and their critical temperatures.

Compounds	T_c (pressure)	References
Low dimensional system		
$(TMTSF)_2PF_6$	1.4 K (6.5 kbar)	[3]
$(TMTSF)_2AsF_6$	1.4 K (9.5 kbar)	[9]
$(TMTSF)_2SbF_6$	0.38 K (10.5 kbar)	[10]
$(TMTSF)_2TaF_6$	1.35 K (11 kbar)	[10]
$(TMTSF)_2ClO_4$	1.4 K	[13]
$(TMTSF)_2ReO_4$	1.2 K (9.5 kbar)	[11]
$(TMTSF)_2FSO_3$	3 K (5 kbar)	[12]
$(DMET)_2Au(CN)_2$	0.8 K(5 kbar)	[45]
$(DMET)_2AuCl_2$	0.83 K	[46]
$(DMET)_2AuBr_2$	1.6 K (1.5 kbar)	[47]
κ-$(DMET)_2AuBr_2$	1.9 K	[48]
$(DMET)_2AuI_2$	0.55 (5 kbar)	[46]
$(DMET)_2IBr_2$	0.58 K	[49]
$(DMET)_2I_3$	0.47 K	[49]
κ-$(MDT\text{-}TTF)_2AuI_2$	4.0 K	[50]
Two dimensional system		
$(BEDT\text{-}TTF)_2ReO_4$	2 K (4 kbar)	[51]
α-$(BEDT\text{-}TTF)_2(I_3)_x(I_2)_{1-x}$	3.3 K	[52]
β_L-$(BEDT\text{-}TTF)_2I_3$	1.5 K	[21]
β_H-$(BEDT\text{-}TTF)_2I_3$	8.1 K (0.5 kbar)	[21]
γ-$(BEDT\text{-}TTF)_2(I_3)_{2.5}$	2.5 K	[53]
θ-$(BEDT\text{-}TTF)_2I_3$	3.6 K	[22]
κ-$(BEDT\text{-}TTF)_2I_3$	3.6 K	[23]
β-$(BEDT\text{-}TTF)_2IBr$	2.7 K	[54]
β-$(BEDT\text{-}TTF)_2AuI_2$	3.4 K	[55]
$(BEDT\text{-}TTF)_3Cl_2 \cdot 2H_2O$	2 K (16 kbar)	[56]
κ-$(BEDT\text{-}TTF)_2Ag(CN)_2 \cdot H_20$	5 K	[57]
$(BEDT\text{-}TTF)_4[Pt(CN)_4] \cdot H_2O$	2 K (6.5 kbar)	[58]
$(BEDT\text{-}TTF)_4[Pd(CN)_4] \cdot H_2O$	1.2 K (7 kbar)	[58]
κ-$(BEDT\text{-}TTF)_4Hg_{2.78}Cl_8$	1.8 K (12 kbar)	[59]
κ-$(BEDT\text{-}TTF)_4Hg_{2.89}Br_8$	0.2 K	[60]
α-$(BEDT\text{-}TTF)_2(NH_4)Hg(SCN)_4$	0.8 K	[61]

Table 1.1 Molecular superconductors and theor critical temperatures. (continued)

Compounds	T_c (pressure)	References
κ-(BEDT-TTF)$_2$Cu(SCN)$_2$	10.4 K	[26]
κ-(BEDT-TTF)$_2$Cu[N(CN)$_2$]Br	11.8 K	[25]
κ-(BEDT-TTF)$_2$Cu[N(CN)$_2$]Cl	12.8 K (0.3 kbar)	[24]
κ-(BEDT-TTF)$_2$Cu[N(CN)$_2$](CN)	11.2 K	[62]
κ-(BEDT-TTF)$_2$Cu$_2$(CN)$_3$	2.8 K (1.5 kbar)	[66]
κ'-(BEDT-TTF)$_2$Cu$_2$(CN)$_3$	3.8 K	[62]
kL-(BEDT-TTF)2Cu(CF$_3$)$_4$•TCE	4.0 K	[64]
κ$_H$-(BEDT-TTF)$_2$Cu(CF$_3$)$_4$•TCE	9.2 K	[65]
κ$_L$-(BEDT-TTF)$_2$Ag(CF$_3$)$_4$•TCE	2.6 K	[66]
κH-(BEDT-TTF)$_2$Ag(CF$_3$)$_4$•TCE	9.4 K, 11.1 K	[66]
β"-(BEDT-TTF)$_4$[(H$_2$O)Fe(C$_2$O$_4$)$_3$]•PhCN	8.5 K	[67]
β"-(BEDT-TTF)$_4$[(H$_2$O)Cr(C$_2$O$_4$)$_3$]•PhCN	6.5 K	[68]
β-(BEDO-TTF)$_3$Cu$_2$(SCN)$_3$	4.5 K	[69]
(BEDO-TTF)$_2$ReO$_4$•H$_2$O	2.5 K	[70]
(DMBEDT-TTF)$_2$ClO$_4$	2.6 K (6 kbar)	[71]
λ-(BETS)$_2$GaCl$_4$	8 K	[29]
λ-(BETS)$_2$GaCl$_3$Br	4 K	[72]
λ-(BETS)$_2$(Fe$_{0.48}$Ga$_{0.52}$)Cl$_4$	4 K	[73]
(DTEDT)[Au(CN)$_2$]$_{0.4}$	~4K	[74]
M(dmit)$_2$ sytem		
(TTF)[Ni(dmit)$_2$]$_2$	1.6 K (7 kbar)	[34]
[(CH$_3$)$_4$N][Ni(dmit)$_2$]$_2$	5.0 K (7 kbar)	[35]
α'-(TTF)[Pd(dmit)$_2$]$_2$	6.5 K (20 kbar)	[36]
α-(TTF)[Pd(dmit)$_2$]$_2$	1.7 K (22 kbar)	[37]
β-[(CH$_3$)$_4$N][Pd(dmit)$_2$]$_2$	6.2 K (6.5 kbar)	[38]
β-[(CH$_3$)$_2$(C$_2$H$_5$)$_2$N][Pd(dmit)$_2$]$_2$	4 K (2.4 kbar)	[39]
α-(EDT-TTF)[Ni(dmit)$_2$]	1.3 K	[40]
β'-[((CH$_3$)$_2$(C$_2$H$_5$)$_2$P][Pd(dmit)$_2$]$_2$	4.0-1.8 K (6.9-10.4 kbar)	[41]

References

[1] (a) D.D. Eley, *Nature*, **162,** 819 (1948). (b) H. Akamatu and H. Inokuchi, *J. Chem. Phys.*, **18**, 810 (1950).

[2] (a) J.P. Ferraris, D.O. Cowan, V. Walatka, Jr., J.H. Perlstein, *J. Ame. Chem. Soc.*, **95**, 948 (1973). (b) L.B. Coleman, M.J. Cohen, D.J. Sandman, F.G. Yamagishi, A.F. Gariro, A.J. Heeger, *Solid State Commun.*, **12**, 1125 (1973).

[3] D. Jerome, A. Mazaud, M. Ribault, K. Bechgaard, *J. Phys. Lett. (Paris)*, **41**, L95 (1980).

[4] G. Saito, T. Enoki, K. Toriumi, H. Inokuchi, *Solid State Commun.*, **42**, 557 (1982) : H. Kobayashi, A. Kobayashi, Y. Sasaki, G. Saito, T. Enoki and H. Inokuchi, *J. Am. Chem. Soc.*, **105**, 297 (1983).

[5] T. Mori, A. Kobayashi, Y. Sasaki, H. Kobayashi, G. Saito, H. Inokuchi, *Bull. Chem. Soc. Jpn.*, **57**, 627 (1984).

[6] (a) K. Krogmann, H.D. Hauseb, *Z. anorg. Chem.*, **358**, 67 (1968). (b) K. Krogmann, *Angew. Chem. Int. Ed. Engl.*, **8**, 35 (1969).

[7] (a) M.M. Ahmad, A.E. Underhill, *J. Chem. Soc., Dalton Trans.*, **1982**, 1065. (b) A. Kabayashi, Y. Sasaki, H. Kobayashi, A. E. Underhill, M.M. Ahmad, *J. Chem. Soc., Chem. Commum.*, **1982**, 390.

[8] See for example: (a) P. Cassoux, L. Valade, H. Kobayashi, A. Kobayashi, R.A. Clark, A.E. Underhill, *Coord. Chem. Review*, **110**, 115 (1990).

[9] M. Ribault, J.P. Pouget, D. Jerome, K. Bechgaard, *P. Phys. Lett.*, **41**, L607 (1980).

[10] S.S.P. Parkin, M. Ribault, D. Jerome, K. Bechgaard, *J. Phys.*, **C14**, 5305 (1981).

[11] S.S.P. Parkin, D. Jerome, K. Bechgaard, *Mol. Cryst. Liq. Cryst.*, **79**, 213 (1982).

[12] R. C. Lacoe, S.A. Wolf, P.M. Chakin, F. Wudl, E. Aharon-Shalom, *Phys. Rev.*, **27**, 1947 (1983).

[13] K. Bechgaard, K. Carneiro, F.B. Rasmussen, M. Olsen, G. Rindorf, C.S. Jacobsen, H.J. Pedersen, J.C. Scott, *J. Am. Chem. Soc.*, **103**, 2440 (1981).

[14] K. Bechgaard, N. Thorup, *Solid State Commun.*, **33**, 1119 (1980)

[15] N. Thorup, G. Rindorf, H. Soling, K. Bechgaarrd, *Acta Crystallogr. B*, **37**, 1236

(1981).

[16] T. Mori, A. Kobayashi, Y. Sasaki, H. Kobayashi, G..Saito, H. Inokuchi, *Bull. Chem. Soc. Jpn*, **57**, 627 (1984).

[17] K. Mortensen, Y. Tomkiewicz, K. Bechgaard, *Phys. Rev. B*, **25**, 3319 (1982).

[18] (a) J.P. Pouget et al., *Mol. Cryst. Liq. Cryst.*, **79**, 129 (1982). (b) S.S.P. Parkin et al., *J. Phys. C3*, **44**, 111 (1983). (c) A. Maaroufi et al., *J. Phys. C3*, **44**, 1091 (1983).

[19] M. Miljak et al., *J. Phys. C3*, **44**, 893 (1983).

[20] D. Jerome, in *The Organic conductors, fundamental and application*, ed, by J-P. Farges, Marcel Dekker,420 (1994).

[21] (a) V.N. Laukhin, E.E.Kostyuchenko, Y.V. Shushko, I.F. Shchegolev, E.B. Yagubski, *JETP Lett.*,**41** 81 (1985). (b) R.P. Shibaeva, V.F. Kaminskii, V.K. Bel'skii, *Sov. Phys. Crystallogr.*, **29**, 409 (1985). (c) K. Murata, M. Tokumoto, H. Anzai, H. Bando, G. Saito, K. Kajimura, T. Ishiguro, *J. Phys. Soc. Jpn.*, **54**, 1236 (1985). (d) E.B. Yagubski, I.F. Shchegolev, V.N. Laukhin, P.A. Kononovich, M.V. Kostyuchenko, A.G. Khomenko, Y.V. Shushko, A.V. Zvarykina, *JETP Lett.*, **49**, 1201 (1984). (e) H. Kobayashi, R. Kato, A. Kobayashi, M. Tokumoto, H. Anzai, T. Ishiguro, *Chem. Lett.*, **1985**, 1924. (f) H. Kuroda, K. Yakushi, H. Tajima, A. Ugawa, Y. Okawa, A. Kobayashi, R. Kato, H. Kobayashi, G. Saito, *Synth. Met.*, **27**, A491 (1988). (g) T. Mori, A. Kobayashi, Y. Sasaki, H. Kobayashi, G. Saito, H. Inokuchi, *Bull. Chem. Soc. Jpn.*, **1984**, 957.

[22] (a) K. Kajita, Y. Nishio, S. Moriyama, W. Sasaki, R. Kato, H. Kobayashi, A. Kobayashi, *Solid State. Commun.*, **64**(10), 1279 (1987). (b) H. Kobayashi, R. Kato, A. Kobayashi, Y. Nishio, K. Kajita, W. Sasaki, *Chem. Lett.*, **1989**, 789 and 833.

[23] (a) R. Kato, H. Kobayashi, A. Kobayashi, S. Moriyama, *Chem. Lett.*, **1987**, 507. (b) K. Kajita, Y. Nishio, S. Moriyama, W. Sasaki, R. Kato, H. Kobayashi, A. Kobayashi, *Solid State. Commun.*, **64**(10), 1279 (1987).

[24] A.M. Kini, U. Geiser, H.H. Wang, K.D. Carson, J.M. Williams, W.K. Knok, K. G. Vandervoort, J.E. Thompson, D.L. Stupka, D. Jung, M-H. Whanbo, *Inorg Chem.*, **29**(14), 2555 (1990).

[25] J.M. Williams, A.M. Kini, H.H. Wang, K.D. Carlson, U. Geiser, L.K. Montgomery, G.J. Phyrka, D.M. Watkins, J.M. Kommers, S.J. Borychuk, A.V.S. Crouch, W.K. Kwok, J.E. Schirber, D.L. Overmyer, D. Jung, M-H. Whangbo, *Inorg. Chem.*, **29**, 3272 (1990).

[26] H. Urayama, H. Yamochi, G. Saito, S. Sato, A. Kawamoto, J. Tanaka, T. Mori, Y. Maruyama, H. Inokuchi, *Chem. Lett.*, **1988**, 463.

[27] (a) A. Kobayashi, R. Kato, T. Naito, H. Kobayashi, *Synth. Met.*, **55-57**, 2078 (1993). (b) L.K. Montgomery, T. Burgin, J.C. Huffman, K.D. Carlson, J.D. Dudek, G.A. Yaconi, L.A. Megna, P.R. Mobley, W.K. Kwok, J.M. Williams, J.E. Shirber, D.L. Overmyer, J. Ren, C. Rovir, M-H. Whangbo, *Synth. Met.*, **55-57**, 2090 (1993). (c) H. Kobayashi, T. Naito, A. Sato, K. Kobayashi, A. Kobayashi, H. Tanaka, T. Saito, M. Tokumoto, L. Brossard, P, Cassoux, *Mol. Cryst. Liq. Cryst.*, **284**, 61 (1996).

[28] H. Kobayashi, T. Udagawa, H. Tomita, K. Bun, T. Naito, A. Kobayashi, *Chem. Lett.*, **1993**, 1559.

[29] A. Kobayashi, T. Udagawa, H. Tomita, T. Naito, H. Kobayashi, *Chem. Lett.*, **1993**, 2179.

[30] G. Steinmecke, R. Kirmse, E. Hoyer, *Z. Chem.*, **15**, 28 (1975).

[31] G. Steinmecke, H-J. Sieler, R. Kirmse, E. Hoyer, *Phos. Sulfur.*, **7**, 49 (1979).

[32] A. Kobayashi, H. Kobayashi, in *Molecular Metals and Superconductors Based on Transition Metal Complexes "Handbook of Organic Conductors " Chapter 5* , ed. by N. Nalwa, John Wiley &Sons (1997).

[33] (a) H. Tajima, T. Naito, M. Tamura, A. Kobayashi, H. Kuroda, R. Kato, H. Kobayashi, R.A Clark. A.E. Underhill, *Solid State Commun.*, **79** 337 (1991). (b) H. Tajima, T. Naito, M. Tamura, A. Kobayashi, H. Kuroda, R. Kato, H. Kobayashi, R.A Clark. A.E. Underhill, *Mol. Cryst. Liq. Cryst.*, **181**, 223 (1990). (c) E. Canadell, S. Ravy, J.P. Pouget, L. Brossard, *Solid State Commun.*, **75**, 633 (1990). (d) E. Canadell, I.E.-I. Rachidi, S. Ravy, J.P. Pouget, L. Brossared, J.P. Legros, *J. Phys. France*, **50**, 2967 (1989).

[34] L. Brossard, M. Ribault, M. Bousseau, L. Valade, P. Cassou, *C. R. Acad. Sci. Paris,*

Ser.II, **302**, 205, (1986).

[35] H. Kim, A. Kobayashi, Y. Sasaki, R. Kato, H. Kobayashi, *Chem. Lett.*, **1987**, 1799.

[36] L. Brossard, H. Hurdequint, M. Ribault, L. Valade, J.P. Legros. P. Cassoux, *Synth. Met.*, **27**, B157 (1988).

[37] L. Brossard, M. Ribault, L. Valade, P. Cassoux, *J. Phys. France*, **50**, 1521 (1989).

[38] A. Kobayashi, H. Kobayashi, A. Miyamoto, R. Kato, R.A. Clark, A.E. Underhill, *Chem. Lett.*, **1991**, 2163.

[39] H. Kobayashi, K. Bun, T. Naito, R. Kato, A. Kobayashi, *Chem. Lett.*, **1992**, 1909.

[40] H. Tajima, M. Inokuchi, A. Kobayashi, T. Ohta, R. Kato, H. Kobayashi, H. Kuroda, *Chem. Lett.*, **1993**, 1235.

[41] R. Kato, Y. Kashimura, S. Aonuma, N. Hanasaki, H. Tajima, *Solid State Commun.*, **105**(9), 561 (1998).

[42] R. Kato, H. Kobayashi, H. Kim, A. Kobayashi, *Chem. Lett.*, **1988**, 865.

[43] H. Kobayashi, R. Kato, A. Kobayashi, *Synth. Met.*, **42**, 2495 (1991).

[44] A. Kobayashi, A. Sato, H. Kobayashi, to be published.

[45] K. Kikuch, M. Kikuchi, T. Namiki, K. Saito, I. Ikemoto, K. Murata, T. Ishiguro, K. Kobayashi, *Chem. Lett.*, **1987**, 931.

[46] K. Kikuchi, K. Murata, Y. Honda, T. Namiki, K. Saito, H. Anzai, K. Kobayashi, T. Ishiguro, I. Ikemoto, *J. Phys. Soc. Jpn.*, **56**, 4241 (1987).

[47] K. Kikuchi, K. Murata, Y. Honda, T. Namiki, K. Saito, H. Anzai, K. Kobayashi, T. Ishiguro, I. Ikemoto, *J. Phys. Soc. Jpn.*, **56**, 2627 (1987).

[48] K. Kikuchi, Y. Honda, Y. Ishikawa, K. Saito, I. Ikemoto, K. Murata, H. Anzai, T. Ishiguro, K. Kobayashi, *Solid State Commun.*, **66**, 405 (1988).

[49] K. Kikuchi, K. Murata, Y. Honda, T. Namiki, K. Saito, H. Anzai, K. Kobayashi, T. Ishiguro, I. Ikemoto, *J. Phys. Soc. Jpn.*, **56**, 3436 (1987).

[50] G.C. Papavassiliou, G.A. Mousdis, J.S. Zambounis, A. Terzis, A. Hountas, B. Hilti, C.W. Mayer, J. Pfeiffer, *Synth. Met.*, **27**, B379 (1988).

[51] S.S. Parkin, E.M. Engler, R.R. Schumaker, R. Lagier, V. Y. Lee, J.C. Scott, R.L. Greece, *Phys. Rev. Lett.*, **50**, 270 (1983).

[52] E.B. Yagubskii, I.F. Schegolev, V.N. Laukihin, R.P. Shibaeva, E.E. Kostyuchenko, A. G. Khomenko, Y.V. Sushko, A.V. Zvarykina, *JETP Lett.*, **40**, 1201 (1984)

[53] R.P. Shibaeva, V.F. Kaminski, E.B. Yagubskii, *Mol. Cryst. Liq. Cryst.*, **119**, 361 (1982).

[54] J.M. Williams, H.H. Wang, M.A. Beno, T.J. Emge, L.M. Sowa, P.T. Copps, F. Behroozi, L.N. Hall, K.D. Carlson, G.W, Crabtree, *Inorg. Chem.*, **23**, 3839 (1984).

[55] H.H. Wang, L. Nunez, G.W. Crabtree, K.D. Carlson, J.M. Williams, L.A. Azevedo, J.F. Kwash, J.E. Schirber, *Inorg. Chem.*, **24**, 2465 (1984).

[56] (a) T. Mori, H. Inokuchi, *Chem. Lett.*, **1987**, 1657. (b) M.J. Rosseinsky, M. Kurmoo, D.R. Talham, P. Day, D. Chasseau, D. Watkin, *J. Chem. Soc., Chem. Commun.*, **1988**, 88.

[57] H. Mori, I. Hirabayashi, S. Tanaka, T. Mori, H. Inokuch, *Solid State Commun.*, **76**, 35 (1990).

[58] T. Mori, K. Kato, Y. Maruyama, H. Inokuchi, H. Mori, I. Hirabayashi, S. Tanaka, *Solid State Commun.*, **82**, 177 (1992).

[59] R.N. Lyubovskaya, R.B. Lyubovskii, R.P. Shibaeva, M.Z. Aldoshina, L.M. Gol'denberg, L.P. Rozenberg, M.L. Khidekel, Y.F. Shul'pyakyva, *JETP Lett.*, **42**, 468 (1985).

[60] R.N. Lyubovskaya, E.A. Zhilyaeva, A.V. Zvarykina, V.N. Laukhin, R.B. Lyubovskii, S.I. Pesotskii, *JETP Lett.*, **45**, 530 (1987).

[61] H. Ito, H. Kaneko, T. Ishiguro, H. Ishimoto, K. Kono, S. Horiuchi, T. Komatsu, G. Saito, *Solid State Commun.*, **85**, 1005 (1993).

[62] T. Komatsu, T. Nakamura, N. Matsukawa, H. Yamochi, G. Saito, H. Ito, T. Ishiguro, M. Kusunoki, K. Sakaguchi, *Solid State Commun.*, **80**, 843 (1991).

[63] U. Geiser, H.H. Wang, K.D. Carson, J.M. Williams, H.A. Charlier, Jr., J.E. Heindl, G.A. Yaconi, B.J. Love, M.W. Lathrop, J.E. Schirber, D.L. Overmyer, J. Ren, M.H. Whambo, *Inorg. Chem.*, **30**, 2586 (1991).

[64] J.A. Schlueter, U. Geiser, J.M. Williams, H.H. Wang, W.K. Kwok, J.A. Fendrich, K.D. Carson, C.A. Achembach, J.D. Dudek, D. Naumann, T. Roy, J.E. Schirber,

W.R. Bayless, *J. Chem. Soc, Chem. Commun.*, **1994**, 1599.

[65] J.A. Schlueter, K.D. Carson, J.M. Williams, U. Geiser, H.H. Wang, U. Welp, W.K. Kwok, J.A. Fendrich, J.D. Dudek, C.A. Achembach, D. Naumann, T. Roy, J.E. Schirber, W.R. Bayless, *Physica C (Amsterdam)*, **230**, 348 (1994).

[66] J.A. Schlueter, K.D. Carson, U. Geiser, H.H. Wang, J.M. Williams, W.K. Kwok, J.A. Fendrich, U. Welp, P.M. Keane, J.D. Dudek, A.S. Komosa, D. Naumann, T. Roy, J.E. Schirber, W.R. Bayless, B. Dorill, *Physica C (Amsterdam)*, **233**, 379 (1994).

[67] A.W. Graham, M. Kurmoo, P. Day, *J. Chem. Soc., Chem. Commun.*, **1995**, 2061.

[68] L. Martin, S.S. Turner, P. Day, F. E. Mabbs, E.J.L. McInnes, *Chem. Commun.*, **1997**, 1367.

[69] M.A. Beno, H.H. Wang, A.M. Kini, K.D. Carlson, U. Geiser, W.K. Kwok, J.E. Thompson, J.M. Williams, J. Ren, M.H. Whamgbo, *Inorg, Chem.*, **29**, 1599 (1990).

[70] S. Kahlish, D. Schweitzer, I. Heinen, S.E. Lan, B. Nuber, H.J. Keller, K. Winzer, H.W. Helberg, *Solid State Commun.*, **80**, 191 (1991).

[71] J.S.Zambounis, CW. Mayer, K. Hanesten, B. Hilti, W. Hofherr, J. Pfeiffer, M. Bünkle, G. Rihs, *Adv. Mater.*, **4**, 33 (1992).

[72] H. Tanaka, A. Kobayashi, T. Saito, K. Kawano, T. Naito, H. Kobayashi, *Adv. Mater.*, **8**(10), 812 (1996).

[73] H. Kobayashi, A. Sato, E. Arai, H. Akutsu, A. Kobayashi, P. Cassoux, *J. Am. Chem. Soc.*, **119**(50) 12392 (1997).

[74] Y. Misaki, N. Higuchi, H. Fujiwara, T. Yamabe, T. Mori, H. Mori, S. Tanaka, *Angew. Chem. Int. Ed. Engl.*, **34**(11), 1222 (1995).

Chapter 2

Experimental

2.1 Introduction

In this chapter, the general synthesis procedures and measurement apparatus used throughout the present study are described.

Firstly, the outlines of the syntheses of (1) dmit$(COPh)_2$ which is the starting material of the dmise ligand (Chapter 3), (2) EDT-TTF and its selenium derivative EDTS (Chapter 4) and (3) the supporting electrolytes are given.

Procedure for preparing single crystals are also described. Conditions of the crystal growths are written in following chapters.

Experimental for the X-ray crystal structure analyses, the measurements of the electrical resistivity and the magnetic susceptibility are described. Temperature dependence of the electrical resistivity and the magnetic susceptibility were measured down to 2 K (Chapter 3-5). X-ray diffraction data were collected at room temperature and at low temperature (down to *ca.* 7 K).

2.2 *Syntheses*

2.2.1 *dmit(COPh)$_2$*

A convenient bulk synthesis of dmit ligand was described for the first time by Steimecke et al. in 1979 [1] and later modified by Valade et al. [2]. The dmit ligand is usually handled as dmit(COPh)$_2$ because Na$_2$(dmit) is unstable. Intermediate product of the zinc-chelate [*n*-(C$_4$H$_9$)$_4$N]$_2$[Ni(dmit)$_2$] (**1**) was prepared, and the subsequent treatment of this chelate with benzoyl chloride stabilized the ligand as dmit(COPh)$_2$ (**2**) by following reported procedures. Outline of the reaction is shown in Scheme 2.1.

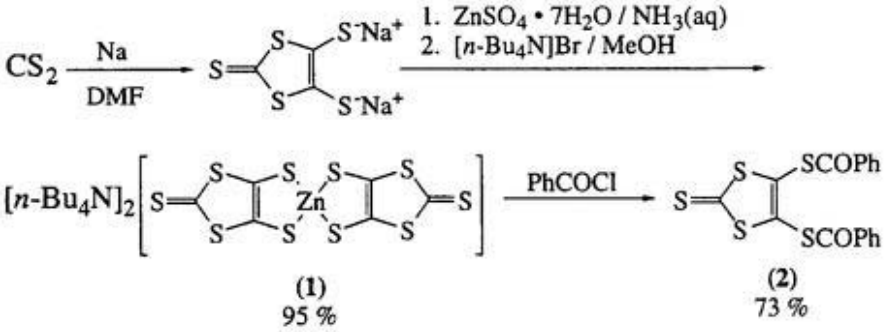

Scheme 2.1 Reaction scheme of the synthesis of dmit(COPh)$_2$ (**2**)

2.2.2 *The nickel-dmise complex*

The dmise ligand was synthesized according to the reference [3] where the modified route of the original one by Cornelissen et al.[4] was adopted. [(*n*-C$_4$H$_9$)$_4$N]$_2$[Ni(dmise)$_2$] (M= Ni and Pd) and [(*n*-C$_4$H$_9$)$_4$N][Ni(dmise)$_2$] were prepared in analogy to the synthesis of the dmit complexes as described by Steimecke et al. [1]. Outline of the reaction is shown in Scheme 2.2.

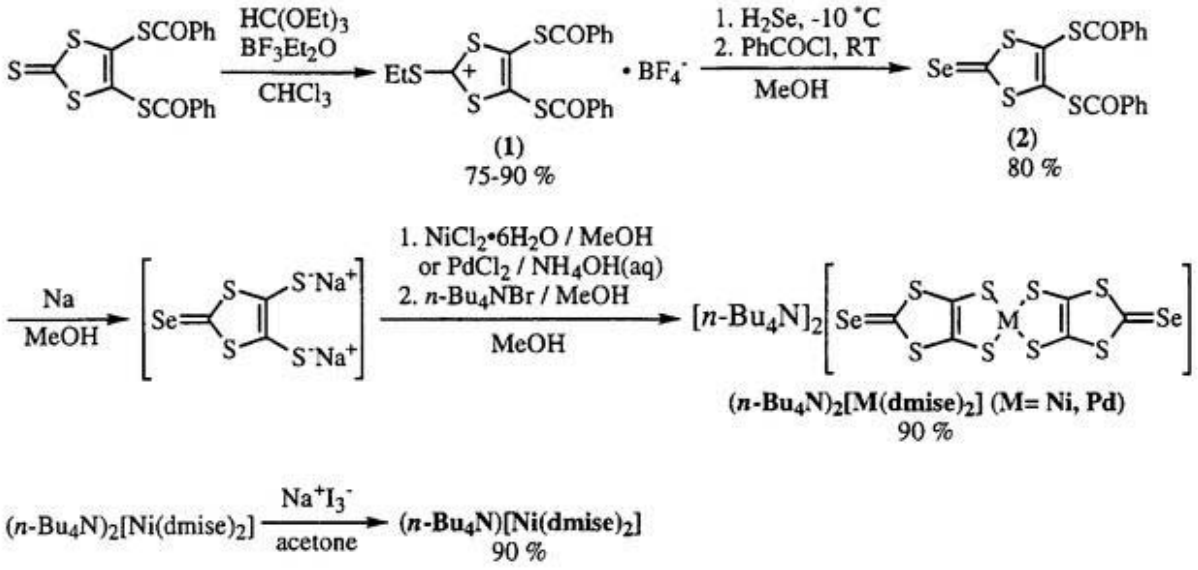

Scheme 2.2 Reaction scheme of the synthesis of $[(n\text{-}C_4H_9)_4N][Ni(dmise)_2]$.

2.2.3 EDT-TTF

Synthesis of EDT-TTF was reported for the first time in 1985 [5]. EDT-TTF was obtained from 4,5-ethylenedithio-1,3-dithiol-2-one (**3**) and 1,3-dithiole-2-thione (**4**) by the standard cross-coupling reaction in triethyl phosphite. Only unsymmetrical molecule EDT-TTF (**5**) was obtained. EDT-TTF and their intermediates were prepared according to the literature [5,6]. Outlines of the syntheses are shown in Schemes 2.3 ~ 2.4.

4,5-ethylenedithio-1,3-dithiol-2-one (3)

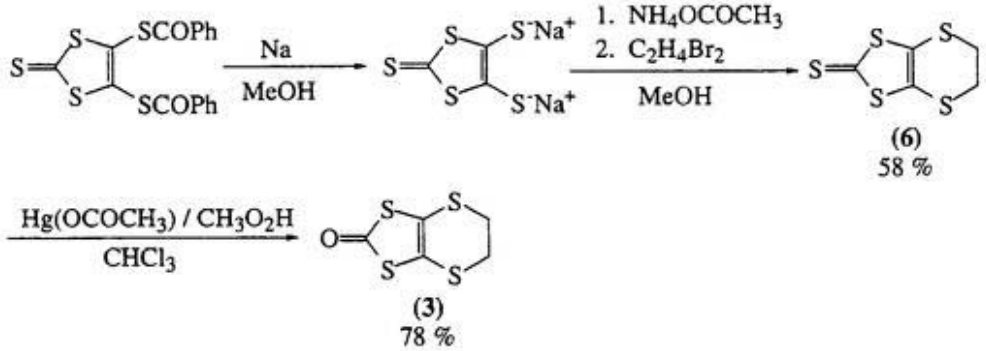

Scheme 2.3 Reaction scheme of 4,5-ethylenedithio-1,3-dithiol-2-one (**3**)

EDT-TTF (5)

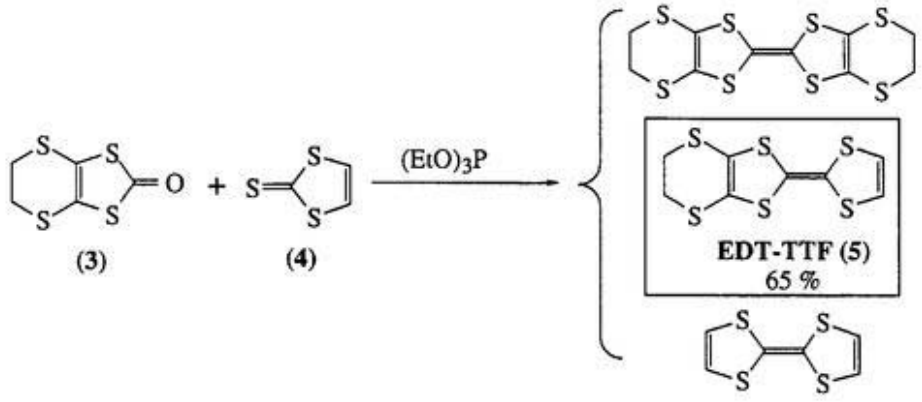

Scheme 2.4 Reaction scheme of synthesis of EDT-TTF (**5**)

2.2.4 EDTS

EDTS which is a selenium analogue of EDT-TTF was synthesized by a reaction of 4,5-ethylenedithio-1,3-dithiole-2-thione (**6**) and 4,5-bis(methoxycarbonyl)-1,3-diselenol-2-one (**7**) [7]. The intermediate (**8**) was prepared by the standard cross-coupling procedure. EDTS (**9**) was obtained by the demethoxycarbonylation.

4,5-bis(methoxycarbonyl)-1,3-diselenol-2-one (7)

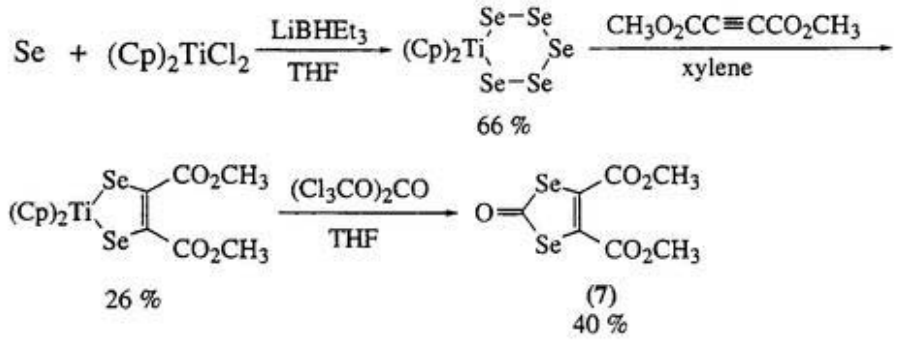

Scheme 2.5 Reaction scheme of the synthesis of 4,5-bis(methoxycarbonyl)-1,3-diselenol-2-one (**7**)

EDTS (9)

A mixture of **6** (1.4 g , 6.1 mg) and **7** (0.1 g, 3.0 mmol) was stirred at 110 °C in 35 ml of toluene under the nitrogen atmosphere. Triethyl phosphite (35 ml) was added to the reaction solution, then the color of the solution turned immediately from yellow to red. This solution was refluxed at 110-120 °C for 2 hours until the solution color changed from red to dark orange. This dark orange solution was evaporated and dried *in vacuo*. The red-purple oilic residue was purified by silica gel column chromatography using carbon disulfide as eluent. The purple fraction was evaporated and dark red oil **(8)** (513 mg) in yield of 33 %.

A red solution of **8** (513 mg, 1.0 mmol) and $LiBr{\bullet}H_2O$ (1.06 g, 10.2 mmol) dissolved in 70 ml of HMPA was evacuated at room temperature for 2 hours in order to remove the amine of solvent. After bubbled by argon gas for 15 minutes, this solution was heated 90 °C for 1 hour and at 110 °C for 1 hours. The reaction mixture was extracted 3 times by benzene and washed water 5 times with distilled water. The extract (benzene solution) was dried over Na_2SO_4 for 50 minutes and the orange portion was evaporated. The orange residue was purified by silica gel column chromatography using carbon disulfide and dichloromethane as eluent. The orange solution was evaporated and dried *in vacuo*. The resulting orange powder were recrystallized from CS_2 to afford the reddish orange needle crystal (166 mg) in yield of 43 %.

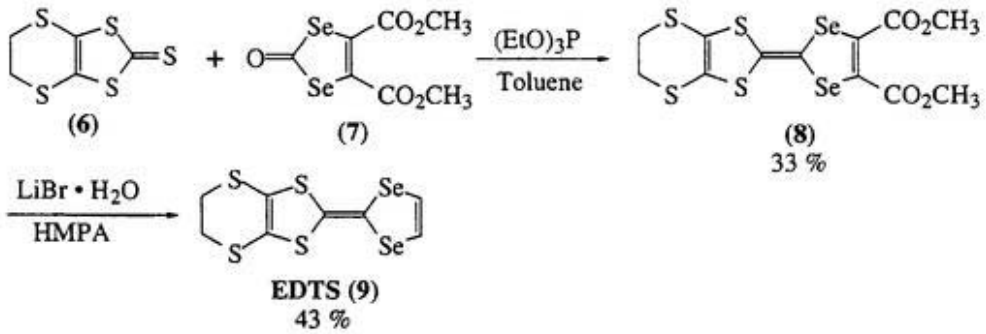

Scheme 2.6 Reaction scheme of the synthesis of EDTS (**9**)

2.2.5 *Supporting electrolytes*

(N,N-dimethylpiperidinium)ClO_4

Methyl iodide (24.4 g, 171 mmol) was added slowly to the solution of 9.8 g (115 mmol) of N-methylpiperidine dissolved in 5 ml of methanol in an ice bath. Immediately white preticipate was appeared. After stirring at room temperature, the solution was cooled at -40 °C. White preticipate (N,N-dimethylpiperidinium iodide) was filtered and dissolved in methanol. Silver perchlorate (3.7 g, 18 mmol) of was dissolved in methanol at room temperature, and added to the methanol solution of N,N-dimethylpiperidinium iodide. White solid of AgCl was precipitated immediately. After filtration of AgCl, and the colorless filtrate was obtained. The filtrate was concentrated and then cooled at -40 °C. White needle like crystal 3.3 g was obtained in yield of 93 %.

$[(C_2H_5)_4N]FeCl_4$ and $[(C_2H_5)_4N]GaCl_4$

To the solution of methanol (120ml) of Fe(III)Cl_3 (17 g, 100 mmol), added 40 ml of ethanol solution of tetraethyl ammonium chloride (16 g, 100 mmol). Yellow solid was produced immediately. This crude material was recrystallized from hot dichloromethane to give yellow needle crystals of $[(C_2H_5)_4N]FeCl_4$ [yield 12.7 g (39 %)].

Colorless needle crystals of $[(C_2H_5)_4N]GaCl_4$ were obtained by the same procedure using $GaCl_3$ instead of $FeCl_3$ [yield 10.5 g (85 %)].

2.3 *Preparations of single crystals*

All the crystals were prepared electrochemically. In order to obtain high quality crystals, it is essential to use pure electrolytes and donor (or acceptor) molecules under anhydrous conditions. The two compartment (H-type) cell was employed. The cell equipped glass filters were used for the electrocrystallization of $M(dmise)_2$ system. Electrodes were platinum wires (1 mmϕ). Solvents were distilled before use, and stored in the refrigerator. Potensiostats used were manufactured by the Equipment Development Center of the Institute for Molecular Science.

Donor (or acceptor) and the supporting electrolyte(s) were brought into the cell in a clean dry box. Proper degassed solvent was poured into the cell under nitrogen atmosphere at room temperature. Either constant current or voltage was applied between the electrodes usually for several days. Black plate or needle crystals of charge-transfer complexes were grown on the cathode.

2.4 *Crystal structure analyses*

X-ray diffractmetry has played an essential role to make clear the electronic states of molecular conductors. For example, the diffuse streaks observed in KCP and (TTF)(TCNQ) provided the first definite evidence of the existence of 1D metal electrons in the molecular crystals and through the observation of three-folded lattice modulations in the insulating phase of the $(DCNQI)_2Cu$ system, the mixed valence of Cu and therefore the existence of π-d hybrid metal band were revealed [8-10].

The temperature is, of course, the most important parameter to study physical properties of solids. Usually, X-ray crystal structure analyses have been made down to about 90 K by flushing cold nitrogen gas toward the sample. However, the development of crystal structure analyses at the lower temperature has been long remained to be made, in spite of the common understanding that the information on the low-temperature crystal structure are inevitable for the precise discussion.

In recent years, new low-temperature X-ray system equipped with liquid helium refrigerator has been established in our laboratory [11]. The minimum temperature is about 7 K. In Chapter 4, the crystal structure analyses above and below the temperature of the electronic (or magnetic) transition will be described.

2.4.1 *Measurements at room temperature*

A standard automated four-circle diffractometer was employed for the room-temperature crystal structure analyses. Samples were mounted on glass capillaries. Intensity data were collected by an automatic four-circle diffractometer (Rigaku AFC-5R or Rigaku AFC-7R) equipped with a rotating anode. Monochromatic Mo Kα X-ray was used. Lattice parameters were determined using 20-27 reflections. Data were collected in the angle range of $2^\circ \leq \theta \leq 60^\circ$ (sometimes 55°) by the ω-2θ scan method rated θ= 8°/min. (sometimes 16 °/min.). The absorption corrections were made empirically .

2.4.2 *Measurements at low temperature*

Data collections system of the diffractometer for low temperature consists of a Weissenberg-type imaging plate, DIP320 (MAC Science), and a helium cryostat, RC102 Cryogenic workstation (Cryo Industries). Camera radius is 150 mm.

Single crystal was mounted on the brass sample rod (8.0 mmϕ) for this equipment. A copper wire (~0.9 mmϕ) and a gold wire (20 μmϕ) were attached to the sample rod. Single crystal was fixed on the gold wire using the gold paste. Cooled helium gas (or liquid helium) was flushed toward the base of sample rod, and the crystal was cooled by the heat conduction. Distance from cooling point to the crystal position was about 45 mm. Temperature was controlled by a temperature control system, LTC-10 Temperature Controller (Conductus).

Monochromatic Mo-Kα X-ray was used for the data collection . Reflection data were collected in the angle range of $0 \leq \phi \leq 186$ ° at an interval of 6° (31 shots of X-ray photographs were taken). In most cases, the lattice parameters were determined by the program WELMS on the basis of two pairs of oscillation and Weissenberg photographs taken on two positions at interval of 90°. The intensity data collection and the subsequent structure analysis were made by using the program DENZO (both of MAC Science).

2.4.3 *Solution and refinement*

Crystal structures were solved by the direct method. Anisotropic or isotropic temperature factors were refined by the full-matrix or block-diagonal least-squares methods using the observed reflections [$I>3.00\sigma(I)$]. The atomic scattering factors were taken from the following reference [12]. Calculations were performed using the teXsan crystallographic software package (Molecular Structure Corporation) [13] or the program UNICS III [14] on a HITAC M-680 computer at the Computer Center of the University of Tokyo.

2.5 *Electrical resistivity and magnetic susceptibility*

Temperature dependence of the electric resistivity was measured down to 2 K by the four-probe method with AC current ranging 10 to 100 μA using Huso Electrical Chemical System HECS 994C1 Multi-channel 4-terminal conductometer. Gold wires (15 μm ϕ, Tanaka Denshi Kogyo K.K.) were fixed by the gold paste (Tokuriki Chemical, No. 8560) on the crystal surface almost along the conducting direction. Cooling samples down to 2 K were performed by means of pumping liquid helium using a cryostat (Ichikawa Vacuum).

Magnetic susceptibility was measured by using 0.5 ~ 5 mg of polycrystalline samples wrapped in the aluminum foil pieces set in a straw. Measurements were performed by use of the SQUID magnetometer, MPMS-7 or MPMS2 (the Quantum Design).

References

[1] (1) G. Steinmecke, R. Kirmse, E. Hoyer, *Z. Chem.*, **15**, 28 (1975). (2) G. Steinmecke, H-J. Sieler, R. Kirmse, E. Hoyer, *Phos. Sulfur.*, **7**, 49 (1979).

[2] L. Valade, M. Bousseau, P. Cassoux, *J. Chem. Soc., Dalton Trans.*, **1985**, 783.

[3] (a) T. Naito, A. Sato, K. Kawano, A. Tateno, H. Kobayashi, A. Kobayashi, *J. Chem.. Soc., Chem. Commun.*, **1995**, 351. (b) T. Naito, *Doctor thesis*, 156 (1995)

[4] J. P. Cornelissen, B. Pomarde, A.L. Spek, D. Reefman, J.G. Haasnoot, J. Reedijk, *Inorg. Chem.*, **32**, 3720 (1993).

[5] (a) H. Tatemitsu, E. Nishikawa, Y. Sakata, S. Misumi, *J. Chem. Soc. Chem. Commun.*, **1985**, 106. (b) R. Kato, H. Kobayashi, A. Kobayashi, *Chem. Lett.*, **1989**, 781.

[6] K.S. Varma, A. Bury, N.J. Harris, A.E. Underhill, *Synthesis*, **1987**, 837.

[7] C.M. Bolinger, T.B. Rauchfuss, *Inorg. Chem.*, **21**, 3947 (1982).

[8] R.Comès, M. Lambert, H. Launois, *Phys.Rev. B*, **8**(2), 571 (1973).

[9] F. Denoyer, F. Comès, A.F. Garito, A.J. Heeger, *Phys. Rev. Lett.*, **35**(7), 445 (1975).

[10] A. Kobayashi, R. Kato, H. Kobayashi, T. Mori, A. Inokuchi, *Solid State. Commun.*, **64**, 45 (1987).

[11] A. Kobayashi, H. Kobayashi, *Solid State Phys.*, **31**(1), 35 (1996).

[12] *International Tables for X-ray Crystallography*, Knoch Press, Barmingham, **4** (1974).

[13] Crystal Structure Analysis Package, Molecular Structure Corporation (1985 and 1992).

[14] T. Sakurai, K. Kobayashi, *Rep. Inst. Phys. Chem. Res.*, **55**, 69 (1979).

Chapter 3

Enhancement of the dimensionality of molecular conductors by the selone substitution of $M(dmit)_2$: $M(dmise)_2$ system (M= Ni, Pd)

The major part of this work has been published; (1) Akane Sato, Hayao Kobayashi, Toshio Naito, Fumiko Sakai, Akiko Kobayashi, *Inorg. Chem.*, **36**(23), 5262 (1997). (2) Akane Sato, Hayao Kobayashi, Akiko Kobayashi, *Chem. Lett.*, **1997**, 1275.

3.1 Introduction

The $Ni(dmit)_2$ complex molecule (dmit = 1,3-dithiole-2-thioxo-4,5-dithiolate) has played an important role in the development of the new molecular conducting systems, from which the molecular superconductor based on the transition metal-complexes has been prepared for the first time [1,2]. Unlike most of the constituent molecules of the crystalline molecular conductors, which are the TTF-like π-donor molecules, $Ni(dmit)_2$ is a π-acceptor molecule. Despite the resemblance in the molecular structures and the modes of molecular arrangements between the $Ni(dmit)_2$ conductors and the BEDT-TTF conductors [BEDT-TTF = Bis(ethylenedithio)tetrathiafulvalene], it has been pointed out that the transverse intermolecular interactions are weak in the $M(dmit)_2$ (M= Ni, Pd) system. Nevertheless, various types of molecular conductors including some stable metallic conductors and eight molecular superconductors have been discovered in the $M(dmit)_2$ (M=Ni, Pd) systems.

Compared with the TTF-like π-donor molecules, $M(dmit)_2$ molecules have the unique advantage that they can interact with each other through the terminal thione groups of the dmit ligands in the direction of the long molecular axis. Such a possibility was suggested ten years ago in $[(C_2H_5)_4N][Ni(dmit)_2]_2$ which was regarded as a precursor of a three-dimensional

molecular metal in spite of its semiconducting properties [3]. Up to now, three-dimensional Fermi-surface of the molecular metal has never determined by the low-temperature physical experiments such as Shbnikov-de Haas and/or de Haas-van Alphen experiments. Of course, there are C_{60} conductors having three-dimensional Fermi surfaces. However, the design of three-dimensional molecular metals based on the planar π molecules will not be so easy, but the development of such system may be one of the important future targets to the chemistry of a molecular conductors.

$M(dmise)_2$ (dmise = 1,3-dithiole-2-selenoxo-4,5-dithiolate) is a π-acceptor molecule analogous to $M(dmit)_2$, where the thione groups are exchanged to the selone groups of the ligands. It may be easily imagined that the three-dimensionality will be enhanced greatly by exchanging thione group to selone group, if the $M(dmise)_2$ conductors with similar structures to the corresponding $M(dmit)_2$ conductors can be obtained.

While some synthesis routes of $M(dmise)_2$ complex had been reported [4-6], the crystal structures and physical properties of the partially oxidized $M(dmise)_2$, α- and β-$[(CH_3)_4N][Ni(dmise)_2]_2$ were reported by Cornelissen et al. for the first time [7,8]. Although these salts exhibited relatively high conduction at the room-temperature (~10 S cm^{-1}), the systems behaved as semiconductors. The most prominent feature in the crystal structure of α-$[(CH_3)_4N][Ni(dmise)_2]_2$ is the extremely short intermolecular Se···Se contact between the two terminal selone groups, which is more than 0.72 Å shorter than the sum of the van der Waals radii of the selenium atoms (i.e., 4.00 Å). However, the calculation of the intermolecular overlap integrals of LUMO's showed that the selone-selone interaction was very small and both α- and β-$[(CH_3)_4N][Ni(dmise)_2]_2$ were suggested to have quasi-one dimensional band structures. These results indicated the difficulty in the design of three-dimensional molecular metals from usual planar π molecules. But the small interaction is not unexpected result in view of the large sensitivity of the π-π overlap integrals to the mutual orbital orientations.

Most of the molecular conductors currently studied have the layered structures, where the neighboring conduction layers constituted by planar π molecules are separated by counter ions between them. Since the layer-layer separation depends on the size of the counter ions, smaller size anions would be preferable to give the large interlayer interactions. In this study,

the possibility of enhancement of the dimensionality by synthesizing new $M(dmise)_2$ conductors with small anions was examined.

In the present study, the metallic conductors of $[(CH_3)_3HN][Ni(dmise)_2]_2$ (**1**) [9] and $[(CH_3)_2H_2N][Ni(dmise)_2]_2$ (**2**) which were suggested possessing the multi-dimensional Fermi surfaces by the electronic band structure calculations were obtained. At the same time, a $Pd(dmise)_2$ conductor with stable metallic state, $Cs[Pd(dmise)_2]_2$ (**4**) was also prepared. However, the crystal structure of $Cs[Pd(dmise)_2]_2$ could not be determined due to the insufficient crystal quality. In addition, the crystals of (N,N-dimethylpiperidinium) $[Ni(dmise)_2]_2$ (**5**) was prepared in order to obtain the first $M(dmise)_2$ system with "spanning overlap molecular arrangements" (see Chapter 1.1.3) and stable metallic state. In this chapter, synthesis, crystal structure and physical properties of $[(CH_3)_xH_{4-x}N][Ni(dmise)_2]_2$ (x = 1-3) (**1**, **2** and **3**), **4** and **5** are described.

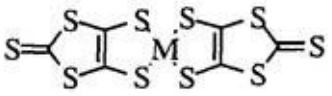

$M(dmit)_2$

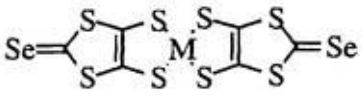

$M(dmise)_2$

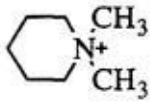

N,N-dimethylpiperidinium cation

3.2 *Experimental*

3.2.1 *Preparation of charge-transfer complexes*

Single crystals of **1**, **2**, **3**, **4** and **5** were obtained by the electrochemical oxidation of the mixture of $[n\text{-}(C_4H_9)_4N][Ni(dmise)_2]$ (4-10 mg) and proper supporting electrolyte (80-135 mg) in acetonitrile or the mixed solution of acetone and acetonitrile (15 ml), according to the procedure mentioned in Chapter 2. Conditions of preparation are shown in Table 3.1.

Table 3.1 Electric conditions obtained good crystalline [cation][$M(dmise)_2]_2$.[a]

Product	electrolyte (mg)		solvent	current (μA)	time (days)	habit
$[Me_3HN][Ni]_2$	$[(n\text{-}Bu)_4N][Ni]$	4.4	AN 15ml	0.2	7	thin plate
	$[Me_3HN]ClO_4$	83				
$[Me_2H_2N][Ni]_2$	$[(n\text{-}Bu)_4N][Ni]$	5.7	AN/AC(1:1)	0.5	5	thin plate
	$[Me_2H_2N]ClO_4$	136	15 ml			
$[MeH_3N][Ni]_2$	$[(n\text{-}Bu)_4N][Ni]$	5.7	AN/AC(1:1)	0.2	7	thin plate
	$[MeH_3N]ClO_4$	80	13ml			
$Cs[Pd]_2$	$[(n\text{-}Bu)_4N]_2[Pd]$	8	AN 15ml	0.8	10	thin plate
	$CsPF_6$	83				(not satisfied)
$(pipe)[Ni]_2$	$[(n\text{-}Bu)_4N][Ni]$	10	AN 15ml	0.2	10	rhombic plate
	$(pipe)ClO_4$	50-80				

[a] Abbreviations in Table 3.1 are : Me= CH_3, Bu= C_4H_9, [Ni]= $[Ni(dmise)_2]$, [Pd]= $[Pd(dmise)_2]$, pipe= N,N-dimethylpiperidinium, AN= acetonitrile, AC= acetone.

3.2.2 *X-ray measurements*

X-ray crystal structure determinations

Crystal structures of **1**, **2**, **3** and **5** were determined at the room temperature. The experimental details and crystal data are listed in Table 3.2. The crystals of **1** and **2** were sealed in the quartz capillaries because they were more or less unstable in the air.

Crystal structures of **1**, **3** and **5** were solved by the direct methods, and that of **2** was solved by the heavy atom methods. The refinements were made by the full-matrix least-squares methods. Anisotropic temperature factors were used for the non-hydrogen atoms and the hydrogen atoms were included in the final calculation. All calculations were performed using the teXsan crystallographic software package of Molecular Structure Corporation [10]. The structure of **2** was refined by the block-matrix least-squares method by using the program UNICS III [11] on a HITAC M-680 computer at the Computer Center of the University of Tokyo. Anisotropic temperature factors were used for the non-hydrogen atoms and the hydrogen atoms were not included in the final calculation.

X-ray oscillation patterns and temperature dependence of the lattice constants

X-ray oscillation patterns and temperature dependence of the lattice constants of **5** were examined down to 7 K.

Several oscillation photographs of the single crystal ($0.75 \times 0.8 \times 0.1$ mm^3) were taken in the temperature range of 295 - 7 K. The oscillation range and the oscillation speed were 3° and 2 °/min, respectively. X-ray exposure time was 45 minutes at a generation power of 8 kW (40 kV × 200 mA).

Temperature dependence of the lattice constants was determined using a single crystal ($0.75 \times 0.35 \times 0.02$ mm^3). Data analyses were performed by a program WELMS.

Table 3.2. Summary of the experimental conditions and crystal data for [cation][Ni(dmise)2]2.

Compound	$[(CH_3)_3HN][Ni(dmise)_2]_2$	$[(CH_3)_2H_2N][Ni(dmise)_2]_2$	$[(CH_3)H_3N][Ni(dmise)_2]_2$	$[C_7H_{16}N][[Ni(dmise)_2]_2$
Crystal data				
Empirical formula	$C_{15}H_{10}NNi_2S_{16}Se_4$	$C_{14}H_8NNi_2S_{16}Se_4$	$C_{13}H_6NNi_2S_{16}Se_4$	$C_{19}S_{16}Se_4Ni_2NH_{16}$
Crystal system	triclinic	triclinic	monoclinic	monoclinic
Space group	$P\bar{1}$	$P\bar{1}$	$P2_1/c$	C2/c
a(Å)	7.606(3)	7.625(3)	7.636(2)	40.15(1)
b(Å)	17.761(3)	17.583(5)	9.545(3)	6.496(4)
c(Å)	6.660(2)	6.526(2)	22.555(6)	13.935(7)
α(deg)	100.27(2)	100.01(2)		
β(deg)	114.93(2)	114.81(5)	92.95(2)	98.19
γ(deg)	81.84(2)	80.82(5)		
V($Å^3$)	800.4(4)	778.4(4)	1641.6(8)	3597(3)
Z	1	1	2	4
Measurement				
Diffractometer	AFC-5R	AFC-7R	AFC-7R	AFC-5R
ρ_{calc}($g\ cm^{-3}$)	2.387	2.425	2.267	2.22
μ(cm^{-1})	67.84	69.74	66.00	60.33
T(K)	296	296	296	296
Total reflections	3969	3046	4289	5017
Unique reflections	3692	2733	3996	4951
R_{int}	0.018	0.017	0.118	0.058
Observation reflections	2400	1759	1634	1896
Solution and refinement[a]				
Solution	Direct methods	Heavy atom methods	Direct methods	Direct methods
Refinment	Full-matrix least-squares	Block-matrix least-squares	Full-matrix least-squares	Full-matrix least-squares
R (Fo) [b]	0.036	0.066	0.058	0.073
R_w (Fo)	0.022 [c]	0.072 [d]	0.058 [c]	0.99 [c]

[a] Calculation of $[(CH_3)_2H_2N][Ni(dmise)_2]_2$ was made using the program UNICS III [11] on a HITAC M-680 computer at the Computer Center of the University of Tokyo. The others was calculated using the teXsan crystallrographic software package of Molecular Structure Corporation [10].

[b] $|F_o| \geq 3\sigma|F_o|$, b $R = \Sigma(|F_o|-|F_c|)/\Sigma|F_o|$, [c] $Rw = [\Sigma w(|F_o|-|F_c|)^2/\Sigma w|F_o|^2]^{1/2}$, $w = 1/\sigma^2(F)$, [d] $Rw = \Sigma w(|F_o|-|F_c|)^2$, $w = 1/\sigma^2(F)$.

3.2.3 *Electrical resistivity measurements*

The temperature dependence of the electrical resistivity was measured by the four-probe method under the constant current ranging from 10 to 100 μA. The four gold wires (15 μmϕ) were bonded on the crystal surface by the gold paint. The resistivities were measured along the long axes of the crystals (almost the molecular stacking directions). Measurements under the high pressure were performed up to 6 kbar for **1** using the clamp-type cell and Daphne oil 7373 (Idemitsu Oil Co. Ltd.) as the pressure medium.

3.2.4 *Band structure calculation*

The band structure calculations were carried out by the extended Hückel method using Slater-type atomic orbitals. The exponents ζ and ionization potentials (eV) for atomic orbitals are listed in Table 3.3.

Table 3.3 The exponents ζ and the ionization potentials (eV) for atomic orbitals.

orbital		ζ	E_i (eV)	orbital		ζ	E_i (eV)
Se	4s	2.112	-20.0	Ni	4s	2.1	-7.34
	4p	1.827	-11.0		4p	2.1	-3.74
	4d	1.5	-6.8		4d	a	-10.6
S	3s	2.122	-20.0	C	2s	1.625	-21.4
	3p	1.825	-11.0		2p	1.625	-11.4
	3d	1.5	-5.44				

[a] Double ζ: 0.5681 χ_1 (5.75) + 0.6294 χ_2 (2.0).

3.2.5 Magnetic susceptibility measurement

Magnetic susceptibly of **5** was measured in the temperature range of 300 to 2 K in the magnetic field of 5 kOe on a SQUID magnetometer by using the polycrystalline sample wrapped with a piece of the aluminum foil.

3.3 $[(CH_3)_xH_{4-x}N][Ni(dmise)_2]_2$ (x= 1, 2 and 3).

3.3.1 Crystal structures

The atomic coordinates of **1**, **2** and **3** are listed in Table 3.4 and the numbering schemes of atoms of the $Ni(dmise)_2$ molecules are shown in Fig.3.1.

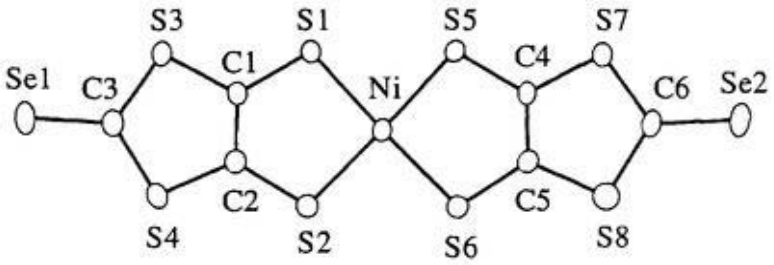

(a)

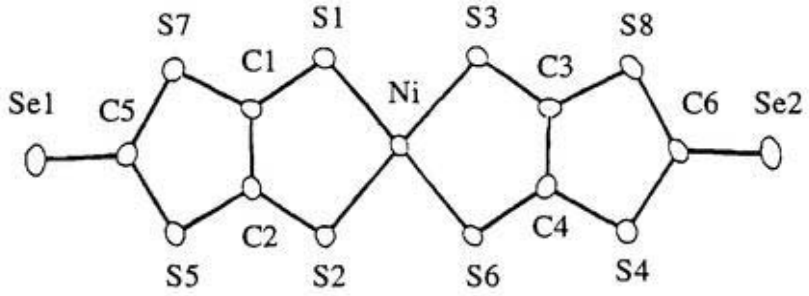

(b)

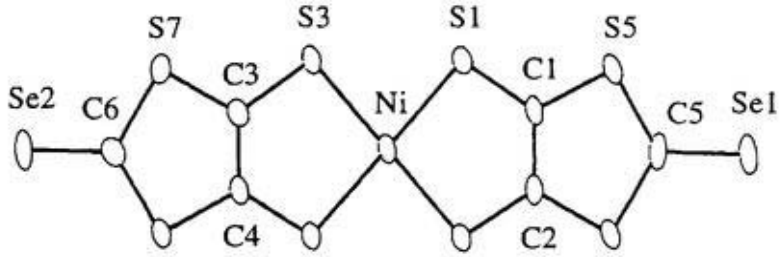

(c)

Fig.3.1. Numbering schemes (a) **1**, (b) **2** and (c) **3** .

Table 3.4. Atomic coordinates of **1** and **2**.

Atom	x	y	z	B_{eq}
(1)				
Se1	0.1765(1)	0.13814(4)	0.0814(1)	4.60(2)
Se2	0.3974(1)	0.93242(4)	0.0699(1)	4.57(2)
Ni	0.2638(1)	0.53380(4)	0.0334(1)	2.45(1)
S1	0.2716(2))	0.47219(8)	0.2878(2)	3.01(3)
S2	0.1991(2)	0.43341(8)	-0.2168(2)	3.06(3)
S3	0.2294(2)	0.30646(8)	0.2844(2)	3.15(4)
S4	0.1620(2)	0.26925(8)	-0.1801(2)	3.33(4)
S5	0.3311(2)	0.63056(8)	0.2926(2)	3.02(3)
S6	0.2509(2)	0.59925(8)	-0.2185(2)	2.91(3)
S7	0.3842(2)	0.79435(8)	0.2833(2)	3.18(4)
S8	0.3085(2)	0.76748(8)	-0.1825(2)	3.25(4)
N	0.910(1)	0.9832(5)	0.455(2)	15.0(4)
C1	0.233(7)	0.3822(3)	0.1533(8)	2.4(1)
C2	0.2008(7)	0.3652(3)	-0.0678(8)	2.6(1)
C3	0.1877(7)	0.2362(3)	0.0609(8)	2.9(1)
C4	0.3357(7)	0.7015(3)	0.1550(8)	2.4(1)
C5	0.3019(7)	0.6880(3)	-0.0675(8)	2.5(1)
C6	0.3637(7)	0.8342(3)	0.0574(8)	2.9(1)
C7	0.964(2)	0.9113(8)	0.522(2)	20.4(6)
C8	1.198(2)	0.9627(10)	0.465(2)	18.6(5)
(2)				
Se1	0.8767(3)	0.9372(1)	0.7585(3)	3.73
Se2	0.6707(3)	0.1373(1)	-0.2513(3)	3.65
Ni	0.7631(3)	0.5355(1)	0.2713(3)	1.98
S1	0.7476(6)	0.6006(2)	0.5779(6)	2.45
S2	0.8281(6)	0.6342(5)	0.1687(5)	2.46
S3	0.4002(6)	0.4340(2)	0.3668(6)	2.64
S4	0.7299(6)	0.3064(2)	-0.2387(6)	2.58
S5	0.8736(6)	0.7999(2)	0.3898(6)	2.78
S6	0.7732(6)	0.4732(2)	-0.0391(6)	2.50
S7	0.7982(6)	0.7699(2)	0.7644(6)	2.84
S8	0.6628(6)	0.2687(2)	0.1340(6)	2.84
N	0.522(8)	-0.025(2)	-0.005(8)	8.43
C1	0.847(2)	0.8379(8)	0.638(2)	2.52
C2	0.685(2)	0.2363(8)	-0.122(2)	2.57
C3	0.700(2)	0.3645(7)	0.150(2)	2.14
C4	0.733(2)	0.3822(7)	-0.028(2)	2.29
C5	0.793(2)	0.6909(8)	0.562(2)	2.35
C6	0.832(2)	0.7046(7)	0.385(2)	2.43
C11	0.376(5)	-0.004(2)	-0.171(4)	4.31
C12	0.623(5)	0.050(3)	0.231(5)	5.31

$$B_{eq} = \frac{8}{3}\pi^2 (U_{11}(aa^*)^2 + U_{22}(bb^*)^2 + U_{33}(cc^*)^2 + 2U_{12}aa^* \cdot bb^* \cdot cos\gamma + 2U_{13}aa^* \cdot bb^* \cdot cos\beta + 2U_{23}aa^* \cdot bb^* \cdot cos\alpha)$$

The crystal structures of **1** and **2** are shown in Fig.3.2. The crystals of **1** and **2** belong to the triclinic system with the space group of P $\bar{1}$. Although the unit cell parameters of **1** and **2** were very similar to each other, these were not isostructural (see Table 3.4). On the other hand, **1** and **2** are isostructural to their dmit analogs, $[(CH_3)_3HN][Ni(dmit)_2]_2$ and $[(CH_3)_2H_2N][Ni(dmit)_2]_2$, respectively [12]. Each unit cell contained two $Ni(dmise)_2$ molecules and one counter cation. The selected bond lengths and angles also are listed in Table 3.5. The $Ni(dmise)_2$ molecules stack along the [100] direction with slightly dimmerizating (3.557 Å and 3.464 Å) in the crystal of **1** while the $Ni(dmise)_2$ molecules stack along the [101] direction with spacing 3.573 Å and 3.522 Å in **2** (Fig.3.3). In each case, the $Ni(dmise)_2$ molecules formed one-dimensional columns. In the crystals of **1** and **2**, the cation located on the inversion center, so that the cation has a positional disorder and the carbon and nitrogen atoms have large thermal parameters. Intermolecular distance between the two chalcogen atoms less than the sum of the van der Waals radii (i.e., S···S, 3.70 Å; S···Se, 3.85 Å; Se···Se, 4.00 Å) of **1** and **2** are listed in Table 3.6. The short intermolecular distances of the chalcogen···chalcogen atoms were observed along the stacking direction of $Ni(dmise)_2$ molecules, in the transverse direction and along the direction of long molecular axis. The Se···Se short contacts along the long axis of the molecules are 3.801(1) Å and 3.486(1) Å in **1**, and 3.504(3) Å and 3.617(3) Å in **2**, respectively. Every Se···Se short contact is longer than 3.277(3) Å for the α-$[(CH_3)_4N][Ni(dmise)_2]_2$ [8].

The intermolecular overlap integrals of LUMO of $Ni(dmise)_2$ calculated for **1** and **2** showed the large intermolecular interactions along the long axis of the molecules, which is quite different from the case of α-$[(CH_3)_4N][Ni(dmise)_2]_2$ [8]. The results of the calculation of band structure for **1** and **2** will be discussed later.

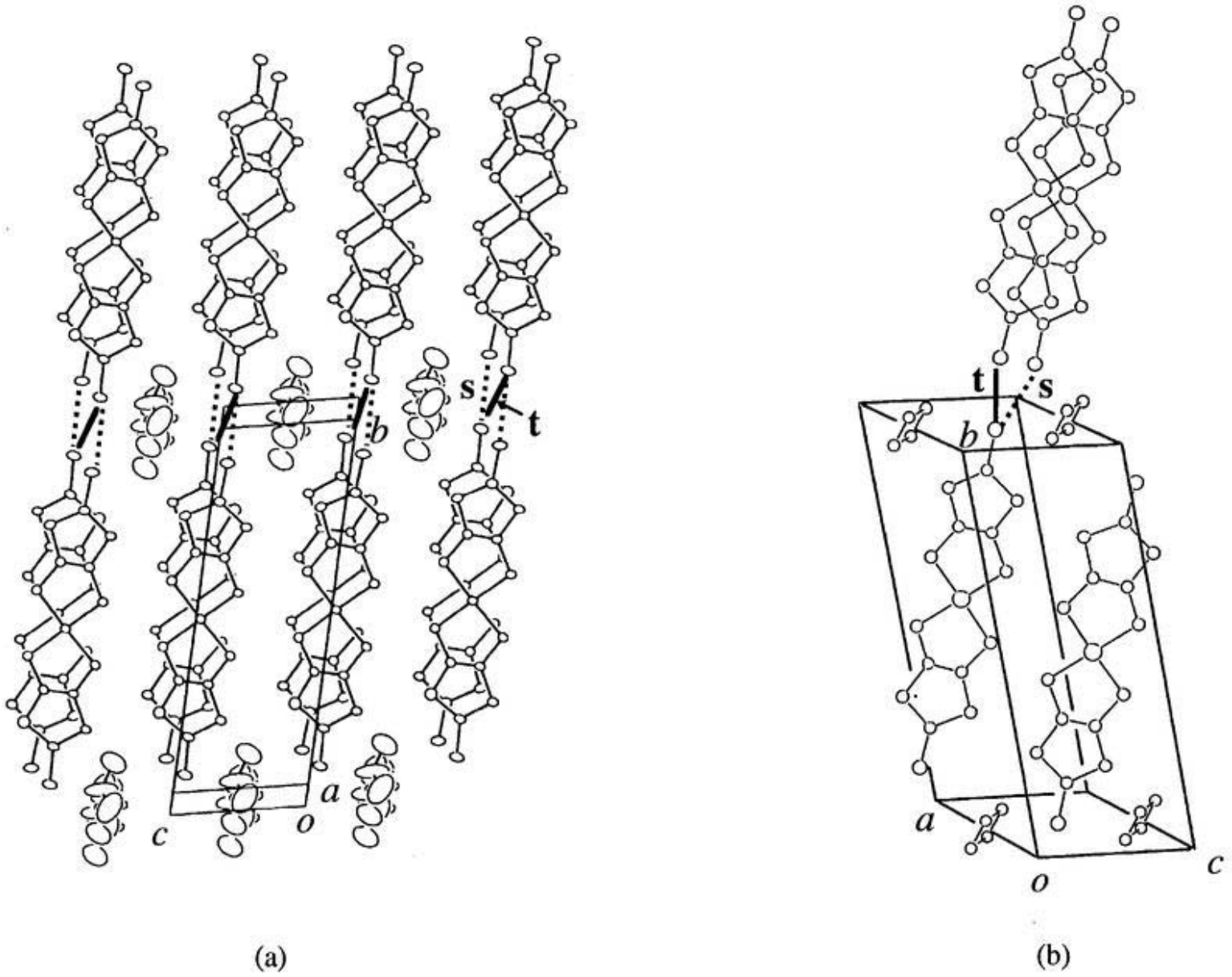

Fig.3.2. Crystal structures of (a) **1** and (b) **2**. s and t correspond to discussions of the intermolecular chalcogen···chalcogen distances and the overlap integrals. $(CH_3)_3HN^+$ and $(CH_3)_2H_2N^+$ cations are disordered.

Table 3.5 Selected bond lengths (Å) and angles (degree) of **1** and **2**.

(1)

	distance / Å		distance / Å
Ni - S1	2.151(2)	S7 - C4	1.730(5)
Ni - S2	2.167(2)	S7 - C6	1.714(5)
Ni - S5	2.155(2)	S8 - C5	1.738(5)
Ni - S6	2.168(2)	S8 - C6	1.741(5)
S1 - C1	1.686(5)	Se1 - C3	1.788(5)
S2 - C2	1.693(5)	Se2 - C6	1.782(5)
S3 - C1	1.737(5)	C1 - C2	1.372(6)
S3 - C3	1.710(5)	C4 - C5	1.374(6)
S4 - C2	1.747(5)	N - C7	1.38(1)
S4 - C3	1.731(5)	N - C8	1.36(1)
S5 - C4	1.696(5)		
S6 - C5	1.710(5)		
	angle / °		**angle / °**
S1 - Ni - S2	92.86(6)	S5 - C4 - C5	121.4(4)
S5 - Ni - S6	93.66(6)	S7 - C4 - C5	115.8(4)
Ni - S1 - C1	102.6(2)	S6 - C5 - C4	121.5(4)
Ni - S2 - C2	101.8(2)	S8 - C5 - C4	115.2(4)
Ni - S5 - C4	102.1(2)	S7 - C6 - S9	112.2(3)
Ni - S6 - C5	101.3(2)	S7 - C6 - Se2	123.4(3)
S1 - C1 - C2	121.2(4)	S8 - C6 - Se2	124.4(3)
S3 - C1 - C2	116.3(4)	C1 - S3 - C3	97.6(2)
S2 - C2 - C1	121.5(4)	C2 - S4 - C3	97.4(2)
S4 - C2 - C1	115.0(4)	C4 - S7 - C6	98.7(2)
S3 - C3 - S4	113.6(3)	C5 - S8 - C6	98.0(2)
S3 - C3 - Se1	122.1(3)	C7 - N - C8	67.7(4)
S4 - C3 - Se1	124.3(3)		

Table 3.5 Selected bond lengths (Å) and angles (degree) of **1** and **2** (Continued)

(**2**)

	distance / Å		distance / Å
Ni - S1	2.165(4)	S7 - C3	1.732(1)
Ni - S2	2.160(5)	S7 - C6	1.74(2)
Ni - S3	2.171(5)	S8 - C4	1.73(1)
Ni - S4	2.154(4)	S8 - C6	1.71(2)
S1 - C1	1.71(2)	Se1 - C5	1.79(1)
S2 - C2	1.70(1)	Se2 - C6	1.80(1)
S3 - C3	1.70(1)	C1 - C2	1.37(3)
S3 - C4	1.70(2)	C3 - C4	1.38(2)
S5 - C1	1.74(1)	N - C11	1.14(5)
S5 - C5	1.73(2)	N - C12	1.16(5)
S6 - C2	1.75(2)		
S6 - C5	1.73(2)		
	angle / °		angle / °
S1 - Ni - S2	93.3(2)	S7 - C3 - C4	115.3(10)
S3 - Ni - S4	92.7(2)	S7 - C6 - S8	114.1(7)
Ni - S1 - C1	102.1(6)	S8 - C4 - C3	116.2(10)
Ni - S2 - C2	101.8(6)	Se1 - C5 - S5	123.6(9)
Ni - S3 - C3	102.5(6)	Se1 - C5 - S6	123.1(10)
Ni - S4 - C4	102.8(6)	Se2 - C6 - S7	124.0(10)
S1 - C1 - C2	121(1)	Se2 - C6 - S8	121.9(9)
S2 - C2 - C1	122(1)	C1 - S5 - C5	97.9(8)
S3 - C3 - C4	121(1)	C2 - S6 - C5	97.6(8)
S4 - C4 - C3	121.4(10)	C3 - S7 - C6	97.2(7)
S5 - C5 - S6	113.2(7)	C4 - S8 - C6	97.3(7)
S5 - C1 - C2	115.6(11)	C11 - N - C12	161(4)
S6 - C2 - C1	115.7(10)		

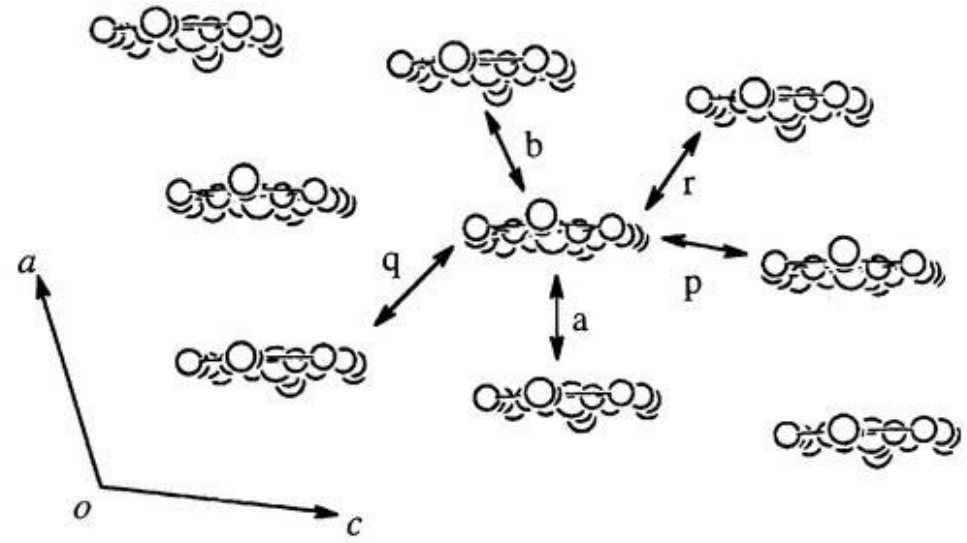

(a)

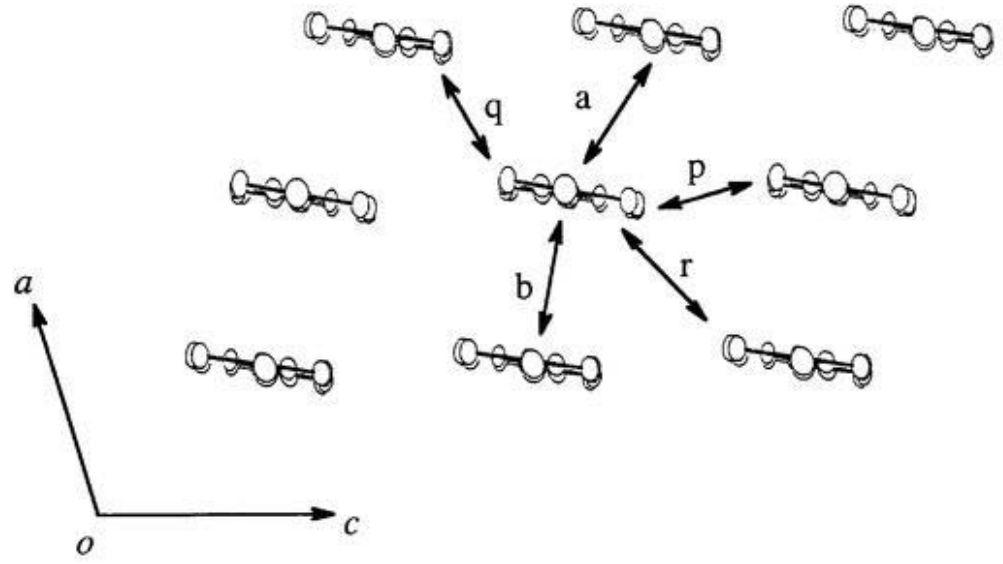

Fig.3.3. End-on projections of (a) **1** and (b) **2**. These figures indicate the schemes of intermolecular short contacts between chalcogen atoms less than the sum of the van der Waals radii and their overlap integrals.

Table 3.6 Intermolecular chalcogen···chalcogen distances in **1** and **2**. a, b, p, q, r, s and t correspond to those shown in Fig.3.3.

	contact	symmetry operation[a]	distance / Å
(1)			
a	S1···S2	(-*x*, -*y*+1, -*z*)	3.606(2)
	S1···S6	(-*x*, -*y*+1, -*z*)	3.677(2)
b	Se1···Se2	(-*x*+1, -*y*+1, -*z*)	3.773(2)
p	S1···S6	(*x*, *y*, *z*+1)	3.690(2)
r	S1···S1	(-*x*+1, -*y*+1, -*z*+1)	3.568(3)
	S1···S5	(-*x*+1, -*y*+1, -*z*+1)	3.661(2)
	S3···S5	(-*x*+1, -*y*+1, -*z*+1)	3.516(2)
	S3···S7	(-*x*+1, -*y*+1, -*z*+1)	3.653(2)
s	Se1···Se2	(*x*, *y*-1, *z*)	3.8007(9)
t	Se2···Se2	(-*x*+1, -*y*+2, -*z*)	3.486(1)
(2)			
a	S4···S4	(-*x*+2, -*y*+1, -*z*)	3.536(7)
	S2···S4	(-*x*+2, -*y*+1, -*z*)	3.647(6)
	S2···S8	(-*x*+2, -*y*+1, -*z*)	3.510(6)
b	S1···S8	(-*x*+1, -*y*+1, -*z*)	3.664(5)
p	S1···S2	(*x*, *y*, *z*+1)	3.600(5)
	S1···S4	(*x*, *y*, *z*+1)	3.564(6)
	S3···S4	(*x*, *y*, *z*+1)	3.633(5)
	S3···S8	(*x*, *y*, *z*+1)	3.615(5)
q	Se1···Se2	(-*x*+2, -*y*+1, -*z*+1)	3.831(3)
s	Se1···Se1	(-*x*+2, -*y*+2, -*z*+2)	3.504(3)
t	Se1···Se2	(*x*, *y*+1, *z*+1)	3.617(3)

[a] This applies on second atom

3 which has a smaller counter cation was expected to give the larger overlap integrals between the two selone groups. However, the Ni(dmise)$_2$ molecular arrangements in the crystal structure of **3** is unexpectedly different from those of **1** and **2**. The structure of **3** is shown in Fig.3.4, and the atomic coordinates and the selected bond lengths and angles are listed in Table 3.7 and Table 3.8, respectively. The crystal belongs to the monoclinic system with the space group of $P2_1/c$. One Ni(dmise)$_2$ molecule and one $(CH_3)H_3N^+$ cation were crystallographically independent. The Ni(dmise)$_2$ molecules were not disordered but distorted. The $(CH_3)H_3N^+$ cation located near the inversion center took two possible orientations with large thermal parameters (N, B_{eq}= 8.8(8) Å^2; C8, B_{eq}= 6.4(10) Å^2). The Ni(dmise)$_2$ molecules stacked with the spacings of 3.601 Å and 3.602 Å along the *a* axis (Fig.3.5). The Ni(dmise)$_2$ molecules stacked almost parallel with the dihedral angle of two independent molecular planes being 0.03°. The Ni(dmise)$_2$ molecules arranged zig-zag in the molecular transverse direction, that is, the Ni(dmise)$_2$ columns were not neighboring each other. The intermolecular distances less than the sum of van der Waals radii between the chalcogen atoms are listed in Table 3.9 (Fig.3.5, Table 3.9). There were no short intermolecular contact between the two selone groups of the Ni(dmise)$_2$ molecules along the long molecular axis direction.

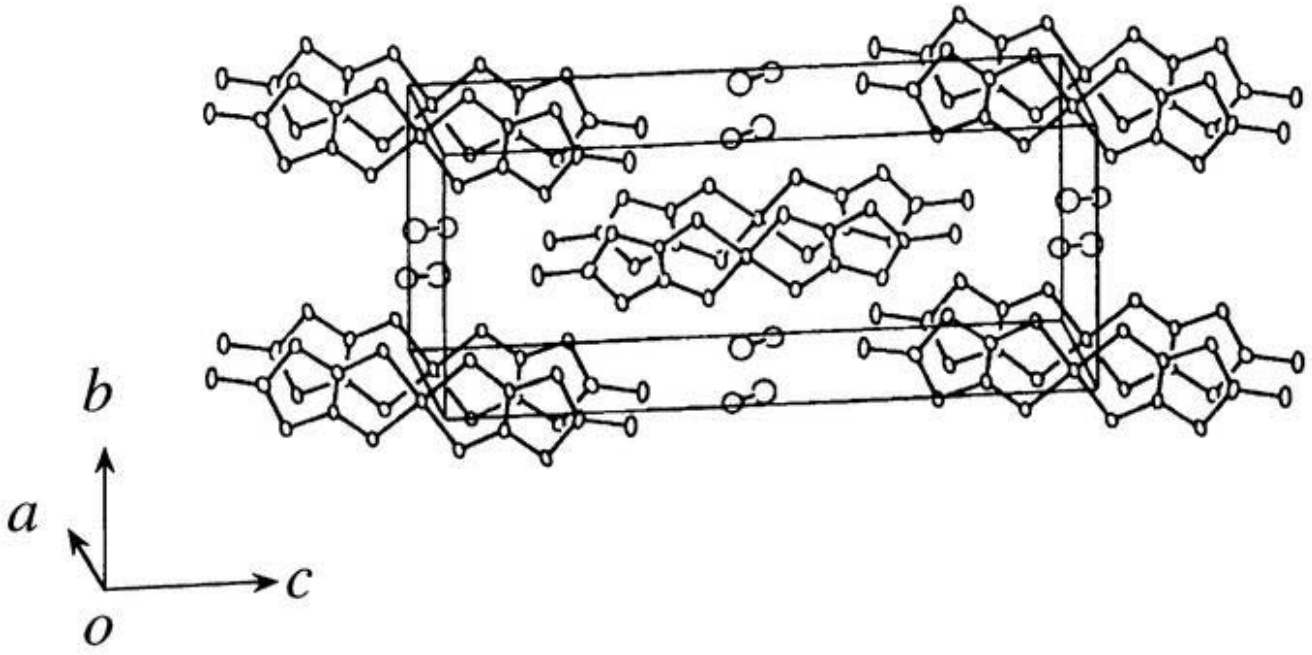

Fig.3.4. Crystal structures of **3**. $(CH_3)H_3N^+$ cations disorderedly occupy two sites.

Table 3.7 Atomic coordinates of **3**.

Atom	x	y	z	B_{eq}
Se1	0.0973(2)	0.9148(2)	0.28915(6)	4.45(4)
Se2	0.4266(2)	1.0840(2)	-0.33389(6)	4.82(4)
Ni	0.2612(2)	1.0059(2)	-0.02214(7)	2.95(3)
S1	0.2831(5)	1.1433(3)	0.0539(1)	3.41(8)
S2	0.1748(5)	0.8335(4)	0.0302(1)	3.94(9)
S3	0.3458(4)	1.1789(4)	-0.0757(1)	3.41(8)
S4	0.2387(5)	0.8641(4)	-0.0967(1)	3.41(8)
S5	0.2091(4)	1.0939(4)	0.1835(1)	3.47(8)
S6	0.1065(5)	0.8062(4)	0.1600(1)	3.51(8)
S7	0.4070(5)	1.1965(4)	-0.2064(1)	3.45(8)
S8	0.3067(4)	0.9091(4)	-0.2270(1)	3.19(8)
N	0.184(4)	1.000(3)	0.500(1)	8.8(8)
C1	0.219(1)	1.039(1)	0.1104(5)	2.8(3)
C2	0.171(1)	0.901(1)	0.0998(5)	2.7(3)
C3	0.347(1)	1.102(1)	-0.1449(5)	2.9(3)
C4	0.302(2)	0.967(1)	-0.1541(5)	2.6(3)
C5	0.138(1)	0.940(1)	0.940(1)	3.0(3)
C6	0.380(2)	1.062(1)	-0.2577(5)	3.5(3)
C8	0.104(5))	0.985(4)	0.447(2)	6.4(10)

$$B_{eq} = \frac{8}{3}\pi^2(U_{11}(aa^*)^2 + U_{22}(bb^*)^2 + U_{33}(cc^*)^2 + 2U_{12}aa^* \cdot bb^* \cdot cos\gamma + 2U_{13}aa^* \cdot bb^* \cdot cos\beta + 2U_{23}aa^* \cdot bb^* \cdot cos\alpha)$$

Table 3.8. Selected bond lengths (Å) and angles (degree) of **3**.

	distance / Å		distance / Å
Ni - S1	2.160(5)	S7 - C3	1.74(2)
Ni - S2	2.150(5)	S7 - C6	1.73(2)
Ni - S3	2.165(5)	S8 - C4	1.74(1)
Ni - S4	2.162(5)	S8 - C6	1.71(2)
S1 - C1	1.71(2)	Se1 - C5	1.79(1)
S2 - C2	1.69(1)	Se2 - C6	1.79(2)
S3 - C3	1.72(2)	C1 - C2	1.39(2)
S4 - C4	1.71(5)	C4 - C5	1.35(2)
S5 - C1	1.73(1)	N - C8	1.35(2)
S5 - C5	1.70(2)		
S6 - C2	1.73(1)		
S6 - C5	1.76(2)		

	angle / °		angle / °
S1 - Ni - S2	92.3(2)	S4 - C4 - C3	120(1)
S3 - Ni - S4	93.3(2)	S8 - C4 - C3	115(1)
Ni - S1 - C1	103.1(5)	S5 - C5 - C6	113.8(8)
Ni - S2 - C2	103.1(5)	S5 - C5 - Se1	124.6(10)
Ni - S3 - C3	101.1(6)	S6 - C5 - Se1	121.6(9)
Ni - S4 - C4	102.3(5)	S7 - C6 - S8	113.4(9)
S1 - C1 - C2	120(1)	S8 - C6 - Se2	122.0(9)
S5 - C1 - C2	115(1)	S8 - C6 - Se2	124.6(9)
S2 - C2 - C1	120(1)	C1 - S5 - C3	98.1(7)
S6 - C2 - C1	115(1)	C2 - S6 - C5	98.7(7)
S3 - C3 - C4	122(1)	C5 - S7 - C6	96.7(8)
S7 - C3 - C4	116(1)	C4 - S8 - C6	97.8(7)

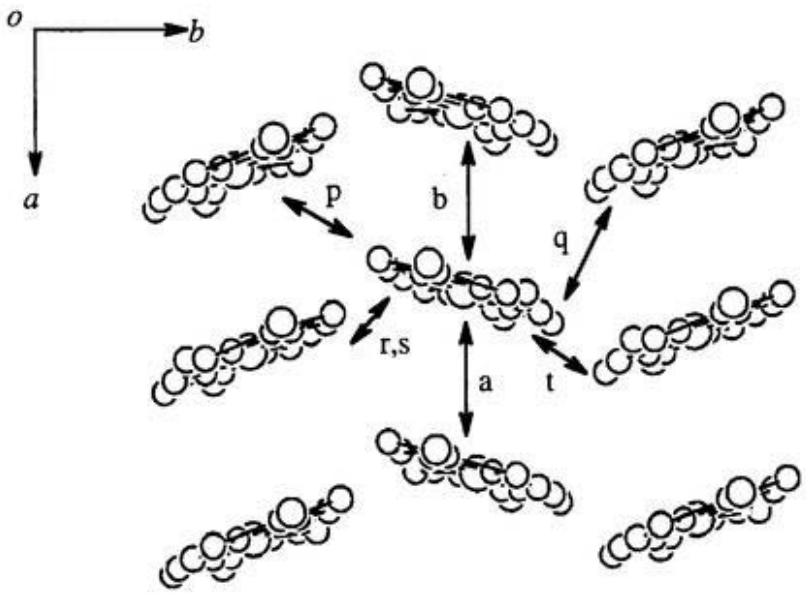

Fig.3.5. End-on projection of **3**: Arrows indicates the direction of the short intermolecular contacts between chalcogen atoms less than the sum of the van der Waals radii and their overlap integrals.

Table 3.9 Intermolecular chalcogen···chalcogen distances in **3** . a, b, q, r and s correspond to Fig.3.5.

	contact	symmetry operation[a]	distance / Å
a	Se1···Se2	$(-x+1, -y+2, -z)$	3.723(3)
	S1···S4	$(-x+1, -y+2, -z)$	3.733(7)
	S2···S3	$(-x+1, -y+2, -z)$	3.49(7)
b	Se1···S8	$(-x, -y+2, -z)$	3.722(5)
q	S7···S8	$(-x+1, y+1/2, -z-1/2)$	3.386(6)
r	Se2···S1	$(-x, -y+2\,1/2, -z-1/2)$	3.755(5)
	Se2···S5	$(-x, -y+2\,1/2, -z-1/2)$	3.529(5)
	S5···S7	$(-x, -y+2\,1/2, -z+1/2)$	3.476(6)
s	Se1···S8	$(x, -y-1\,1/2, z+1/2)$	3.511(5)
	Se1...S4	$(x, -y+1\,1/2, z+1/2)$	3.817(5)
	S6···S8	$(x, -y+1\,1/2, z+1/2)$	3.560(6)

[a] This applies on the second atom.

3.3.2 *Electrical resistivities*

Figure 3.6 shows the temperature dependence of the electrical resistivity of **1**. The conductivity was 100 S cm^{-1} around room temperature. Although the crystal quality was not sufficient, some crystals exhibited weakly metallic behavior even at ambient pressure. In the low temperature region, the resistivity gradually increased. The activation energy below 25 K was 0.055 eV. Such behavior is similar to that of $[(CH_3)_3HN][Ni(dmit)_2]_2$ [12]. However, unlike **1**, the resistivity behavior of $[(CH_3)_3HN][Ni(dmit)_2]_2$ was reported to be sample-dependent. Under high pressures, the metallic range extended down to ca. 150 K at 3 kbar and down to ca. 60 K at 6 kbar.

Figure 3.7 shows the temperature dependence of the electrical resistivity of **2**. The electrical conductivity of **2** was *ca.* 30 S cm^{-1} around room temperature. The resistivity was almost independent on the temperature in the high temperature region and increased gradually below 100 K. The activation energy around 60 K was 0.04 eV. The sluggish resistivity increase may be related to the insufficient quality of the crystal.

The conductivity of **3** was 4.5 S cm^{-1} around the room temperature. The temperature dependence of electrical resistivity is semiconductive in the whole temperature range (Fig.3.8). The activation energy was 0.072 eV.

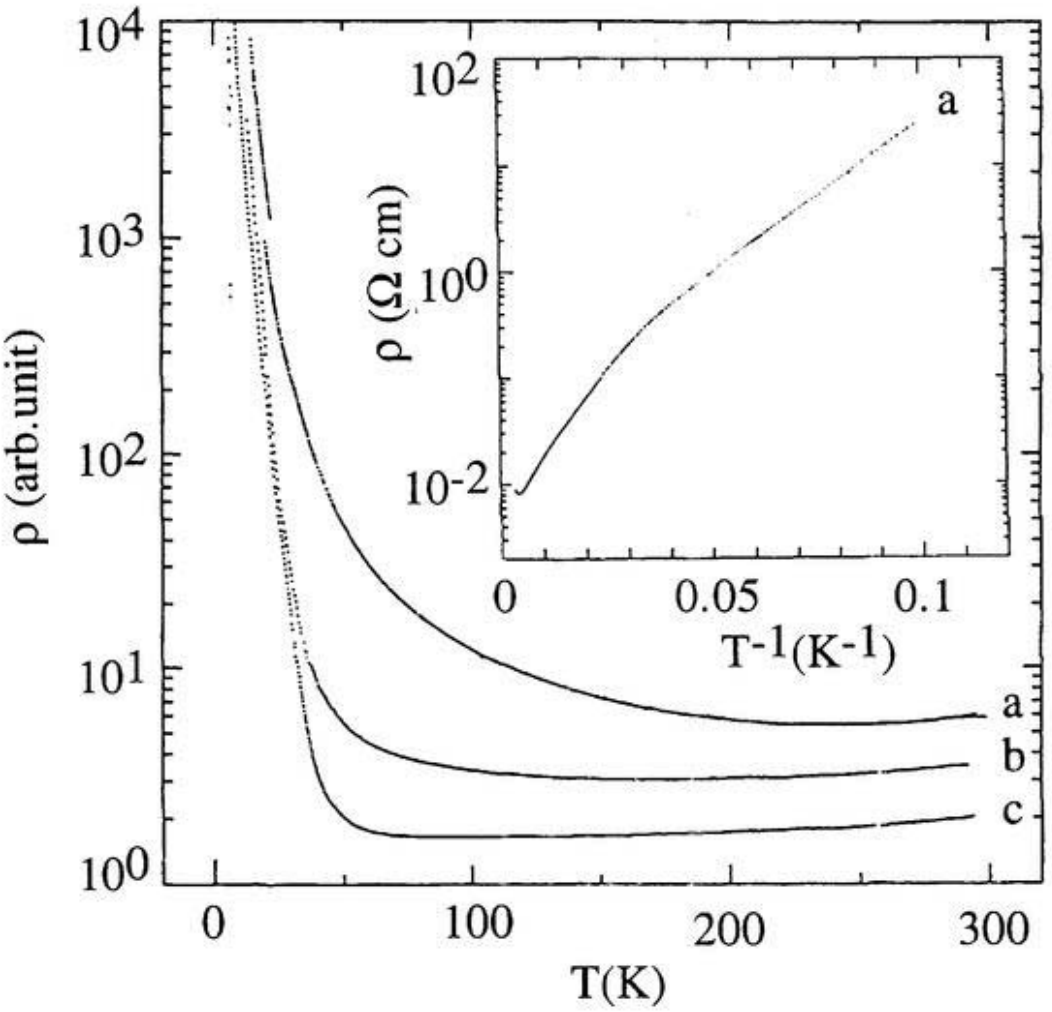

Fig.3.6. Temperature dependence of electrical resistivities of **1**: (a) at ambient pressure, (b) at 3 kbar and (c) at 6 kbar. The conductivity was about 100 S cm^{-1} at room temperature and ambient pressure. The activation energy below 25 K was 0.055 eV.

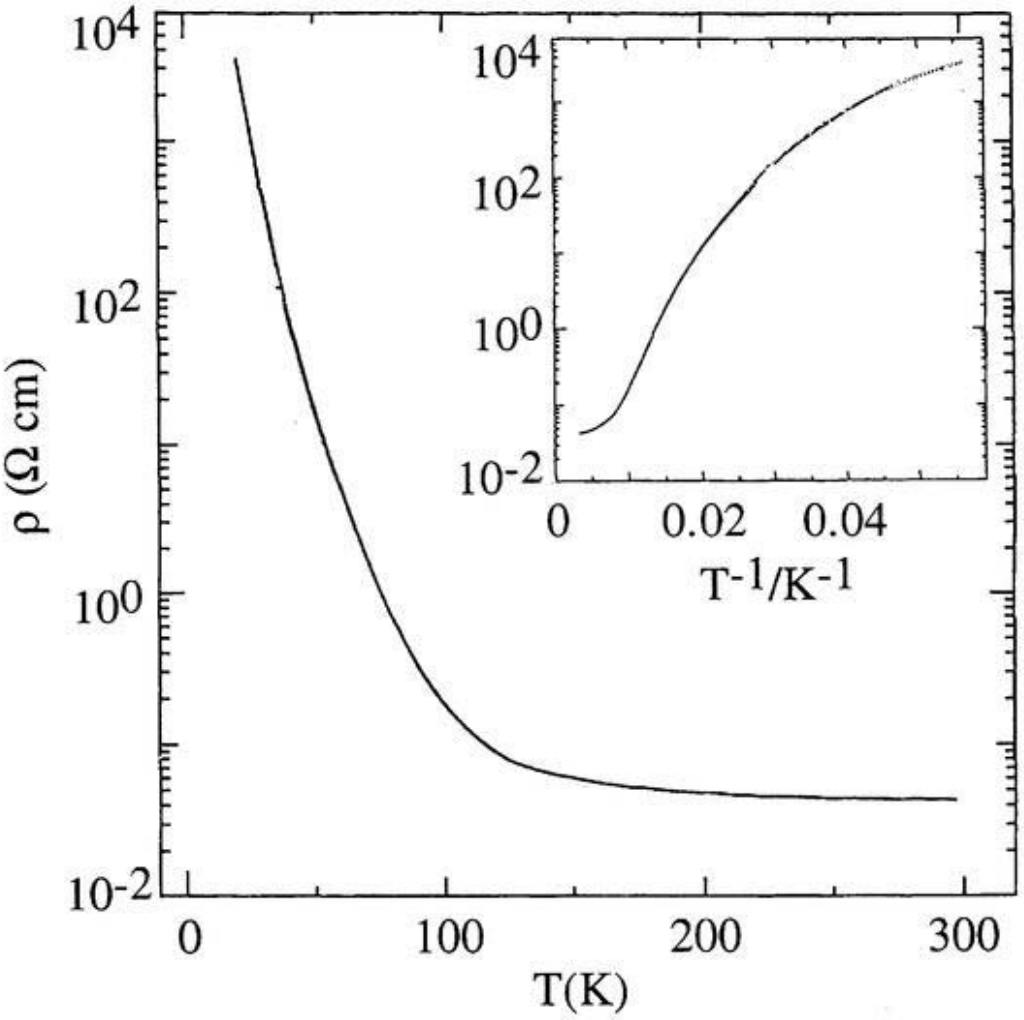

Fig.3.7. Temperature dependence of electrical resistivity of **2** at ambient pressure. Conductivity was about 30 S cm^{-1} at room temperature. The activation energy in the range of 54- 61 K was 0.04 eV.

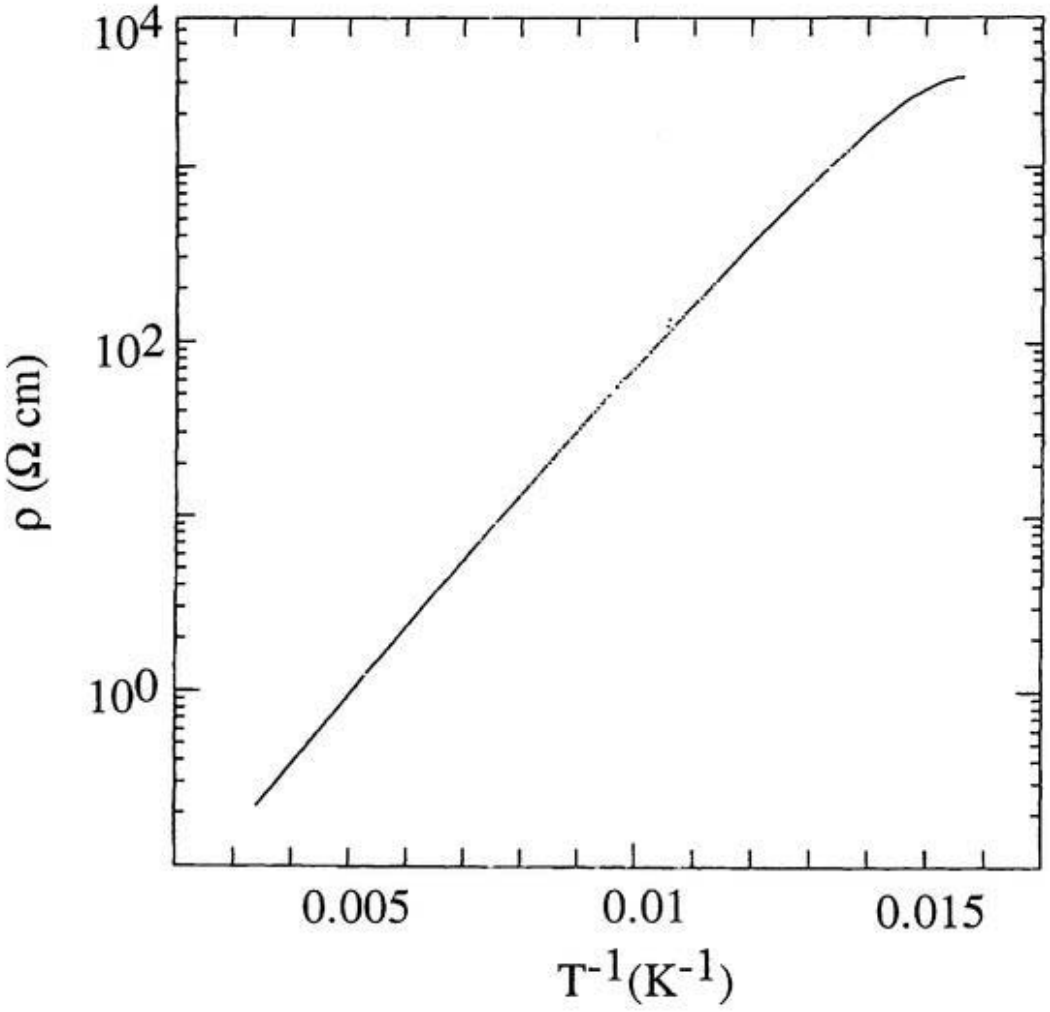

Fig.3.8. Temperature dependence of electrical resistivity of **3**. Conductivity was about 4.5 S cm^{-1} at room temperature and at ambient pressure. The activation energy was 0.072 eV.

3.3.3 Band structures

Because the $Ni(dmise)_2$ molecules were stacked without dimerizing in the crystals of **1** and **2**, it is considered that the HOMO-LUMO inversion will not occur in these systems. The tight-binding band structure calculations were performed by the simple extended Hückel method using the LUMO of $Ni(dmise)_2$. The overlap integrals are given in Table 3.10. Since $|a|$ and $|b|$ take similar values, the $Ni(dmise)_2$ stack can be regarded as regular stack from the viewpoint of electronic band structure. The overlap integrals q in **1** and r in **2** have large values. This suggests that these salts have stronger transverse interactions compared with $M(dmit)_2$ compounds having similar arrangements. In addition, the overlap integrals of the molecules across the cation layer have fairly large value ($2.0 - 3.0 \times 10^{-3}$) in **1** and **2**. This is in striking contrast to the case of α-$[(CH_3)_4N][Ni(dmise)_2]_2$, which has small overlap integrals along the direction of the long axis of the molecule [8].

Figure.3.9 shows the calculated Fermi surfaces of the two compounds. The cross sections of Fermi surfaces in the a^*b^* and b^*c^* planes showed closed Fermi surfaces. Since the Fermi surfaces gave closed cross sections in two different directions, these two $Ni(dmise)_2$ conductors can be regarded as essentially three-dimensional conductors. The weak metallic nature of these systems should be related to the relatively small overlap integrals (transfer integrals) of LUMO's. The low crystal quality and the positional disorder in the cation layers are also undesirable for the enhancement of the metallic nature of the system. In addition, the low-temperature semiconductive properties may not be intrinsic nature for these $Ni(dmise)_2$ salts. Anyway, the result of the band structure calculations clearly shows a way to design the stable three-dimensional molecular metal composed of planar π-molecules.

Table 3.10. Intermolecular overlap integrals ($\times 10^3$) of $Ni(dmise)_2$ in **1-3**. a, b, p, q, r, s and t correspond to those in Figures 3.3 and 3.5, respectively.

	1	**2**	**3**
a	12.7	-14.9	-21.4
b	-14.0	13.4	7.11
p	0.2	0.2	0.25
q	-4.9	1.3	0.25
r	1.3	-6.5	0.24
s	3.0	2.0	0.24
t	0.7	2.9	0.34

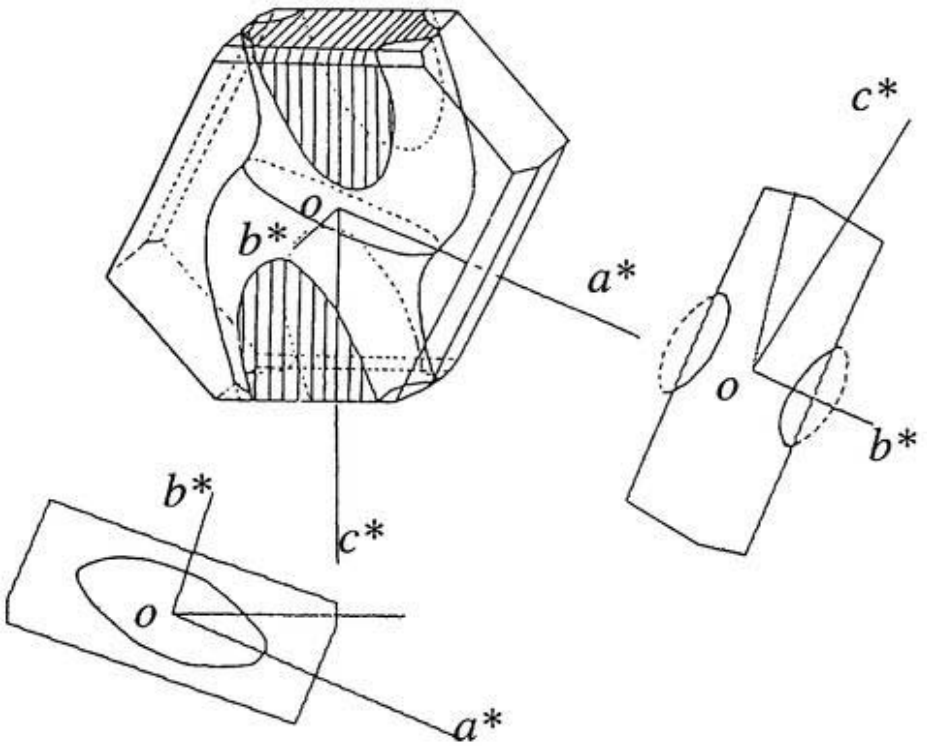

(a)

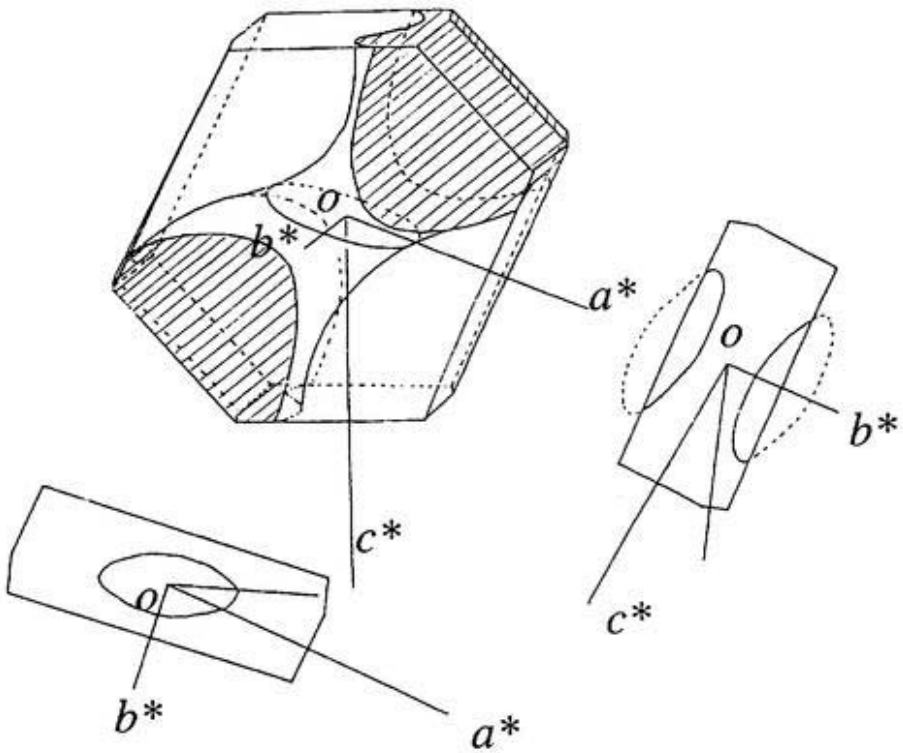

(b)

Fig.3.9. Calculated Fermi surfaces of (a) **1** and (b) **2**.

3.4 *Cs[Pd(dmise)$_2$]$_2$*

Because of the poor quality of the crystal of **4**, a complete crystal structure determination was not successful. Composition of the cation and the anion was determined by EPMA (electron probe microanalysis). The X-ray oscillation photographs showed that the shortest lattice constants was about 4 Å. The weak diffuse streaks were also observed between the layer of main Bragg spots. This lattice constant suggested that the crystal was not isostructural to Cs[Pd(dmit)$_2$]$_2$ (Cs[Pd(dmit)$_2$]$_2$; monoclinic, C2/c, a= 14.490(4) Å, b= 6.2629(14) Å, c= 30.601(7) Å, β= 90.58(2) °, V= 2777.02 Å^3, Z= 4) [13]. The resistivity decreased slowly with decreasing temperature down to 4.2 K. The weak temperature dependence may be related to the poor quality of the crystals (see Fig.3.11).

Anyway, **4** is the first example of a M(dmise)$_2$ compound which has metallic conductivity down to 4 K. The trials of the preparation of the single crystals of sodium and potassium salts have not been successful. However, considering the fact that among the M(dmit)$_2$ conductors extensively studied so far, there are only a few systems having stable metallic state down to low temperature, the stable metallic state of **4** will be interesting. In the case of M(dmit)$_2$ conductors, all the compounds with stable metallic state have the characteristic molecular arrangements called "spanning overlap mode". But the lattice constant of 4 Å of **4** indicates that M(dmise)$_2$ conductors can have stable metallic states even in the different molecular arrangements (probably the molecules are arranged regularly with the periodic unit of 4 Å). Although the dimensionality of the metallic state of **4** could not be analyzed, the stable metallic state suggests two- or three-dimensional nature of the system. Since the size of the Cs^+ ions is much smaller than that of $(CH_3)_xH_{4-x}N^+$ cations, the selone···selone contacts will be much closer. A good single crystal of (alkali metal)[M(dmise)$_2$]$_2$ may realize a possibility of stable molecular metal system with three-dimensional Fermi surface at low temperature.

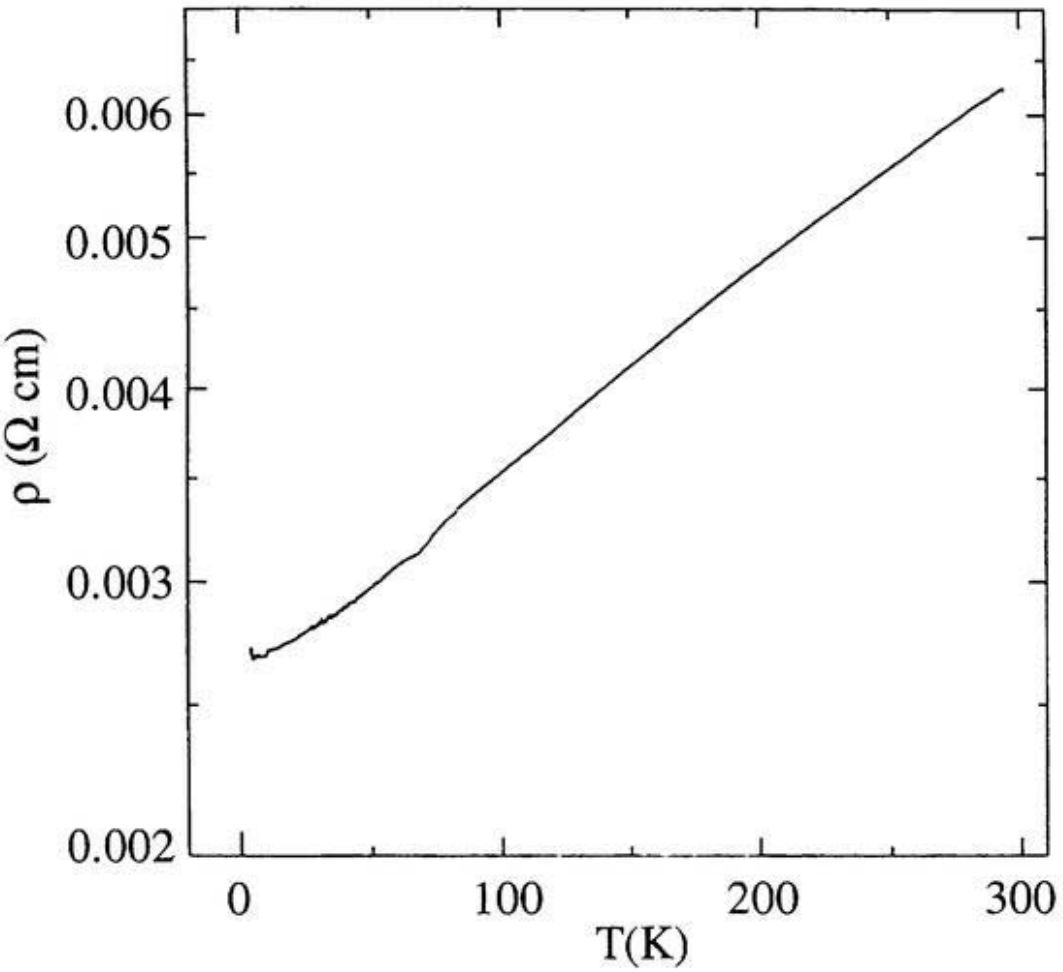

Fig.3.10. Temperature dependence of electrical resistivity of **4**.

3.5 *(N,N-dimethylpiperidinium)[Ni(dmise)$_2$]$_2$*

3.5.1 Crystal structure

The numbering scheme of Ni(dmise)$_2$ and crystal structure of (N,N-dimethylpiperidinium)[Ni(dmise)2]2 (**5**) are shown in Fig.3.11. The crystal belonged to the monoclinic system and the space group is C2/c. The atomic coordinates are listed in Table 3.11. The unit cell of **5** contains eight Ni(dmise)$_2$ molecules and four N,N-dimethylpiperidinium cations. One Ni(dmise)$_2$ molecule is crystallographically independent and the N,N-dimethylpiperidinium cations are heavily disordered on a 2-fold axis. In Fig.3.11(b), two plausible positions of the disordered six-membered ring of the N,N-dimethylpiperidinium cations are presented, which were founded out though the difference syntheses and refined isotropically. Some electronic density peaks were remained around the cation site, but it was impossible that these peaks were assigned to the two methyl groups.

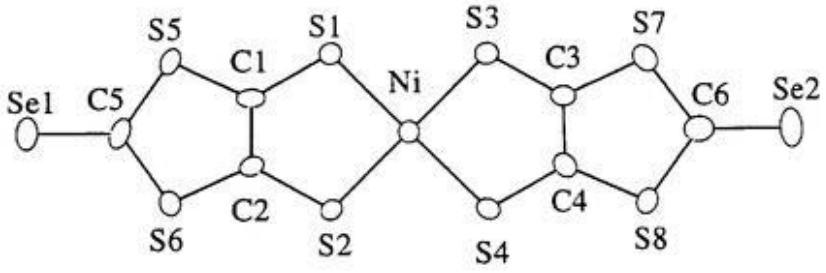

(a)

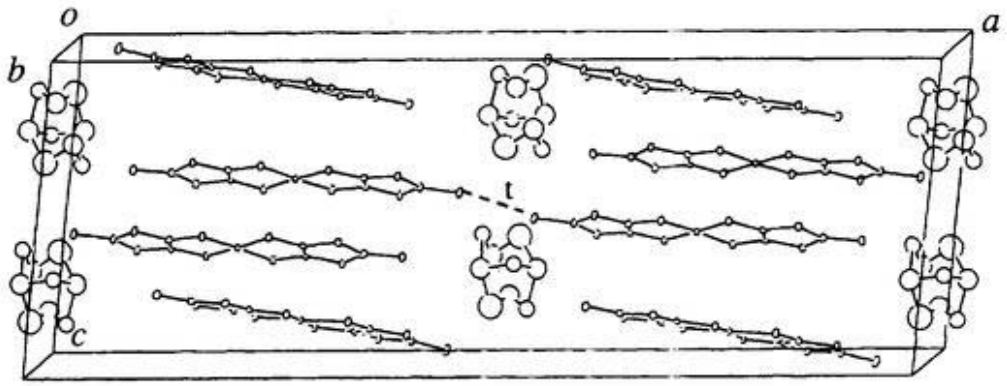

(b)

Fig.3.11. (a) Numbering scheme of Ni(dmise)$_2$ and (b) crystal structure of **5**. The cations are heavily disordered. Two plausible positions of the disordered six-membered rings of cations are presented. Se···Se distance (t) is 3.48 Å.

Table 3.11. Atomic coordinates of **5**.

Atom	*x*	*y*	*z*	B_{eq}
Se1	0.89388(8)	-0.1173(6)	0.6703(2)	5.30(9)
Se2	0.54279(8)	0.4800(5)	0.5424(2)	5.39(9)
Ni	0.71868(8)	0.1835(5)	0.6144(2)	2.43(7)
S1	0.7653(2)	0.3534(1)	0.6405(5)	3.1(2)
S2	0.7443(2)	-0.106(1)	0.6068(5)	3.2(2)
S3	0.6930(2)	0.4751(9)	0.6148(5)	2.8(2)
S4	0.6720(2)	0.011(1)	0.5930(5)	3.5(2)
S5	0.8379(2)	0.210(1)	0.6635(5)	3.4(2)
S6	0.8184(2)	-0.213(1)	0.6337(5)	3.9(2)
S7	0.6181(2)	0.578(1)	0.5871(5)	3.5(2)
S8	0.5995(2)	0.155(1)	0.5631(5)	4.1(2)
N11	0.5000	0.249(9)	0.2500	14(2)
C1	0.7955(6)	0.166(4)	0.643(2)	2.8(1)
C2	0.7855(6)	-0.040(3)	0.630(2)	2.4(6)
C3	0.6507(6)	0.405(4)	0.596(2)	2.5(6)
C4	0.6413(6)	0.202(4)	0.586(2)	2.9(6)
C5	0.8520(7)	-0.044(4)	0.656(2)	3.5(7)
C6	0.5855(6)	0.407(4)	0.565(2)	4.1(7)
C12	0.513(4)	0.00(2)	0.141(8)	37(5)
C13	0.488(3)	-0.16(1)	0.184(6)	25(3)
C14	0.472(2)	-0.02(1)	0.132(4)	15(1)
C15	0.453(2)	0.14(1)	0.206(6)	16(2)
C16	0.469(3)	0.09(2)	0.248(9)	23(4)

$$B_{eq} = \frac{8}{3}\pi^2(U_{11}(aa^*)^2 + U_{22}(bb^*)^2 + U_{33}(cc^*)^2 + 2U_{12}aa^* \cdot bb^* \cdot cos\gamma + 2U_{13}aa^* \cdot bb^* \cdot cos\beta + 2U_{23}aa^* \cdot bb^* \cdot cos\alpha)$$

Intramolecular distances and angles of the $Ni(dmise)_2$ molecule are shown in Table 3.12. The $Ni(dmise)_2$ molecules are arranged in two types of crystallographically independent overlap modes without forming usual column structure. These overlap-modes are shown in Figs.3.12(b-c), which are denoted as mode-I and -II. In the mode-I, one $Ni(dmise)_2$ molecule (B') overlaps the two adjacent molecules (A and A'), where the angle of molecules $\angle$ A-B'-A' is 33.1° (Fig. 3.12(a)). This mode (mode-I) which is the so-called "spanning overlap mode" was also found in three dmit conductors, α- and γ-$[(CH_3)_2(C_2H_5)_2N][Ni(dmit)_2]_2$ and (N,N-dimethylpiperidinium)$[Ni(dmit)_2]_2$ [14-16]. This overlap mode intensified the transverse interaction in the $M(dmit)_2$ or $M(dmise)_2$ system, because the intercolumner interaction appears through the bridging molecule. In fact, α- and γ-$[(CH_3)_2(C_2H_5)_2N][Ni(dmit)_2]_2$ and (N,N-dimethylpiperidinium)$[Ni(dmit)_2]_2$ are the stable metallic conductors with two dimensional Fermi surfaces [15-17]. On the other hand, in the mode-II, $Ni(dmise)_2$ molecules usually stack in parallel with each other. The intermolecular distance is 3.505 Å and the slip distances in the molecular overlap are 1.793 Å and 2.037 Å toward the transverse and the long molecular axis direction in the mode-II [Fig.3.12(b)]. The dihedral angles are 10.4° and 0° in the modes of A and B, respectively (Fig.3.13). End-on projection of the molecular arrangement and the intermolecular short contacts are given in Fig. 3.14 and its caption. In addition to the short contacts on the bc plane, there is a short intermolecular distance of 3.48 Å between the two terminal selone groups [Fig. 3.12(a)].

Table 3.12 Selected bond lengths (Å) and angles (degree) of $Ni(dmise)_2$ molecule in **5**.

	distance / Å		distance / Å
Ni - S1	2.168(6)	S7 - C3	1.71(2)
Ni - S2	2.149(6)	S7 - C6	1.71(3)
Ni - S3	2.159(6)	S8 - C4	1.69(3)
Ni - S4	2.167(6)	S8 - C6	1.73(3)
S1 - C1	1.72(2)	Se1 - C5	1.73(3)
S2 - C2	1.70(3)	Se2 - C6	1.76(3)
S4 - C4	1.74(3)	C1 - C2	1.40(3)
S3 - C3	1.74(2)	C3 - C4	1.37(3)
S5 - C1	1.71(3)		
S5 - C5	1.75(2)		
S6 - C2	1.73(2)		
S6 - C5	1.73(3)		
	angle / °		**angle / °**
S1 - Ni - S2	92.9(2)	S4 - C4 - C3	119(2)
S3 - Ni - S4	92.8(2)	S7 - C3 - C4	115(2)
Ni - S1 - C1	104.0(7)	S3 - C3 - C4	120(2)
Ni - S2 - C2	103.4(7)	S8 - C3 - C4	116(2)
Ni - S3 - C3	103.0(7)	S7 - C6 - S8	111(1)
Ni - S4 - C4	101.8(7)	S7 - C6 - Se2	124(1)
S1 - C1 - C2	119(2)	S8 - C6 - Se2	123(1)
S5 - C1 - C2	115(1)	C1 - S5 - C5	99(1)
S2 - C2 - C1	121(1)	C2 - S6 - C5	99(1)
S6 - C2 - C1	114(1)	C3 - S7 - C6	98(1)
S3 - C3 - S4	120(2)	C4 - S8 - C6	98(1)
S5 - C5 - Se1	124(1)		
S6 - C5 - Se1	124(1)		

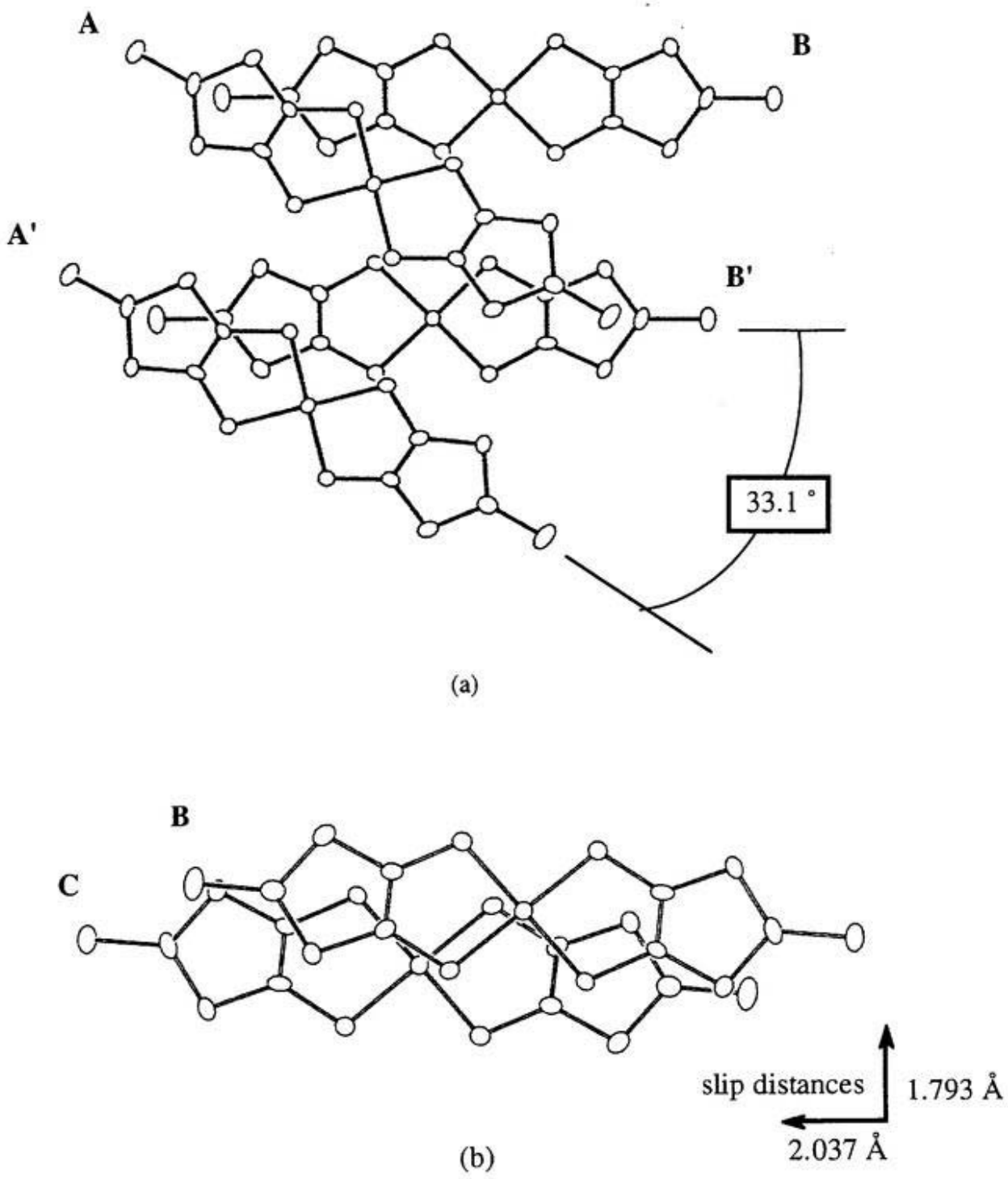

Fig.3.12. Two overlapping modes for the Ni(dmise)$_2$ molecules of **5** : (a) mode-I (spanning overlap mode) (b) mode-II.

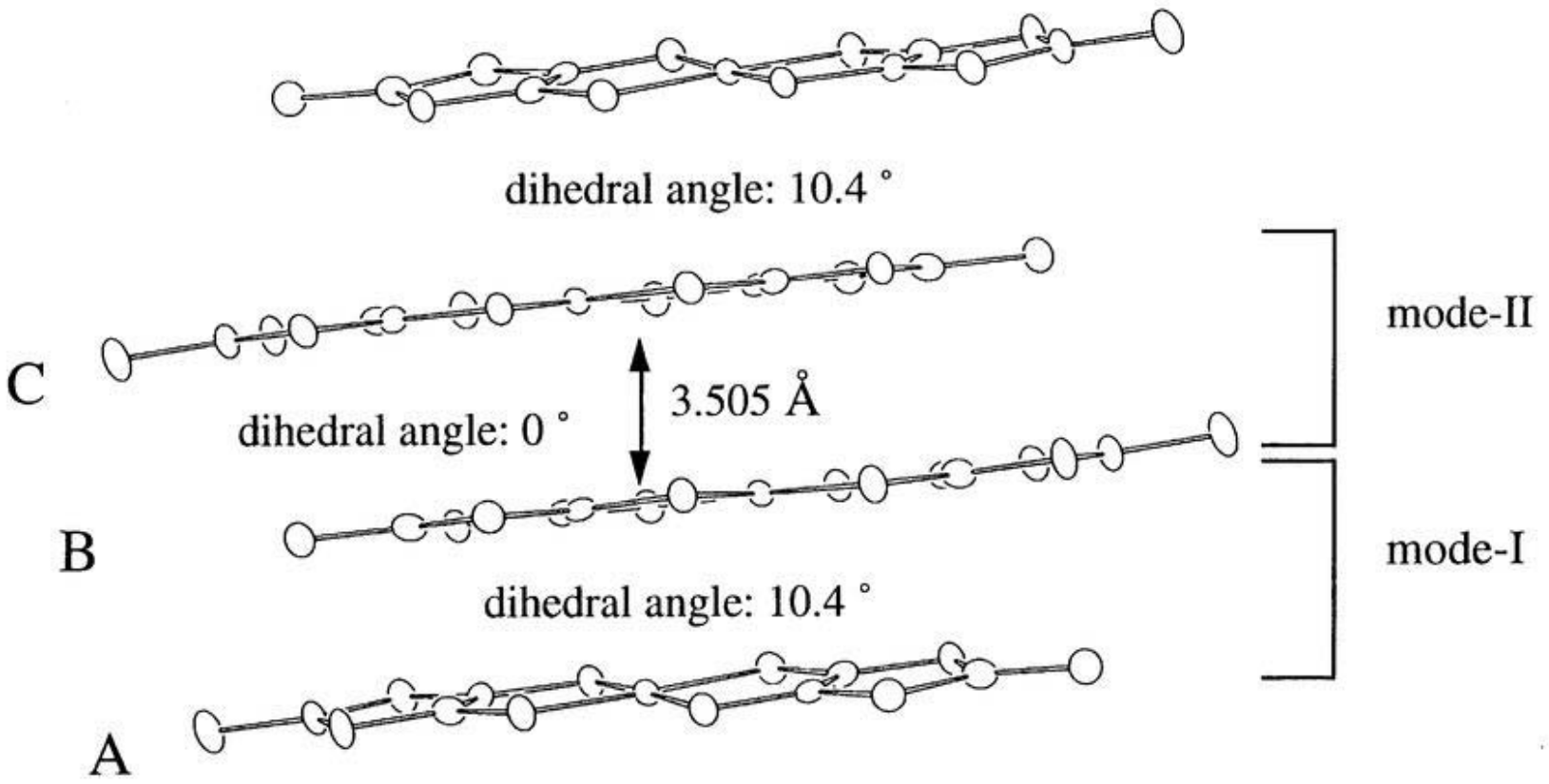

Fig.3.13. $Ni(dmise)_2$ stacking modes of **5**. The mode -I and -II mean two types of the overlap modes.

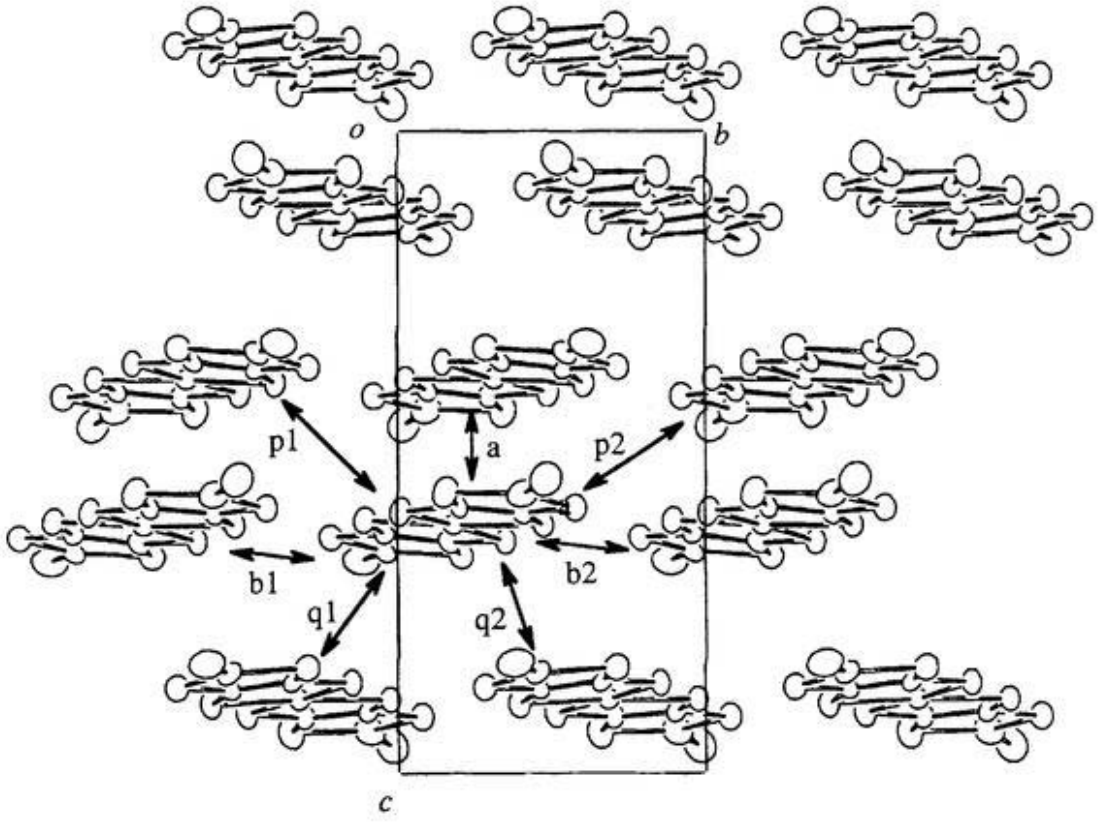

Fig.3.14. End-on projection of **5**. Short contacts between chalcogen atoms: (a) Se1...S7 3.568(7) Å (b1) S4···S7 3.54(1) Å, S2···S3 3.425(9) Å; (b2) S1···S6 3.54(1) Å, S1···S2 3.628(9) Å, S3···S4 3.583(9) Å; (p1) S2···S2 3.60(1) Å; (q1) Se1···Se7 3.698(8) Å; (q2) 3.606(9) Å.

3.5.2 *Electrical resistivity*

The conductivity of **5** is *ca.* 70 Scm^{-1} at the room temperature. As shown in Fig.3.15, the temperature dependence of the electrical resistivity of **5** shows that the metallic state continues down to 2 K. **5** is the first stable metallic $M(dmise)_2$ salt whose crystal structure has been determined. The conductivity at 2 K is 70 times larger than that of the room temperature. A large decrease in the electrical resistivity is also observed in three $Ni(dmit)_2$ conductor with the "spanning overlap mode" which stabilizes the metallic electronic state. A kink is observed at 250 K on the temperature dependence of the electrical resistivity.

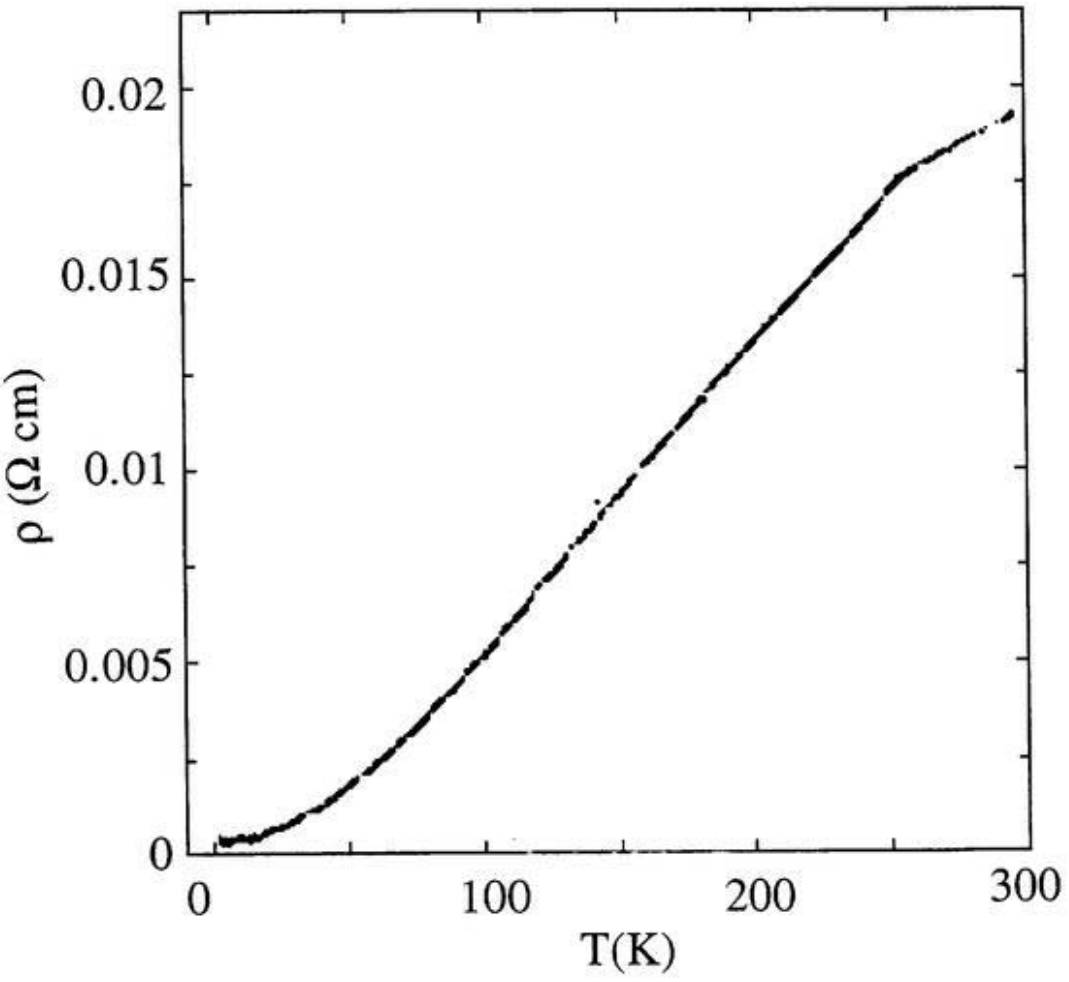

Fig3.15. Temperature dependence of the electrical resistivity of **5**.

3.5.3 X-ray oscillation photographs and temperature dependence of the lattice constants

X-ray oscillation photographs and the temperature dependence of the lattice constants of **5** were examined in order to obtain some information on the resistivity anomaly at 250 K. X-ray oscillation photographs of the *bc* plane down to 7 K are shown in Fig.3.16. Extra reflection spots are appeared below 250 K along the *b*-axis which is the molecular transverse direction. In this temperature region, the resistivity shows anomaly and crystal structure changes into a five-folded superstructure. Since the metallic conductivity is not affected so seriously by the appearance of superstructure, it is suggested that this structural change in the arrangement of $Ni(dmise)_2$ molecular forming the conduction paths is not large. This $Ni(dmit)_2$ analog, (N,N-dimethylpiperidinium)$[Ni(dmit)_2]_2$ which also has the same structural transition in the same temperature region, was reported that the structural transition originated the order-disorder transition of the counter cations [17].

No anomaly was observed on the temperature dependence of the lattice constants except for the appearance the five-folded superstructure (see Fig.3.18). Temperature dependence of the *a*-axis was independent on the temperature, and those of the *b*- and *c*- axes were shortened linearly down to 7 K with the thermal expansion coefficients of 3.3×10^{-5} K^{-1} and 8.1×10^{-5} K^{-1} respectively.

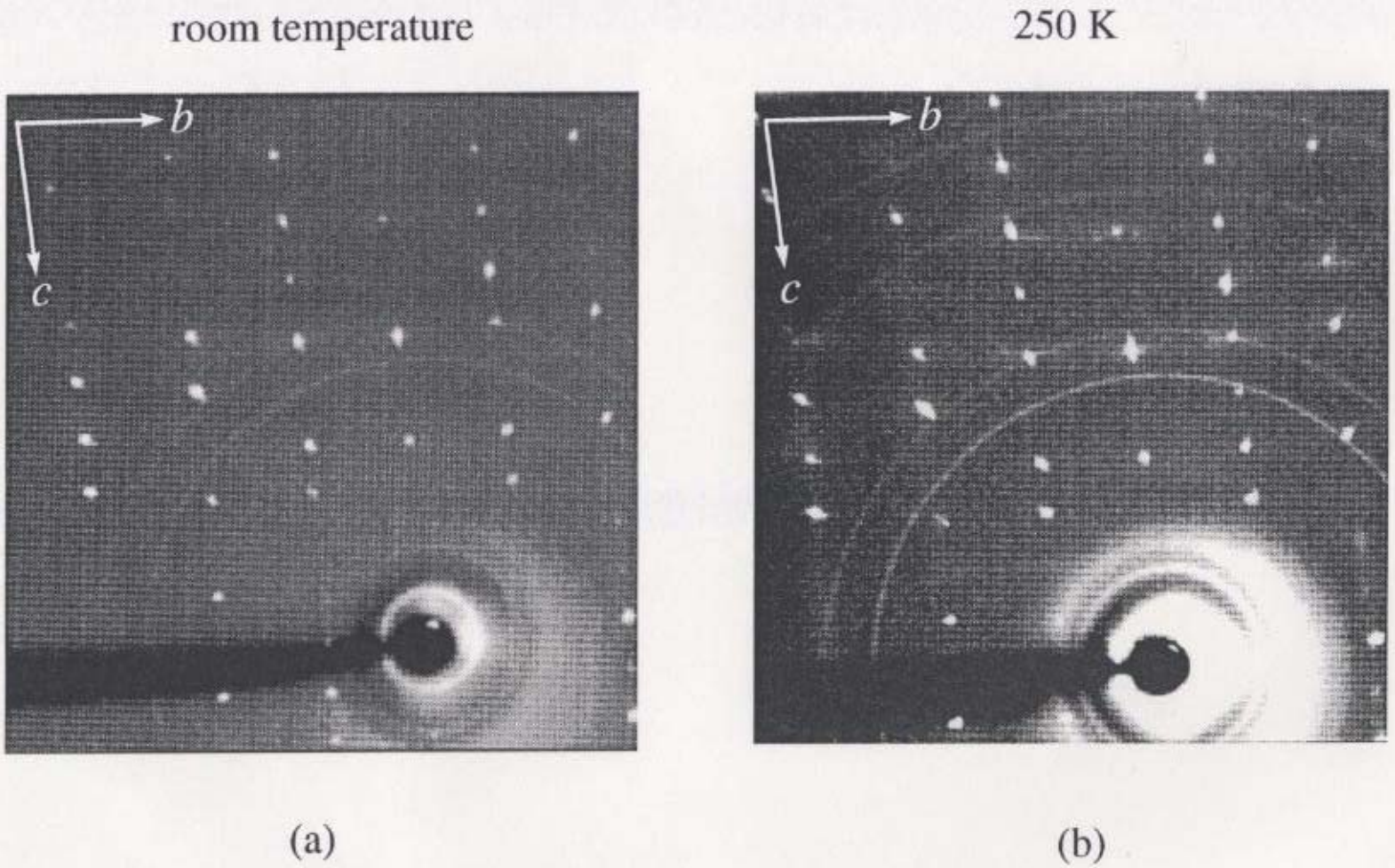

Fig. 3.16. X-ray oscillation photographs of **5** at (a) room temperature, (b) 250 K, (c) 100 K and (d) 7 K.

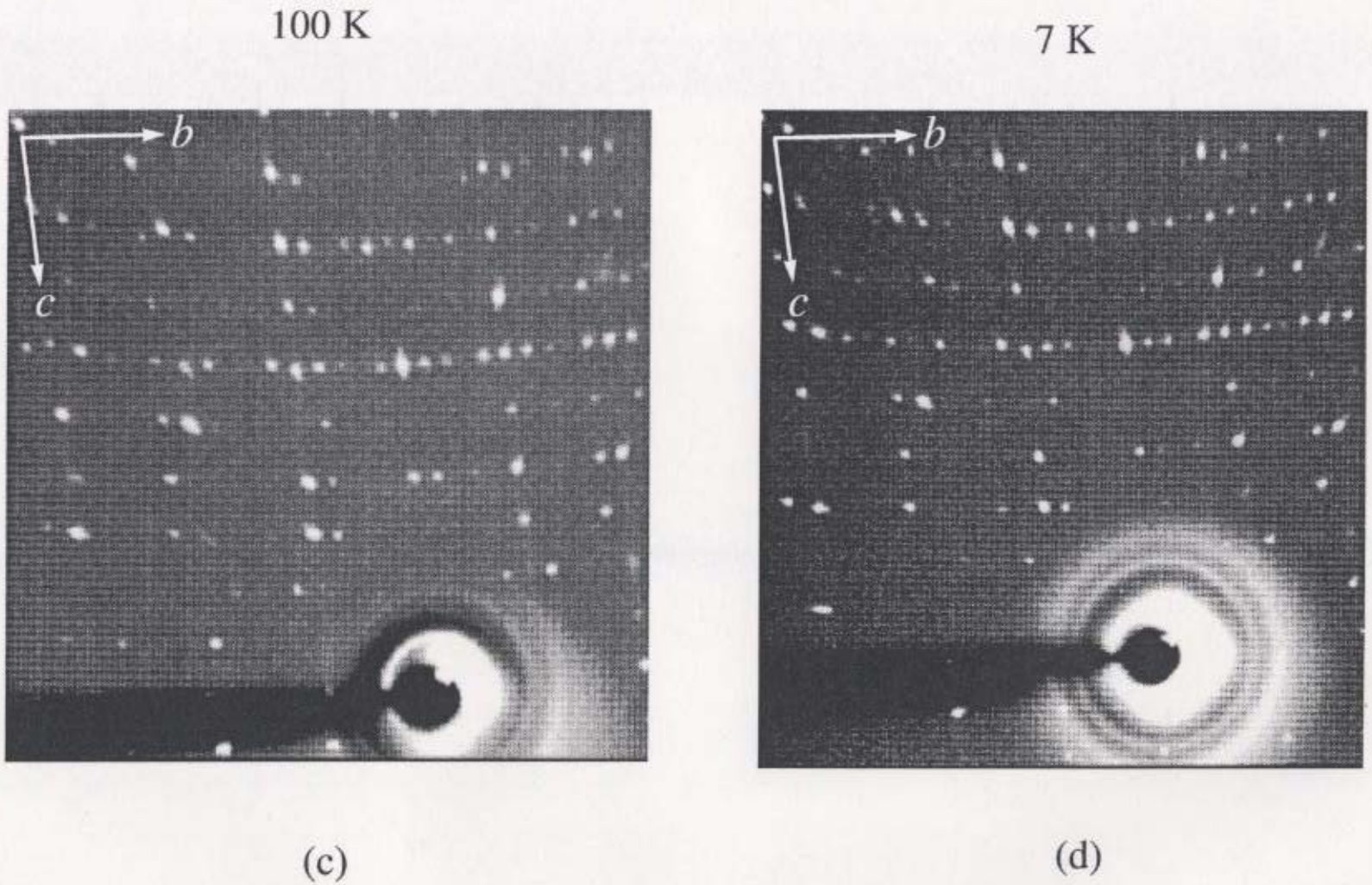

Fig. 3.16. X-ray oscillation photographs of **5** at (a) romm temperature, (b) 250 K, (c) 100 K and (d) 7 K. (continued)

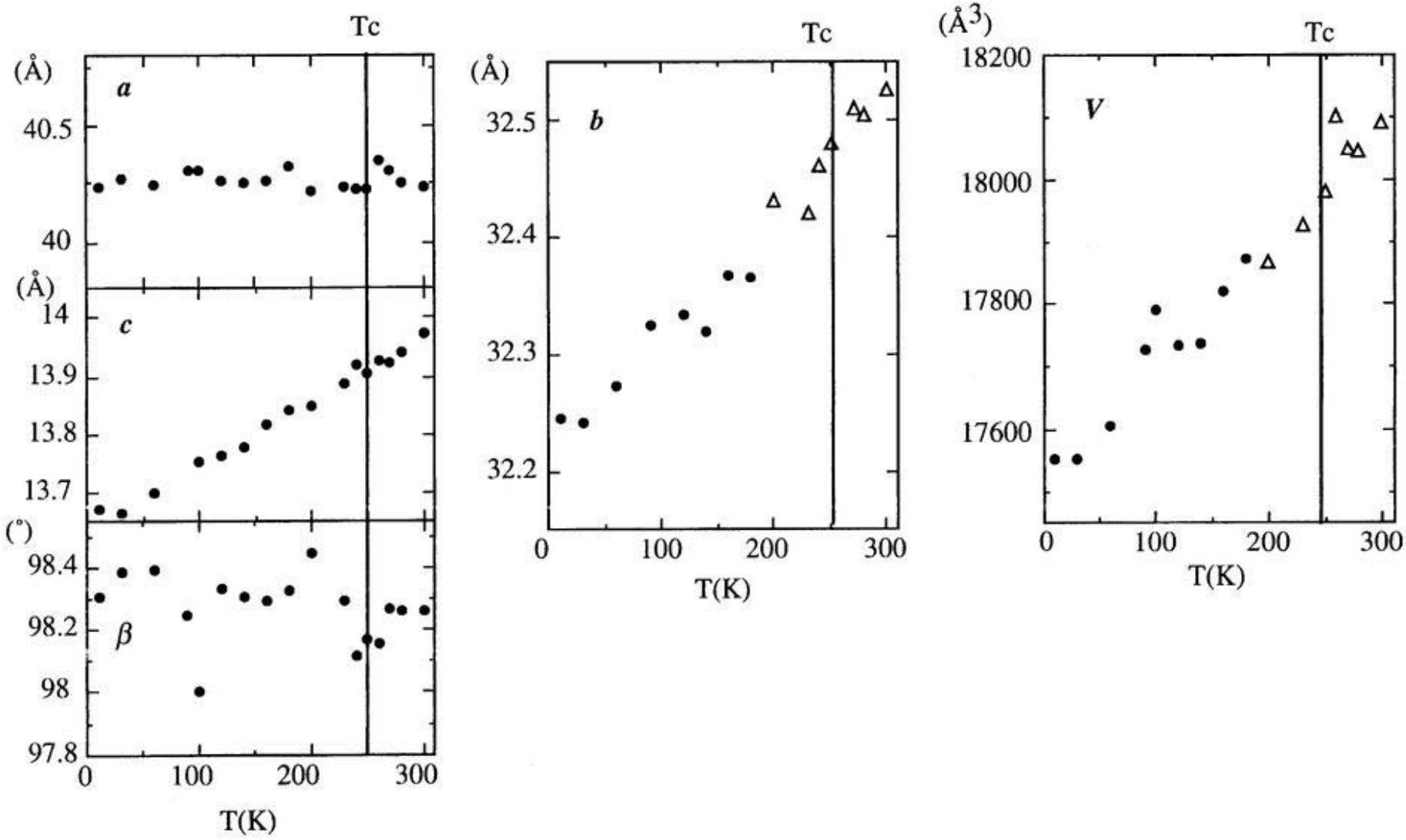

Fig. 3.17 . Temperature dependence of the lattice constants for 5. ●marks mean raw data and △marks mean the values converted raw data to 5-folded perioddic lattice constants.

3.5.4 *Magnetic susceptibility*

Temperature dependence of the magnetic susceptibility was shown in Fig.3.18. The diamagnetic core distributions were calculated according to Pascal's law [18]. In contrast to the resistivity, the susceptibility showed no distinct anomaly at 250 K. Since the observed paramagnetic susceptibility was unexpectedly large (χ_{RT}= 8.4 × 10^{-4} emu/mol), the susceptibility measurement was carried out on the different sample. The essentially the same results were obtained. The magnitude of the susceptibility at room temperature corresponds to 70 % of the paramagnetic susceptibility due to the localized S=1/2 spins. The susceptibility takes a broad maximum around 200 K, which is reminiscent of the Bonner-Fisher behavior of one-dimensional Heisenberg chain. Fitting of the experimental results by the one-dimensional Heisenberg model of S=1/2 was examined according to the following equation [19]:

$$\chi_M = \left(\frac{Ng^2\mu_B 2}{k_B T}\right) \Big/ \left(\frac{A + Bx + Cx^2}{1 + Dx + Ex^2 + Fx^3}\right) \qquad \cdots\cdots\cdots\cdots (1)$$

where $x = \frac{|J|}{k_B T}$

A = 0.25, B = 0.14995, C = 0.30094, D = 1.9862, E = 0.68854, F = 6.0626.

The term of $[(Ng^2\mu_B{}^2) / k_B]$ is calculated to be 1.500 erg G^{-1} mol^{-1}, where g is assumed to be 2.00. When the equation 1 is fitted to the result of susceptibility, $[(Ng^2\mu_B{}^2) / k_B]$ = 1.86~1.95 erg G^{-1} mol^{-1} was obtained. The $|J|$ value was ~150 K. This result indicates that the 120-130 % of spins are localized on each $Ni(dmise)_2$ dimer. Above calculation indicates that the electronic property of this system is inconsistent with the simple metal model, where the temperature independent Pauli-like susceptibility behavior is expected. It might be possible that the localized spins and π conduction electrons coexist in this system. Similar susceptibility behavior has been also observed in the $M(dmit)_2$ analogs such as α-$[(CH_3)_2(C_2H_5)_2N][Ni(dmit)_2]_2$ and (N,N-dimethylpiperidinium)$[Ni(dmit)_2]_2$. There must be a common origin for these unusual electronic properties of $Ni(dmiX)_2$ conductor (X= t and se) with the spanning overlap molecular arrangement. It might be imagined that unique π-d electron systems are realized in these complexes with stable metallic states.

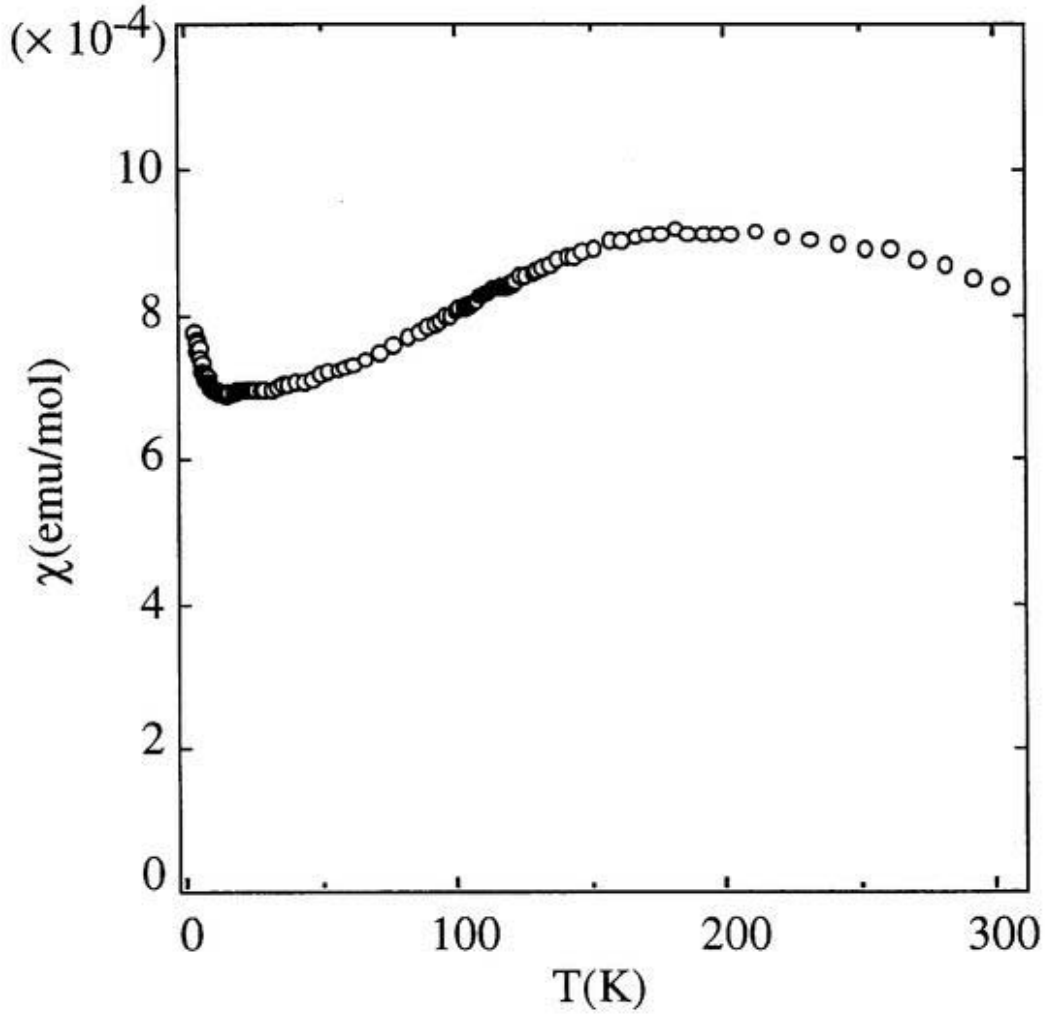

Fig.3.18. Temperature dependence of the magnetic susceptibility of **5**. Magnetic susceptibility was corrected by subtracting the calculated diamagnetic contribution.

3.6 *Summary*

Some new $M(dmise)_2$ conductors were synthesized and their electrical conductivities were studied.

1 exhibited weak-metallic behavior around room temperature. The tight-binding band structure calculation suggested that **1** and **2** had three-dimensional Fermi surfaces. The intermolecular interactions between the selenium atoms in the selone group should be very effective to extend the dimensionality of $M(dmise)_2$ systems.

4 kept metallic behavior down to 4 K at ambient pressure for the first time among the $M(dmise)_2$ conductors.

5 was the first $M(dmise)_2$ complex with stable metallic state down to 2 K, whose crystal structure had been determined. The electrical resistibity showed anomaly around 250 K. Below 250 K, crystal structure changed into a five-folded superstructure along the *b*-axis which was the molecular transverse direction. The magnetic susceptibility had a maximum of 9.2×10^{-4} emu mol^{-1} around 200 K.

References

[1] P. Cassoux, L. Valade, H. Kobayashi, A. Kobayashi, R.A. Clark , A. E. Underhill, *Coord. Chem. Rev.*, **110**, 115 (1991).

[2] L. Brossard, M. Ribault, L. Valade, P. Cassoux, *Physica B & C (Amsterdam)*, ***143***, 378 (1986).

[3] R. Kato, T. Mori, A. Kobayashi, Y. Sasaki, H. Kobayashi, *Chem. Lett.*, **1988**, 865.

[4] V.Y. Khodorkozskii, J. Kreicberga, K.A. Balodis, O.Y. Neiland, *Izv. Akad. Nauk Latv. SSR, Ser. Khim., 1988*, 120.

[5] H. Kobayashi, R. Kato, A. Kobayashi, *Synth. Met.*, **42**, 2495 (1991).

[6] B. Olk, R-M. Olk, J. Sieler, E. Hoyer, *Synth. Met.*, **42**, 2585 (1991).

[7] J.P. Cornelissen, D. Reefman, G. Haasnoot, A.L. Spek, J. Reedijik, *Reel Trav. Chim. Pays-Bas.*, **110**, 345 (1991).

[8] J. P. Cornelissen, B. Pomarde, A.L. Spek, D. Reefman, J.G. Haasnoot, J. Reedijk, *Inorg. Chem.*, **32**, 3720 (1993).

[9] (a) T. Naito, A. Sato, K. Kawano, A. Tateno, H. Kobayashi, A. Kobayashi, *J. Chem.. Soc., Chem. Commun.*, **1995**, 351. (b) T. Naito, *Doctor thesis*, 154 (1995).

[10] Crystal Structure Analysis Package, Molecular Structure Corporation, **1985 & 1992**.

[11] Sakurai, T. ; Kobayashi, K.; *Rep. Inst. Phys. Chem. Res.*, **55,** 69.(1979).

[12] (a) B. Pomarede, B. Garreau, I. Malfant, L. Valade, P. Cassoux, J.P. Legros, A. Audouard, L. Brossard, J.P. Ulmet, M.L. Doublet , E. Canadel, *Inorg. Chem.*, **74**, 91 (1991). (b) J.P. Ulmet, M. Mazzaschi, C. Tejel, P. Cassoux, L. Brossard, *Solid State Commun.*, **74**, 91 (1990). (c) J.P. Legros, L. Valade, B. Barreau, B. Pomarede, P. Cassoux, L. Brossard, S. Dybois, A. Audouard, J.P. Ulmet, *Synth. Met.*, **1993**, 2146.

[13] A.E. Underhill, R.A. Clark, I. Marsden, M. Allan, R.H. Friend, H. Tajima, T. Naito, M. Tamura, H. Kuroda, A Kobayashi, H. Kobayashi, E. Canadell, S. Ravy , J.P. Pouget, *J. Phys.; Condens. Matter*, **3**, 933 (1991).

[14] (a) R. Kato, H. Kobayashi, H. Kim, A. Kobayashi, Y. Sasaki, T. mori, H. Inokuchi,

Chem. Lett., **1988**, 865. (b) R. Kato, H. Kobayashi, H. kim, A. Kobayashi, Y. Sasaki, T. mori, H. Inokuchi, *Synth. Met.*, **27**, B359 (1988).

[15] H. Kobayshi, R. Kato, A. Kobayashi, Synth. Met., 42, 2495 (1991)

[16] A. Kobayashi, A. Sato, H. Kobayashi, to be published.

[17] A. Kobayashi, T. Naito, H. Kobayashi, *Synth. Met.*, **70**, 1047 (1995).

[18] "Landolt-Börnsrein", Neue Serie II/11, Springer-Verlag (1981).

[19] *Extended Linear Chain Compounds*, **3**, 45 ed. by J.S. Miller (1983).

Chapter 4

Crystal structures and physical properties of the low dimensional conductors based on the EDT-TTF and analogous donor molecules

4.1 Introduction

Since $(TMTSF)_2PF_6$ (TMTSF = tetramethyltetraselenafulvalene) was reported to be the first organic superconductor in 1980, $(TMTSF)_2X$ (X=PF_6, AsF_6, ClO_4,...) family has been studied intensively, where not only the superconducting phases of seven organic superconductors but also the novel field induced spin density wave (FISDW) phase have been disclosed. Except the ambient-pressure superconductor $(TMTSF)_2ClO_4$, most of $(TMTSF)_2X$ superconductors undergo SDW transitions (antiferromagnetic insulating transition) around 10 K at ambient pressure. The critical pressure depends on the anions. The sulfur-analogues, $(TMTTF)_2X$ (TMTTF = tetramethyltetrathiafulvalene) have been also developed. In contrast with $(TMTSF)_2PF_6$, the electrical resistivity of $(TMTTF)_2PF_6$ is metallic in the high temperature region, but becomes to be semiconductive below 220 K. The room temperature conductivity of $(TMTTF)_2PF_6$ is 50 S cm^{-1}, which is about one order of magnitude smaller than that of $(TMTSF)_2PF_6$. Magnetic properties of $(TMTTF)_2PF_6$ is of the non-magnetic state below 20 K. Since there is no order-disorder transition in the system having centrosymmetrical anions, the magnetic transition of $(TMTTF)_2PF_6$ is not originated from the anion ordering. Nevertheless weak superlattice reflections analogous to Peierls distortion is observed. That is, $(TMTTF)_2PF_6$ is considered to take a spin-Peierls state below 20 K [1-3].

The study of low-dimensional conductors by comparing $(TMTSF)_2X$ family and

$(TMTTF)_2X$ family (called TMs family), have given numbers of suggestions in understanding of the ground states in the low dimensional conductors [1-3]. Natures of TM_2X family are interpreted based on the effects of the "chemical pressure" by the anion sizes and the substitution of the chalcogen atoms. The "general pressure-temperature diagram" of TM_2X has been proposed by Jérome [9]. According to his diagram shown in Fig.4.1 where the "chemical pressure" of $(TMTTF)_2PF_6$ is taken to be "zero pressure", TM_2X system is in the spin-Peiels state at 0-8 kbar, and turns to SDW phase at 8-33 kbar. In the pressure range of 33-50 kbar, the phase boundary is in the superconducting phase. According to this diagram, the electronic properties of $(TMTSF)_2PF_6$ can be converted into that of $(TMTSF)_2PF_6$ by applying 27 kbar. That is, the exchange of S atoms to Se atoms is considered to produce the "effective pressure (chemical pressure)" in the crystal of TM system.

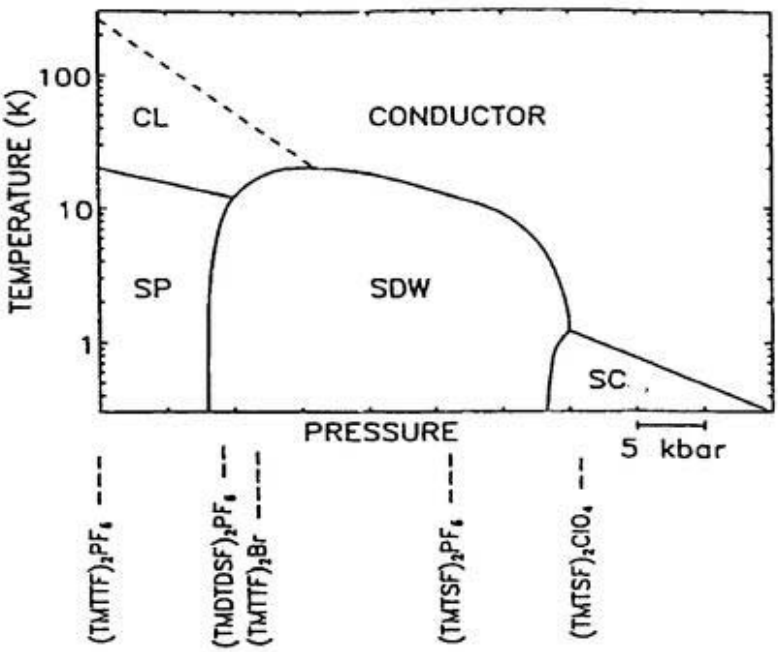

Fig.4.1. General phase diagram of TM_2X series. Abbreviations were SP, SDW and SC refer to spin-Peierls, spin density wave and superconducting ground states, respectively. The dashed line denotes the limit between the metal-like and the charge localized (CL) behavior [3].

EDT-TTF (= ethylenedithiotetrathiafulvalene) is one of the simplest unsymmetrical TTF-like π donor molecules. Organic conducting salts based on EDT-TTF with inorganic anions and

organic metal complexes [i.e. AuI_2^-, $Au(CN)_2^-$, TaF_6^-, AsF_6^-, PF_6^-, ReO_4^-, ClO_4^-, BF_4^-, $Ni(dmit)_2^-$, $Pd(dmit)_2^-$ and $Ni(dmise)_2^-$] have been reported [4-6]. These compounds are highly conductive at room temperature, but insulating at low temperatures except for α- (EDT-TTF)[Ni(dmit)$_2$] and α'- and γ-(EDT-TTF)[Pd(dmit)$_2$] whose ground states are superconductor and (semi)metal. The low-dimensional electronic structure was suggested from the extend Hückel band calculations. X-Ray oscillation photographs down to 13 K and the magnetic susceptibility behavior of (EDT-TTF)$_2$TaF$_6$ showed that the metal-insulator (MI) transition is caused by the development of the charge density wave (CDW) [7]. For the purpose of the enhancement the dimensionality in EDT-TTF system, selenium-substituted analogs of EDT-TTF have been synthesized [8-9]. EDT-TTF and the selenium-substituted donors salts (which are called here "EDTs family" in the present thesis) with the magnetic or non-magnetic anions were synthesized in order to study the effects of anions on their physical properties.

EDT-TTF, EDST and EDTS salts were expected to give good systems to see the effect of "chemical pressure" to the conduction electrons by Se-substitution: two "ethylenedithiodiselenadithiafulvalene (EDT-DSDTTF) are called "EDTS" or "EDST" depending on the selenium positions. Crystal structures, electrical conductivities and magnetic susceptibilities of (EDT-TTF)$_2$GaCl$_4$ (**1**), (EDT-TTF)$_2$FeCl$_4$ (**2**), (EDST)$_2$GaCl$_4$ (**3**), (EDST)$_2$FeCl$_4$ (**4**), (EDTS)$_2$GaCl$_4$ (**5**), (EDTS)$_2$FeCl$_4$ (**6**) will be discussed with referring to the general *P-T* phase diagram of TMs family.

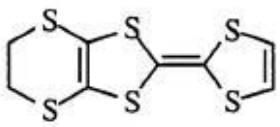

EDT-TTF

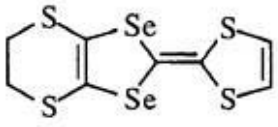

EDST

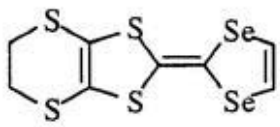

EDTS

4.2 *Experimental*

4.2.1 Sample preparation

Single crystals of **1-6** were obtained by the electrical oxidation in a two compartment glass H-cell equipped with platinum wires as the electrodes. A 20 cm^3 of solutions of dichloromethane containing a 10 mg of donor (EDT-TTF, EDST or EDTS) and a 100 mg of $[(C_2H_5)_4N]MCl_4$ (M= Ga^{3+} or Fe^{3+}) were applied by a constant current of 0.9 μA at 20 °C under the nitrogen atmosphere, according to the procedure mentioned in Chapter 2. Black plate- or rod-like shaped crystals were yielded. Conditions of the preparation are given in Table 4.1.

Table 4.1 Electrolytic conditions for obtaining good crystalline D_2MCl_4s (D= EDT-TTF, EDST, EDTS; M= Ga, Fe)[a]

Products	electrolyte (mg)		current (μA)	time (days)
$(EDT\text{-}TTF)_2GaCl_4$	EDT	8.8	1.0	12
	$GaCl_4$	88		
$(EDT\text{-}TTF)_2FeCl_4$	EDT	5.7	1.0	5
	$FeCl_4$	136		
$(EDST)_2GaCl_4$	EDST	10.8	1.0	27
	$GaCl_4$	105		
$(EDST)_2FeCl_4$	EDST	10.3	1.0	27
	$FeCl_4$	87.3		
$(EDTS)_2GaCl_4$	EDTS	11.5	0.9	8
	$GaCl_4$	108		
$(EDTS)_2FeCl_4$	EDTS	10.4	0.9	8
	$FeCl_4$	99		

[a] Abbreviations in Table. 5.1 are: EDT = EDT-TTF, $FeCl_4$ = $[(C_2H_5)_4N]FeCl_4$, $GaCl_4$ = $[(C_2H_5)_4N]GaCl_4$.

4.2.2 *X-ray measurements*

Structure determinations

Crystal structures of all of compounds (**1-6**) were determined at room temperature and those of **3** and **5** were also determined at low temperature. Crystallographic data for all of compounds are summarized in Table 4.2.

Each crystal structure was solved by the direct methods and refined the full-matrix least squares methods. Hydrogen atoms were located on the position calculated with B= 4.0 Å^2. Non-hydrogen atoms adopted the anisotropic parameters. Final refinements were performed including hydrogen atoms.

X-ray oscillation patterns and temperature dependence of the lattice constants

Several oscillation photographs were taken down to 7 K by using the single crystals of **1** (2.25 × 1.51 × 0.5 mm^3), **2** (2.0 × 0.5 × 0.15 mm^3), **3** (0.70 × 0.45 × 0.1 mm^3) and **5** (3.25 × 1.05 × 0.85 mm^3). Crystal was oscillated with 2 ° of the oscillation range and 2 °/min. of the oscillation speed. X-ray exposure times and the X-ray generation powers are as follows: **1**, 45 min., 12 kW (47 kV × 260 mA); **2**, 45 min., 12.7 kW (47 kV × 270 mA); **3**, 45 min., 12.5 kW (50 kV × 250 mA); **5**, 60 min., 12.2 (47 kV × 260 mA).

Temperature dependence of the lattice constants of **3** was measured down to 7 K.

4.2.3 *Electrical resistivity measurements*

Temperature dependencies of the electrical resistivities were measured along the donor stacking direction (// the c-axis) in the range of 4 - 300 K at ambient pressure. Measurements under the high pressure were performed up to 16 kbar for $(EDST)_2GaCl_4$ using the clamp-type cell and Daphne oil 7373 (Idemitsu Oil Co. Ltd.) as the pressure medium.

4.2.4 Magnetic susceptibility measurements

The magnetic susceptibilities were measured by a SQUID magnetometer down to 2 K. Polycrystalline samples wrapped in aluminum foils were set in the straws. Applied magnetic fields were as follows: 5 kOe and 70 kOe for three $GaCl_4$ salts of **1**, **3** and **5**; 5 kOe and 10 kOe for three $FeCl_4$ salts of **2**, **4** and **6**.

Magnetic anisotropy of **5** was measured using *ca.* 3 mg of a single crystal which was put on a capsule with a small amount of Apiezon M grease. A 10 kOe of magnetic fields were applied to parallel to the *a*-, *b*- and *c*-axes.

Magnetic susceptibilities were obtained by subtracting the diamagnetic contributions. The diamagnetic contributions were calculated according to the Pascal's law.

Table 4.2. Summary of measurements and crystal data of **1-6.**

	1	**2**	**3**		**4**
formula	$C_{16}Cl_4H_{12}Ga_1S_{12}$	$C_{16}Cl_4H_{12}Fe_1S_{12}$	$C_{16}Cl_4H_{12}Ga_1S_8Se_4$		$C_{16}Cl_4H_{12}Fe_1S_8Se_4$
temperature/K	293	293	293	17	293
dimension/mm^{-3}	0.20x0.45x0.08	0.50x0.25x0.03	0.30x0.4x0.10	0.35x0.20x0.15	0.20x0.10x0.50
color, shape	black, plate	black, plate	black, plate	black, plate	black, plate
formula mass	800.52	786.65	988.12	988.12	974.25
diffractometer	Rigaku AFC-7R	Rigaku AFC-5R	Rigaku AFC-7R	DIP320	Rigaku AFC-5R
crystal system	monoclinic	monoclinic	monoclinic	monoclinic	monoclinic
space group	$P2_1/m$	$P2_1/m$	$P2_1/m$	$P2_1/m$	$P2_1/m$
a/Å	6.586(4)	6.587(3)	6.647(2)	6.6090	6.645(5)
b/Å	30.438(4)	30.419(4)	30.714(4)	30.4510	30.701(4)
c/Å	7.091(4)	7.081(4)	7.138(5)	6.9270	7.136(5)
β/degrees	100.09(5)	100.04(4)	100.14(4)	100.257	100.03(6)
V/$Å^3$	1399(1)	1397(1)	1434(1)	1385.99	1433(1)
Z	2	2	2	2	2
Dc/g cm^{-3}	1.899	1.870	2.29	2.37	2.26
F_{000}	798.00	788.00	942.00	942.00	932.00
μ (Mo-Kα)/cm^{-1}	22.69	18.28	69.99	72.45	65.69
scan rate/degree min^{-1}	16.0	8.0	16.0	——	8.0
scan width/degree	0.68 + 0.30 tan θ	0.63 + 0.50 tan θ	1.05 + 0.30 tan θ	——	1.00 + 0.50 tanθ
$2\theta_{max}$/degree	55.0	60.0	55.0	61	60.0
total reflections	3563	4477	3642	10923	4590
unique reflections	3297	4167	3371	4295	4274
R_{int}	0.053	0.035	0.055	0.048	0.032
reflections used ($I>3\sigma(I)$)	1164	1945	2348	2502	2287
R^a , $R_w{}^b$	0.058, 0.046	0.044, 0.035	0.029, 0.021	0.083, 0.110	0.042, 0.044
good of fitness	1.96	1.34	2.02	6.39	1.38
ρ_{max}, $\rho_{min.}$/$e^-Å^{-3}$	0.74, -0.55	0.55, -0.46	0.59, -0.60	3.88, -2.91	0.91, -0.62

[a] $|F_o| \geq 3\sigma|F_o|$, [b] $R = \Sigma(|F_o|-|F_c|)/\Sigma|F_o|$, [b] $Rw = [\Sigma w(|F_o|-|F_c|)^2/\Sigma w|F_o|^2]^{1/2}$, $w = 1/\sigma^2(F)$.

Table 4.2. Summary of measurements and crystal data of **1-6** (continued).

	5		**6**
formula	$C_{16}Cl_4H_{12}Ga_1S_8Se_4$		$C_{16}Cl_4H_{12}Fe_1S_8Se_4$
temperature/K	293	7	293
dimension/mm^{-3}	0.20x0.45x0.08	0.50x0.25x0.03	0.30x0.3x0.30
color, shape	black, plate	black, plate	black, plate
formula mass	988.12	988.12	974.25
diffractometer	Rigaku AFC-5R	DIP 320	Rigaku AFC-5R
crystal system	monoclinic	monoclinic	monoclinic
space group	$P2_1/m$	$P2_1/m$	$P2_1/m$
a/Å	6.543(6)	6.632	6.646(4)
*b*Å	30.395(7)	30.402	30.352(4)
c/ Å	7.251(7)	7.0891	7.247(3)
β/degree	100.37(8)	100.472	100.36(4)
V/Å^3	1440(2)	1405.5	1438.0(9)
Z	2	2	2
Dc/g cm^{-3}	2.28	2.33	2.25
F_{000}	942.00	942.00	932.00
μ (Mo-Kα)/cm^{-1}	69.1	70.8	65.5
scan rate/degree min^{-1}	8.0	——	8
scan width/degree	0.68 + 0.50 tan θ	——	0.68 + 0.50 tan θ
$2\theta_{max}$/degree	60.0	61	60.0
total reflections	4624	12473	4612
unique reflections	4305	4394	4295
R_{int}	0.041	0.058	0.034
reflections used ($I>3\sigma(I)$)	2480	2525	2351
R[a], R_w[b]	0.039, 0.065	0.091, 0.111	0.038, 0.047
good of fitness	1.00	7.25	1.38
ρ_{max}, $\rho_{min.}$/e$^-$Å^{-3}	0.51, -0.59	0.55, -0.46	0.51, -0.51

[a] $|F_o| \geq 3\sigma|F_o|$, b $R = \Sigma(|F_o|-|F_c|)/\Sigma|F_o|$, [b] $Rw = [\Sigma w(|F_o|-|F_c|)^2/\Sigma w|F_o|^2]^{1/2}$, $w = 1/\sigma^2(F)$.

4.3 *Crystal and electronic structures*

The molecular structures and the atomic numbering schemes of **1-6** were shown in Fig.4.2 and the atomic coordinates listed in Table 4.3. All compounds were isostructural to each other. Crystal structures belonged to the monoclinic system, $P2_1/m$ of centrosymmetrical space group. Bond lengths and angles of **1-6** are listed in Table 4.4.

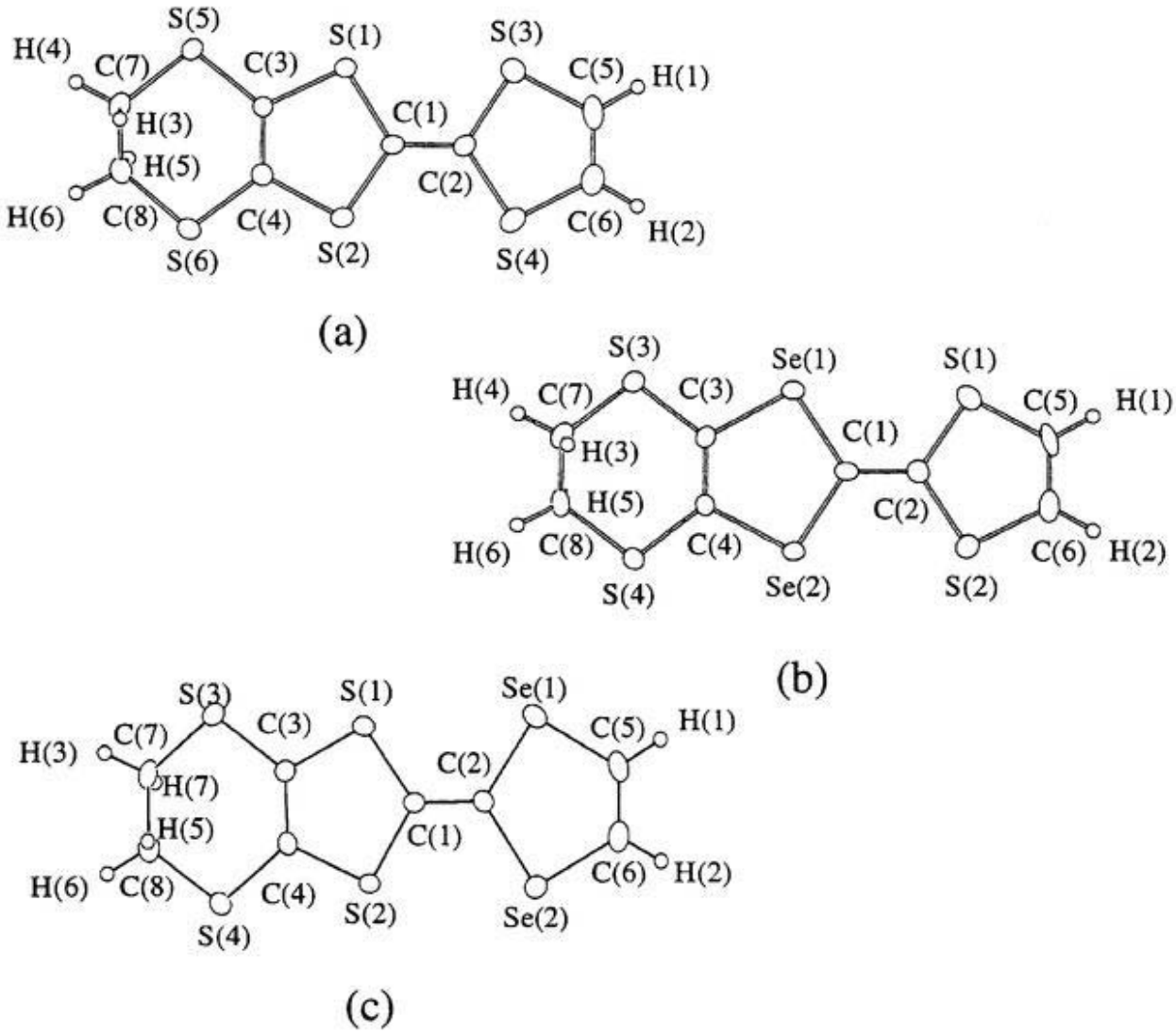

Fig.4.2. Molecular structures and the atomic numbering schemes of **1-6**.

Table 4.3. Atomic Coordinates of **1-6** at the room temperature.

Atom	*x*	*y*	*z*	B_{eq}
(1)				
Ga	0.2518(2)	0.2500	0.1212(3)	3.23(5)
Cl(1)	0.3099(6)	0.2500	-0.1701(6)	4.1(1)
Cl(2)	-0.0775(6)	0.2500	0.1163(6)	5.3(1)
Cl(3)	0.3834(5)	0.19176(9)	0.2689(4)	5.74(9)
S(1)	0.1716(3)	0.45003(8)	0.7664(4)	2.84(7)
S(2)	-0.2627(4)	0.47630(8)	0.6965(4)	2.87(7)
S(3)	0.3096(4)	0.55075(9)	0.8178(4)	3.30(7)
S(4)	-0.1224(4)	0.57873(9)	0.7486(4)	3.37(7)
S(5)	0.0932(4)	0.35471(8)	0.7382(4)	3.45(7)
S(6)	-0.4294(4)	0.38662(9)	0.6519(4)	3.47(7)
C(1)	-0.007(1)	0.4923(3)	0.745(1)	2.4(2)
C(2)	0.052(1)	0.5343(3)	0.769(1)	2.6(3)
C(3)	-0.010(1)	0.4074(3)	0.727(1)	2.5(3)
C(4)	-0.211(1)	0.4195(3)	0.694(1)	2.4(2)
C(5)	0.260(2)	0.6063(3)	0.821(1)	3.5(3)
C(6)	0.060(2)	0.6186(3)	0.790(1)	3.9(3)
C(7)	-0.132(1)	0.322(3)	0.643(1)	3.4(3)
C(8)	-0.319(2)	0.3341(3)	0.726(1)	3.6(3)
H(1)	-0.1707	0.3276	0.5035	3.3395
H(2)	-0.106	0.2615	0.6564	3.3395
H(3)	-0.2735	0.3335	0.8648	3.6574
H(4)	-0.4199	0.3110	0.6974	3.6574
H(5)	0.3734	0.6285	0.8458	3.9899
H(6)	0.0213	0.6507	0.7906	3.6574
(2)				
Fe	0.2499(2)	0.2500	0.6175(2)	3.20(3)
Cl(1)	0.3832(3)	0.30912(5)	0.7660)	5.83(5)
Cl(2)	0.3060(3)	0.2500	0.3214(3)	4.07(5)
Cl(3)	-0.0831(3)	0.2500	0.6134(4)	5.37(6)
S(1)	0.1710(2)	0.42985(4)	0.2653(2)	2.68(3)
S(2)	-0.2639(2)	0.47621(4)	0.1970(2)	2.77(3)
S(3)	0.3098(2)	0.55065(5)	0.3173(2)	3.15(3)
S(4)	-0.1225(2)	0.57874(5)	0.2495(2)	3.25(3)
S(5)	0.0917(2)	0.35467(4)	0.2362(2)	3.34(3)
S(6)	-0.4305(2)	0.38675(5)	0.1514(2)	3.45(3)
C(1)	-0.079(7)	0.4926(2)	0.2469(7)	2.3(1)
C(2)	0.0518(7)	0.5355(2)	0.2677(7)	2.4(1)
C(3)	-0.0127(7)	0.4075(1)	0.2249(7)	2.4(1)
C(4)	-0.2097(7)	0.4200(2)	0.1952(7)	2.4(1)
C(5)	0.2592(10)	0.6063(2)	0.3220(8)	4.0(2)
C(6)	0.0638(9)	0.6188(2)	0.2908(8)	3.8(1)
C(7)	-0.1338(8)	0.3225(2)	0.1427(8)	3.4(1)
C(8)	-0.3214(8)	0.3336(2)	0.72266(8)	3.4(1)
H(1)	-0.1701	0.3272	0.0042	3.3849
H(2)	-0.1038	0.2916	0.1597	3.8549
H(3)	-0.2806	0.3334	0.3653	3.9008
H(4)	-0.4245	0.3111	0.1953	3.9008
H(5)	0.3711	0.6278	0.3474	4.6654
H(6)	0.0264	0.6500	0.2918	4.3319

$$B_{eq} = \frac{8}{3}\pi^2(U_{11}(aa^*)^2 + (U_{22}(bb^*)^2 + (U_{33}(cc^*)^2 + 2U_{12}aa^*bb^*\cos\gamma + 2U_{13}aa^*cc^*\cos\beta + 2U_{23}bb^*cc^*\cos\alpha)$$

Table 4.3. Atomic Coordinates of **1-6** at the room temperature (continued).

Atom	*x*	*y*	*z*	B_{eq}
(3)				
Se(1)	0.19269(6)	0.45132(2)	0.77771(7)	2.53(1)
Se(2)	-0.27622(6)	0.47834(2)	0.69950(7)	2.6(1)
Ga	0.25667	0.2500	0.1401(1)	3.13(2)
Cl(1)	0.3156(2)	0.2500	-0.1497(3)	4.12(5)
Cl(2)	-0.0707(2)	0.2500	0.1319(3)	5.11(6)
Cl(3)	0.3868(2)	0.19220(5)	0.2885(2)	5.68(4)
S(1)	0.3082(2)	0.55531(4)	0.8098(2)	3.00(3)
S(2)	-0.1228(2)	0.58144(4)	0.7391(2)	3.07(3)
S(3)	0.0953(2)	0.35438(4)	0.7523(2)	3.39(3)
S(4)	-0.4217(2)	0.38462(4)	0.6650(2)	3.33(3)
C(1)	-0.0016(5)	0.4963(2)	0.7516(5)	2.2(1)
C(2)	0.0524(6)	0.5387(1)	0.7638(6)	2.2(1)
C(3)	-0.0099(6)	0.4068(1)	0.7367(6)	2.3(1)
C(4)	-0.2043(6)	0.4182(1)	0.7062(6)	2.29(10)
C(5)	0.2546(7)	0.6100(2)	0.8056(7)	3.7(1)
C(6)	0.0591(7)	0.6220(2)	0.7738(7)	3.6(1)
C(7)	-0.1242(6)	0.3214(1)	0.6610(7)	3.5(1)
C(8)	-0.3133(6)	0.3327(2)	0.7422(7)	3.4(1)
H(1)	-0.1607	0.3248	0.5219	4.0327
H(2)	-0.0929	0.2907	0.6808	4.0327
H(3)	-0.2725	0.3328	0.8806	3.7996
H(4)	-0.4150	0.3102	0.7134	3.7996
H(5)	0.3654	0.6318	0.8285	4.2275
H(6)	0.0200	0.6537	0.7687	4.2661
(4)				
Se(1)	0.77664(8)	0.47845(2)	0.80015(9)	2.63(1)
Se(2)	0.30789(8)	0.45135(2)	0.72301(9)	2.68(1)
Fe	0.2450(2)	0.2500	0.3631(2)	3.20(3)
Cl(1)	0.1869(4)	0.2500	0.6567(4)	4.33(6)
Cl(2)	0.5752(4)	0.2500	0.3696(5)	5.33(7)
Cl(3)	0.1142(3)	0.19164(7)	0.2137(3)	5.83(6)
S(1)	0.6232(2)	0.58162(6)	0.7603(2)	3.11(4)
S(2)	0.1916(2)	0.55527(5)	0.6905(2)	3.04(4)
S(3)	0.9223(2)	0.38472(6)	0.8348(3)	3.37(4)
S(4)	0.4064(2)	0.35432(5)	0.7485(3)	3.40(4)
C(1)	0.5006(8)	0.4965(2)	0.7487(8)	2.3(1)
C(2)	0.4471(8)	0.5388(2)	0.7343(8)	2.4(1)
C(3)	0.7062(8)	0.4183(2)	0.7951(8)	2.4(1)
C(4)	0.5103(8)	0.4064(2)	0.7626(8)	2.4(1)
C(5)	0.440(1)	0.62172)	0.7252(10)	3.8(2)
C(6)	0.248(1)	0.6103(2)	0.6939(10)	3.8(2)
C(7)	0.8152(9)	0.3323(2)	0.7575(9)	3.5(2)
C(8)	0.6267(10)	0.3213(2)	0.8394(9)	3.4(2)
H(1)	0.7783	0.3324	0.6233	4.3498
H(2)	0.9141	0.3104	0.7962	4.3498
H(3)	0.6583	0.3248	0.9734	3.8856
H(4)	0.5934	0.2916	0.8104	3.8856
H(5)	0.4760	0.6516	0.7324	4.7722
H(6)	0.1433	0.6321	0.6676	4.3782

$$B_{eq} = \frac{8}{3}\pi^2 (U_{11}(aa^*)^2 + (U_{22}(bb^*)^2 + (U_{33}(cc^*)^2 + 2U_{12}aa^*bb^* \cos\gamma + 2U_{13}aa^*cc^* \cos\beta + 2U_{23}bb^*cc^* \cos\alpha)$$

Table 4.3. Atomic Coordinates of **1-6** at the room temperature (continued).

atom	*x*	*y*	*z*	B_{eq}
(5)				
Se(1)	-0.1289(1)	0.58161(2)	0.2544(1)	2.96(1)
Se(2)	0.33443(10)	0.54959(2)	0.33509(10)	2.95(1)
Ga	0.2460(2)	0.2500	0.6114(2)	3.04(2)
Cl(1)	0.3709(4)	0.30846(7)	0.7620(4)	5.55(6)
Cl(2)	0.3165(4)	0.2500	0.3312(4)	4.29(7)
Cl(3)	-0.0839(4)	0.2500	0.5911(5)	5.01(7)
S(1)	-0.2574(2)	0.47541(5)	0.1837(2)	2.67(3)
S(2)	0.1727(2)	0.44890(5)	0.2555(2)	2.66(3)
S(3)	-0.4238(3)	0.38593(6)	0.1365(3)	3.31(4)
S(4)	0.0946(3)	0.35374(6)	0.2267(3)	3.35(4)
C(1)	-0.0046(9)	0.4916(2)	0.2411(8)	2.3(1)
C(2)	0.0561(9)	0.5342(2)	0.2720(9)	2.3(1)
C(3)	-0.2048(9)	0.4189(2)	0.1820(9)	2.4(1)
C(4)	-0.0087(9)	0.4066(2)	0.2140(9)	2.3(1)
C(5)	0.081(1)	0.6226(2)	0.315(1)	3.6(2)
C(6)	0.274(1)	0.6094(2)	0.350(1)	3.8(2)
C(7)	-0.316(1)	0.3330(2)	0.206(1)	3.3(2)
C(8)	-0.126(1)	0.3222(2)	0.125(1)	3.6(2)
H(1)	0.0501	0.6541	0.3233	4.0705
H(2)	0.3796	0.6310	0.3857	4.3520
H(3)	-0.4175	0.3102	0.1638	3.9065
H(4)	-0.2816	0.3310	0.3384	3.9065
H(5)	-0.1537	0.3265	-0.0070	4.1790
H(6)	-0.0931	0.2909	0.1462	4.1790
(6)				
Se(l)	-0.1280(1)	0.58180(3)	0.2557(1)	2.79
Se(2)	0.3348(1)	0.54957(3)	0.3357(1)	2.81
Fe	0.2433(2)	0.2500	0.6064(2)	2.91
Cl(1)	0.3689(4)	0.30912(8)	0.7590(4)	5.37
Cl(2)	0.3137(5)	0.2500	0.3225(5)	4.22
Cl(3)	-0.0890(5)	0.2500	0.5857(6)	4.76
S(1)	-0.2575(3)	0.47550(6)	0.1834(3)	2.53
S(2)	0.1728(3)	0.44881(6)	0.2549(3)	2.53
S(3)	-0.4254(3)	0.38592(7)	0.1342(3)	3.17
S(4)	0.0933(3)	0.35359(6)	0.2242(3)	3.25
C(1)	-0.0040(10)	0.4917(2)	0.2410(10)	2.12
C(2)	0.057(1)	0.5342(2)	0.274(1)	2.28
C(3)	-0.207(1)	0.4188(2)	0.180(1)	2.33
C(4)	-0.010(1)	0.4064(2)	0.213(1)	2.28
C(5)	0.086(1)	0.6228(3)	0.320(1)	3.48
C(6)	0.275(1)	0.6095(3)	0.354(1)	3.57
C(7)	-0.319(1)	0.3322(3)	0.202(1)	3.35
C(8)	-0.128(1)	0.3221(3)	0.120(1)	3.40
H(1)	0.0501	0.6541	0.3233	4.07
H(2)	0.3796	0.6310	0.3857	4.35
H(3)	-0.4175	0.3102	0.1638	3.91
H(4)	-0.2816	0.3310	0.3384	3.91
H(5)	-0.1537	0.3265	-0.0070	4.18
H(6)	-0.0931	0.2909	0.1462	4.18

$$B_{eq} = \frac{8}{3}\pi^2(U_{11}(aa^*)^2 + (U_{22}(bb^*)^2 + (U_{33}(cc^*)^2 + 2U_{12}aa^*bb^*\cos\gamma + 2U_{13}aa^*cc^*\cos\beta + 2U_{23}bb^*cc^*\cos\alpha)$$

As shown in Fig.4.3(a), the unit cell contains four donors on the general positions and two anions on the mirror planes. One donor molecule and a half of anion were crystallographically independent.

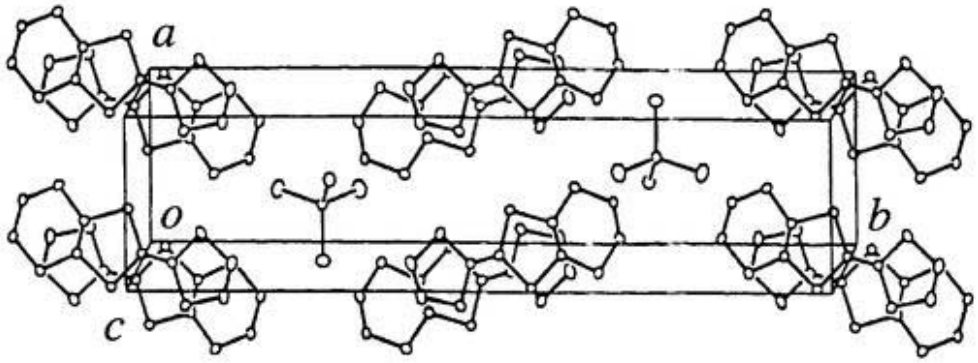

(a)

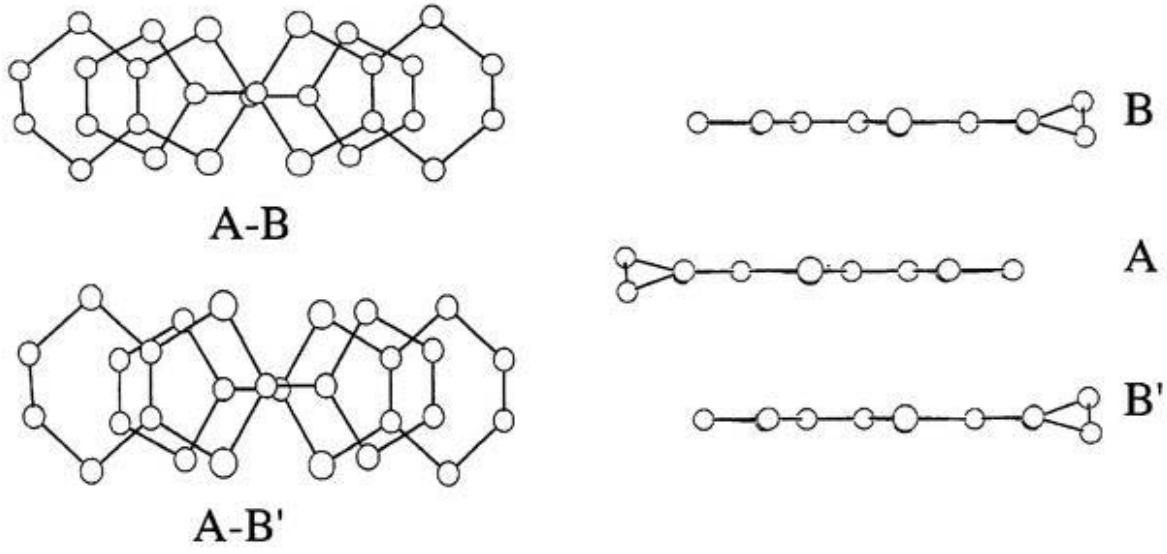

(b) (c)

Fig.4.3. (a) The crystal structure, (b) overlapping modes and (c) side view of the columns of donors of **1**.

The donor molecules were almost flat and the ethylene group took the eclipsed type conformation (Fig.4.3(b)). The distances of the central double bonds of C1-C2 [1.34(1) Å for

1, 1.365(6) Å for **2**, 1.378(6) Å for **3**, 1.344(8) Å for **4**, 1.363(8) Å for **5**, 1.362(9) Å for **6**] were longer than the normal double bond length (1.33 Å) of the ethylene. The distances of C7-C8 of the single bonds were slightly shorter than the single bond length (1.54 Å) : 1.50(1) Å for **1**, 1.501(7) Å for **2**, 1.515(6) Å for **3**, 1.510(9) Å for **4**, 1.52(1) Å for **5**, 1.52(1) Å for **6**. Moieties of ethylene was in ordered conformation. Table 4.5 shows the deviating distances of two of carbon atoms in the ethylene groups (C7 and C8) from the molecular least-square planes which were defined by the six central atoms of the fulvalene moieties. The deviation of C7 from the plane was smaller than that of C8. The deviation of C8 are largest in EDST salts and smallest in EDTS salts. In the crystals of **5** and **6**, C7 was close to the least-square plane (**5**, 0.114 Å; **6**, 0.134 Å) and C8 was 0.711-0.703 Å away from the least-square plane.

Table 4.5. The deviating distances of the ethylene moieties from the molecular least-squares planes.

Compound	1	2	3	4	5	6
C7	0.245 Å	0.250 Å	0.264 Å	0.326 Å	0.114 Å	0.134 Å
C8	0.554 Å	0.553 Å	0.507 Å	0.480 Å	0.703 Å	0.703 Å

Similar to $(EDT\text{-}TTF)_2X$ (X= AuI_2^-, $Au(CN)_2^-$, TaF_6^-, AsF_6^-, PF_6^-, ReO_4, ClO_4^- and BF_4^-) [1], donor molecules were stacked to form diadic columns along the *c*-axis. The donor molecules overlap to each other in the head-to-tail manner (Figs.4.3(b) and (c)). Intermolecular distances of A···B and A···B' [see Fig. 4.3(c)] of **1**-**6** were as follows : **1**, 3.550Å and 3.525 Å; **2**, 3.538 Å and 3.522 Å; **3**, 3.60 Å and 3.556 Å; **4**, 3.609 Å and 3.557 Å; **5**, 3.532 Å and 3.667 Å; **6**, 3.533 Å and 3.672 Å. The difference in A···B and A···B' distances becomes larger in the order of EDT-TTF salts (**1**,**2**) < EDST salts (**3**,**4**) < EDTS salts (**5**,**6**).

Intermolecular distances of the chalcogen atoms shorter than the sum of the van der Waals radii are listed in Table 4.6. The selenium-substituted derivatives of **3**-**6** have

significantly shorter intermolecular distances between the chalcogen atoms than **1** and **2** in the transverse direction. Intermolecular overlap integrals of HOMOs of **1**, **3** and **5** were calculated (Table 4.7).

The intra- and interdimer overlap integrals (a and b) in each compound were almost the same but the those of **3** and **5** were much larger than those of **1**. On the other hand, the magnitudes of the overlapping integrals in the side-by-side direction (p) and diagonal direction (r and q) of **3** and **5** were 100 times larger than those of **1**. According to the overlap integrals, it is considered that the introduction of the selenium atoms certainly makes the intermolecular interactions increase. Since the ratios of overlap integral in intrastack (t_S) to interstack (t_t), t_S/t_t, were 10-100 in **1**-**6**, the electronic structures of $(EDT)_2MCl_4$ systems are essentially one-dimensional. The ratio of intermolecular interactions a/b (Table 4.7) were larger in the order of EDST (**3**) < EDTS (**5**) < EDT-TTF salts (**1**). The substituting position for the chalcogen atom and the conformation of ethylene moiety give a strong influence on the electronic structure of the system. The band dispersion curves and the Fermi surfaces calculated on the basis of the extended Hückel approximation are shown in Fig.4.5. Each compound had a three-quarter filled band because of the 2:1 ratio of the donors and anions. The band widths of **1**, **3** and **5** were 1.3, 3.1, 2.3 eV, respectively.

Table 4.4. Bond lengths and angles of **1-6** at the room temperature.

	distance / Å			distance / Å	
	(1)	**(2)**		**(1)**	**(2)**
S1-C1	1.735(3)	1.745(5)	C1-C2	1.34(1)	1.365(6)
S1-C3	1.753(9)	1.734(5)	C3-C4	1.35(1)	1.333(6)
S2-C4	1.762(9)	1.747(5)	C5-C6	1.35(1)	1.324(7)
S3-C2	1.746(9)	1.736(5)	C7-C8	1.50(1)	1.501(7)
S3-C5	1.723(10)	1.726(6)	M-Cl1	2.166(4)	2.188(2)
S4-C2	1.764(9)	1.735(5)	M-Cl2	2.162(4)	2.191(3)
S4-C6	1.70(1)	1.717(6)	M-Cl3	2.162(3)	2.189(3)
S5-C3	1.737(9)	1.745(5)			
S5-C7	1.804(10)	1.806(5)			
S6-C4	1.738(8)	1.754(5)			
S6-C8	1.796(10)	1.810(5)			

	angle / °	
	(1)	**(2)**
Cl(1) - M - Cl(2)	109.2(2)	110.5(1)
Cl(1) - M - Cl(3)	109.8(1)	109.84(7)
Cl(1) - M - Cl(3)	109.8(1)	108.88(7)
Cl(2) - M - Cl(3)	108.9(1)	109.84(7)
Cl(2) - M - Cl(3)	108.9(1)	108.88(7)
Cl(3) - M - Cl(3)	110.2(2)	108.8(1)
C(1) - S(1) - C(3)	95.9(4)	95.6(2)
C(1) - S(2) - C(4)	95.4(4)	95.2(2)
C(2) - S(3) - C(5)	96.0(5)	94.5(3)
C(2) - S(4)- C(6)	95.9(5)	94.6(3)
C(3) - S(5) - C(7)	101.2(4)	101.0(2)
C(4) - S(6) - C(8)	100.5(4)	100.8(2)
S(1) - C(1) - S(2)	115.5(5)	114.9(3)
S(1) - C(1) - C(2)	121.2(7)	121.8(4)
S(2) - C(1) - C(2)	123.2(8)	123.3(4)
S(3) - C(2) - S(4)	113.1(5)	115.2(3)
S(3) - C(2) - C(1)	123.5(7)	121.9(4)
S(4) - C(2) - C(1)	123.4(7)	122.8(4)
S(1) - C(3) - S(5)	115.2(5)	114.4(3)
S(1) - C(3) - C(4)	116.3(7)	116.2(4)
S(5) - C(3) - C(4)	128.5(7)	129.4(4)
S(2) - C(4) - S(6)	114.2(5)	113.7(3)
S(2) - C(4) - C(3)	116.9(7)	118.1(4)
S(6) - C(4) - C(3)	128.9(7)	128.2(4)
S(3) - C(5) - C(6)	116.9(8)	117.6(4)
S(4) - C(6) - C(5)	118.1(8)	118.0(4)
S(5) - C(7) - C(8)	114.1(7)	114.4(4)
S(6) - C(8) - C(7)	114.3(7)	113.5(4)

Table 4.4. Bond lengths and angles of **1-6** at the room temperature. (continued)

	distance / Å			distance / Å	
	(3)	**(4)**		**(3)**	**(4)**
Se1-C1	1.879(4)	1.890(5)	C1-C2	1.348(6)	1.344(8)
Se2-C1	1.880(4)	1.875(6)	C3-C4	1.320(5)	1.333(7)
Se2-C4	1.905(4)	1.912(6)	C5-C6	1.331(6)	1.306(9)
S1-C2	1.750(4)	1.749(6)	C7-C8	1.515(6)	1.510(9)
S1-C5	1.715(5)	1.718(7)	M-Cl1	2.171(2)	2.196(3)
S2-C2	1.744(4)	1.746(6)	M-Cl2	2.166(2)	2.187(3)
S2-C6	1.722(5)	1.730(7)	M-Cl3	2.168(2)	2.186(2)
S3-C3	1.750(4)	1.751(6)			
S3-C7	1.802(4)	1.806(7)			
S4-C4	1.758(4)	1.739(6)			
S4-C8	1.795(5)	1.806(6)			

	angle / °	
	(3)	**(4)**
C(1) - Se(1) - C(3)	93.3(2)	93.1(3)
C(1) - Se(2) - C(4)	92.8(2)	93.9(2)
Cl(1) - M - Cl(2)	108.85(8)	108.8(1)
Cl(1) - M - Cl(3)	110.01(6)	110.16(8)
Cl(1) - M - Cl(3)	110.01(6)	110.16(8)
Cl(2) - M - Cl(3)	109.00(5)	108.80(9)
Cl(2) - M - Cl(3)	109.00(5)	108.80(9)
Cl(3) - M - Cl(3)	109.95(9)	110.1(1)
C(2) - S(1) - C(5)	95.2(2)	94.6(3)
C(2) - S(2) - C(6)	95.2(2)	94.6(3)
C(3) - S(3) - C(7)	101.9(2)	102.0(3)
C(4) - S(4) - C(8)	101.3(2)	101.9(3)
Se(1) - C(1) - Se(2)	115.5(2)	115.1(3)
Se(1) - C(1) - C(2)	122.2(3)	122.2(4)
Se(2)- C(1) - C(2)	122.3(3)	122.6(4)
S(1) - C(2) - S(2)	114.1(3)	114.4(4)
S(1) - C(2) - C(1)	122.2(3)	123.7(4)
S(2) - C(2) - C(1)	123.7(3)	122.0(5)
Se(1) - C(3) - S(3)	112.8(2)	112.1(3)
Se(1) - C(3) - C(4)	118.6(3)	119.9(4)
S(3) - C(3) - C(4)	128.6(3)	128.0(5)
Se(2) - C(4) - S(4)	111.7(2)	113.1(3)
Se(2) - C(4) - C(3)	119.8(3)	118.0(4)
S(1) - C(4) - C(3)	128.5(3)	128.9(5)
S(1) - C(5) - C(6)	117.9(4)	118.6(5)
S(2) - C(6) - C(5)	117.7(4)	117.8(5)
S(3) - C(7) - C(8)	113.9(3)	112.9(5)
S(4) - C(8) - C(7)	113.8(3)	14.3(5)

Table 4.4. Bond lengths and angles of **1-6** at the room temperature. (continued)

	distance / Å			distance / Å	
	(5)	**(6)**		**(5)**	**(6)**
S1-C1	1.728(6)	1.732(7)	C1-C2	1.363(8)	1.362(9)
S2-C1	1.743(6)	1.743(7)	C3-C4	1.334(8)	1.346(9)
S2-C4	1.750(6)	1.756(7)	C5-C6	1.32(1)	1.30(1)
Se1-C2	1.883(6)	1.885(7)	C7-C8	1.52(1)	1.52(1)
Se1-C5	1.864(8)	1.885(9)	M-Cl1	2.171(2)	2.193(3)
Se2-C2	1.882(6)	1.879(7)	M-Cl2	2.165(3)	2.191(4)
Se2-C6	1.870(8)	1.871(8)	M-Cl3	2.170(4)	2.186(4)
S3-C3	1.748(6)	1.743(7)			
S3-C7	1.796(7)	1.812(8)			
S4-C4	1.744(6)	1.740(7)			
S4-C8	1.793(8)	1.803(8)			

	angle / °	
	(5)	**(6)**
C(2) - Se(1) - C(5)	92.5(3)	92.0(3)
C(2) - Se(2) - C(6)	92.6(3)	92.6(3)
Se(1) - C(5) - H(2)	145.31	145.72
Cl(1) - M - Cl(1)	109.9(1)	109.8(2)
Cl(1) - M - Cl(2)	110.1(1)	110.3(1)
Cl(1) - M - Cl(3)	108.90(9)	108.8(1)
Cl(1) - M - Cl(2)	110.1(1)	110.3(1)
Cl(1) - M - Cl(3)	108.90(9)	108.8(1)
Cl(2) - M - Cl(3)	108.8(1)	108.6(2)
C(1) - S(1) - C(3)	95.4(3)	95.8(3)
C(1) - S(2) - C(4)	95.7(3)	95.7(3)
C(3) - S(3) - C(7)	100.7(3)	101.1(4)
C(4) - S(4) - C(8)	100.8(3)	100.7(4)
S(1) - C(1) - S(2)	114.8(3)	114.8(4)
S(2) - C(1) - C(2)	121.4(5)	121.5(5)
Se(1) - C(2) - Se(2)	115.3(3)	115.3(4)
Se(1) - C(2) - C(1)	123.1(5)	123.0(5)
Se(2) - C(2) - C(1)	121.7(4)	121.7(5)
S(1) - C(3) - S(3)	113.7(3)	114.3(4)
S(1) - C(3) - C(4)	117.5(5)	117.0(5)
S(3) - C(3) - C(4)	128.8(5)	128.7(6)
S(2) - C(4) - S(4)	114.5(3)	114.5(4)
S(2) - C(4) - C(3)	116.5(5)	116.6(5)
S(4) - C(4) - C(3)	129.0(5)	128.9(6)
Se(1) - C(5) - C(6)	120.1(5)	120.1(6)
Se(2) - C(6) - C(5)	119.5(6)	120.0(6)
S(3) - C(7) - C(8)	113.7(5)	112.7(6)
S(4) - C(8) - C(7)	113.7(5)	113.8(6)

Table 4.6 Intermolecular short contacts between the chalcogen atoms in **1-6** at room temperature.[a]

		1	2		3	4		5	6
a	S(2)-S(3)	3.605(5)	3.599(2)	Se(2)-S(1)	3.694(1)	3.692(2)	Se(1)-S(2)	3.734(2)	3.734(2)
	S(1)-S(4)	3.621(5)	3.612(2)	Se(1)-S(2)	3.699(1)	3.699(2)	Se(2)-Se(1)	3.696(2)	3.692(2)
b	S(1)-S(4)	3.714(5)	3.707(2)	Se(1)-S(2)	3.773(2)	3.750(2)	Se(1)-S(2)	3.772(2)	3.775(2)
	S(2)-S(3)	3.702(5)	3.693(2)	Se(2)-S(1)	3.749(2)	3.774(2)	Se(2)-S(1)	3.781(2)	3.782(2)
p1	S(1)-S(6)	3.477(5)	3.459(2)	Se(1)-S(4)	3.484(1)	3.479(2)	Se(2)-S(1)	3.836(3)	3.833(2)
	S(5)-S(6)	3.455(5)	3.446(2)	Se(3)-S(4)	3.502(2)	3.506(3)	S(2)-S(3)	3.525(3)	3.519(3)
p2		none	none	Se(1)-Se(2)	3.762(1)	3.760(3)	Se(1)-Se(2)	3.841(3)	3.839(2)
				Se(2)-S(1)	3.822(1)	3.812(2)	S(3)-S(4)	3.518(4)	3.517(3)
q		none	none	Se(2)-Se(2)	3.969(1)	3.969(2)	Se(1)-S(3)	3.848(3)	3.839(2)

[a] Se···Se ≤ 4.0 Å, Se···S ≤ 3.85 Å, S···S ≤ 3.7 Å.

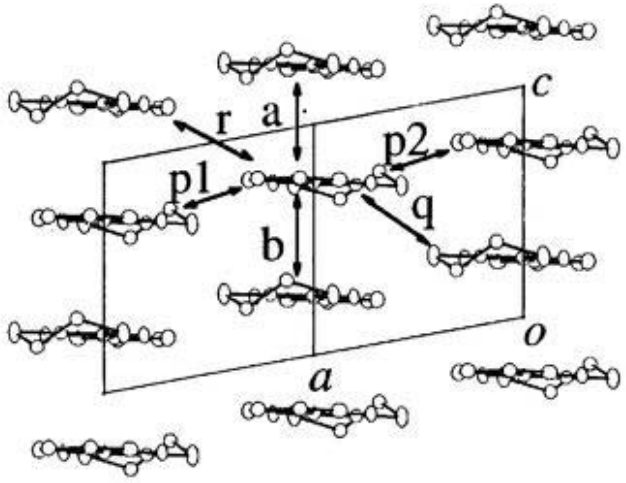

Table 4.7. The Overlap integrals of **1**,**3** and **5**.

	1	**3**	**5**
a	29.3	61.3	40.8
b	25.2	59.8	44.7
a/b	1.16	1.02	1.09 (=b/a)
p1=p2	0.04	4.8	3.06
q	6.13	24.4	19.4
r	5.3	11.8	8.83

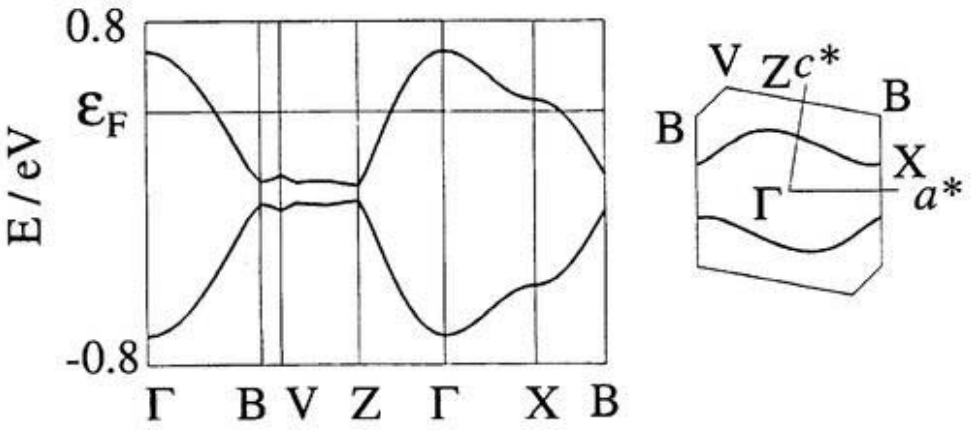

(a)

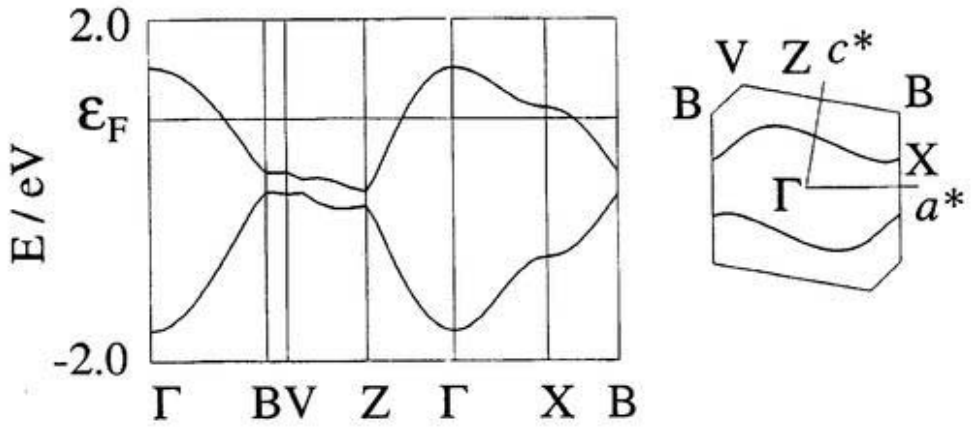

(b)

Fig.4.5. Calculated band structures and Fermi surfaces of (a) **1**, (b) **3** and (c) **5**.

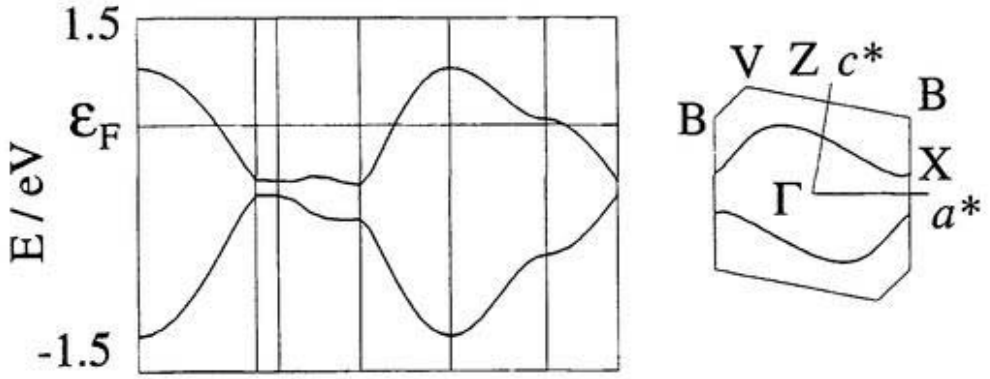

(c)

Fig.4.5. Calculated band structures and Fermi surfaces of (a) **1**, (b) **3** and (c) **5**. (continued)

The bond lengths of Ga-Cl are 2.162-2.171 Å and the angles of ∠ Cl-Ga-Cl are in the range of 108.8 -110.1° (Table 4.4). Those of Fe-Cl and ∠ Cl-Fe-Cl are 2.186-2.193 Å and 108.0-110.3 °, respectively. The Fe-Cl length is about 0.024-0.022 Å longer than Ga-Cl. In the $FeCl_4$ salts (**2**, **4** and **6**) which were prepared with expecting the interactions between the spins of Fe^{3+} ions and π electrons of donors, the short contacts between the Cl atoms and the chalcogen atoms shorter than the sum of the corresponding van der Waals radii were observed : **2**, Cl1 ··· S6 3.616 Å , Cl2 ··· S5 3.492 Å; **4**, Cl3 ··· S3 3.637 Å, Cl1 ··· S4 3.533 Å; **6**, Cl1 ··· S3 3.655 Å, Cl2 ··· S4 3.488 Å. Therefore some interactions were expected between donors and anions. The distances of Fe···Fe were 7.08 Å and 6.58 Å in **2**, 7.14 Å and 6.65 Å in **4** and 7.25 Å and 6.65 Å in **6**. The chalcogen···chalcogen and Cl···chalcogen network in the crystals of **2**, **4** and **6** as shown in Fig.4.6.

4.4 *Physical properties*

4.4.1 Electrical resistivities

As shown in Fig.4.8(a), the temperature dependences of resistivities of **1** and **2** were semiconductive. Resistivity behaviors of **1** and **2** were similar to each other. The conductivities at room temperature (ρ_{RT}) were 4-10 S cm^{-1}. As shown in Fig.4.7(b), the logρ *vs.*. T^{-1} plot could not be fitted by a single linear relationship. The activation energies (E_a) were estimated to be 17 meV and 12 meV in the temperature range of 100-200 K and 40-100 K, respectively. The magnitudes of Ea were relatively small which were consistent with the fairly large value of ρ_{RT}. Although the non-linearity of the logρ-T^{-1} plot around room temperature suggested the smaller band gap (2 E_a) around the room temperature, the metallic behavior did not appear up to 5 kbar.

Since the band width is enhanced by introducing the selenium atoms, the metallic nature might be expected in the EDST and EDTS systems. In fact, unlike EDT-TTF salts (**1**,**2**), those of **3**-**6** were metallic. Each conductivity was in the range of 4-30 S cm^{-1} at room temperature which was as same as for EDT-TTF salts. Resistivity behaviors of these salts were similar. The electrical conductivities were metallic down to around 40 K and the small increasing of the resistivity were observed at lower temperature. The resistivity decreased gradually down to about 40 K ($\rho_{RT}/\rho_{40K} \approx -0.5$) and the resistivity increase below 40 K dependent on samples. Typical resistivity behaviors were shown in Figs.4.7(c) and (d). The calculated activation energies were about 1 meV at 20-35 K.

Resistivity measurements at high pressure were carried out on **3**. Although the metallic region became wider, the resistivity increase could not be suppressed completely up to 16 kbar (Fig.4.8).

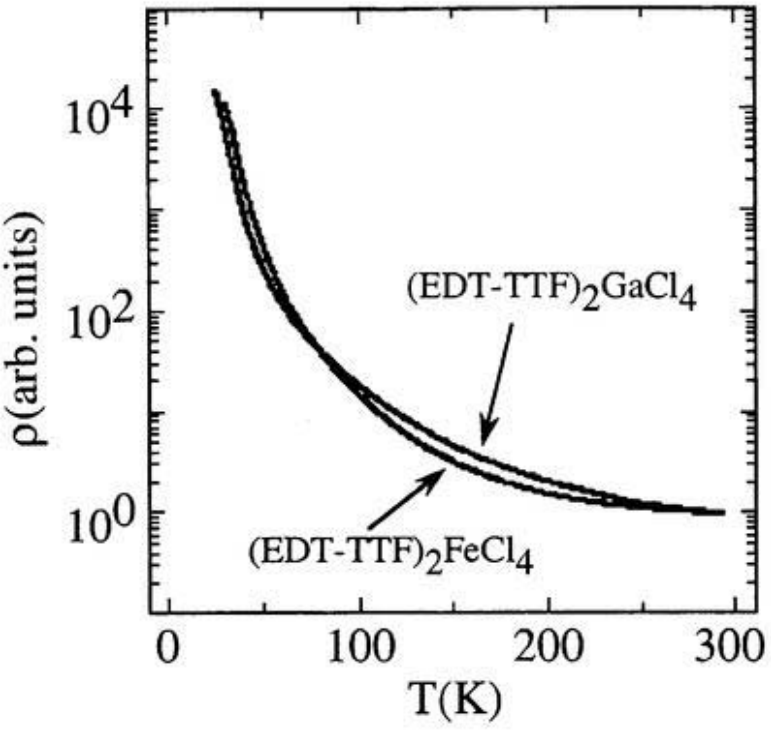

(a)

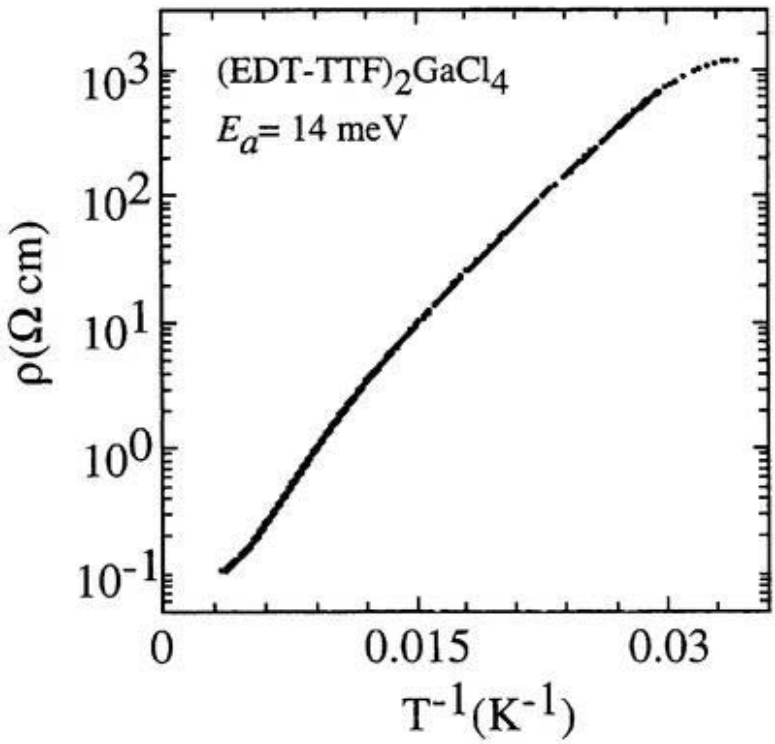

(b)

Fig.4.7. Temperature dependences of the electrical resistivities of **1** - **6** : (a) logρ-T plots of **1** and **2**, (b) logρ-T^{-1} plot of **1**, (c) logρ-T plots of **3** and **4** and (d) logρ-T plots of **5**.

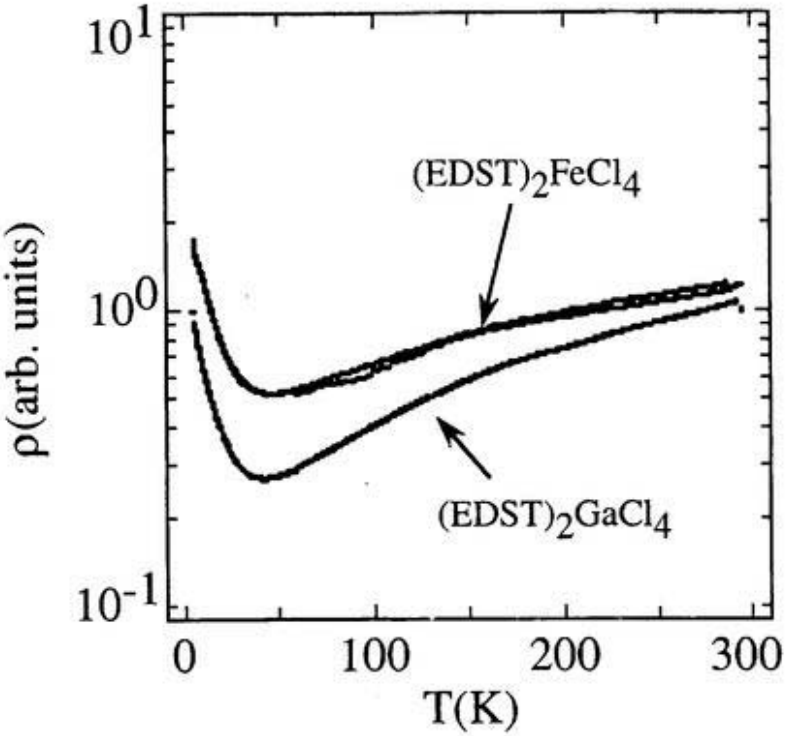

(c)

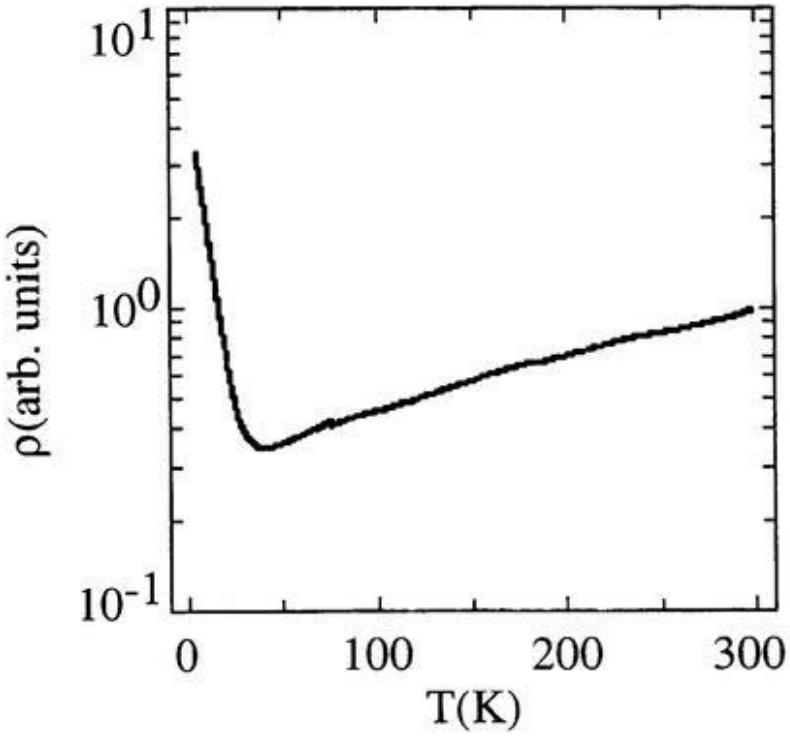

(d)

Fig.4.7. Temperature dependences of the electrical resistivities of **1** - **6** : (a) logρ-T plots of **1** and **2**, (b) logρ-T^{-1} plot of **1**, (c) logρ-T plots of **3** and **4** and (d) logρ-T plots of **5**. (continued)

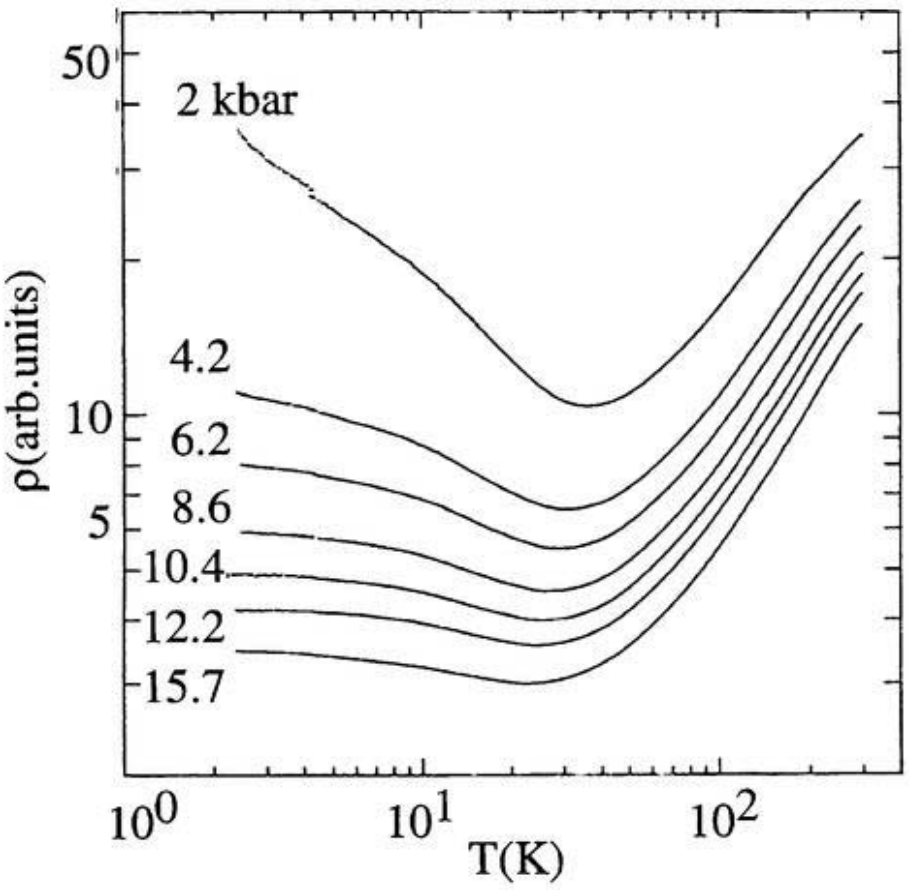

Fig.4.8. Temperature dependences of the electrical resistivities under high pressure of **3**.

4.4.2 Magnetic susceptibilities

Temperature dependences of the magnetic susceptibilities of polycrystalline samples of **1**, **3** and **5** are shown in Fig.4.9. Due to the small absolute value of magnetization, the data points were somewhat scattered.

According to the resistivity behavior, the conduction electrons of **1** were expected to be almost localized. Localized spin system usually exhibits the Curie-like behavior, however, the paramagnetic susceptibility of **1** decreased gradually with lowering temperature in the temperature range of 70-300 K. The magnitude of susceptibility at room temperature was about 1.6×10^{-4} emu/mol which was the same order of the magnitude of the Pauli paramagnetic susceptibility of the usual organic metal. Susceptibility which was subtracted the Curie's impurity contribution from the observed data dropped toward zero below 50 K. Sharp decrease of the susceptibility below 50 K was observed not only under the low magnetic field but also at 70 kOe (the highest magnetic field examined), that is, field independent. Thus, the susceptibility behavior of **1** suggested the non-magnetic ground state.

Temperature dependences of the magnetic susceptibilities of **3** and **5** were resemble to that of **1**. The magnetic susceptibilities decreased gradually down to 40 K (= T_{MI}) and decreased abruptly. However, unlike **1**, **3** and **5** seemed to have the constant values at low temperature (see the insets of Figs.9b and 9c). The magnitude of susceptibilities at room temperature of **3** and **5** were about (1.6 or 2) $\times 10^{-4}$ emu/mol which is a little larger than that of **1**. The sharp decreases of susceptibilities were also observed under the magnetic field of 70 kOe for the both samples. The susceptibilities of the single crystal of **5** were also measured for the magnetic field parallel to the *a*-, *b*- and *c*- axes. Drops of susceptibilities below 40 K were observed for each axis, that is, the decrease in susceptibilities of **5** were isotropic (Fig.4.10). Therefore, the possibilities of SDW ground states are ruled out for **3** and **5** .

On the other hand, the temperature dependences of the susceptibilities of the three salt with $FeCl_4^-$, **2**, **4** and **6**, satisfied the Curie's law as shown in Fig.4.11. The large susceptibility suggested the high-spin state of Fe ions. Assuming that S= 5/2 and g = 2, the spin concentrations of **2**, **4** and **6** were estimated to be 0.98, where the susceptibility of π conduction electrons was neglected. The Curie-Weiss plot of the susceptibility suggested the

weak magnetic interaction between Fe ions (θ< -1.4 K).

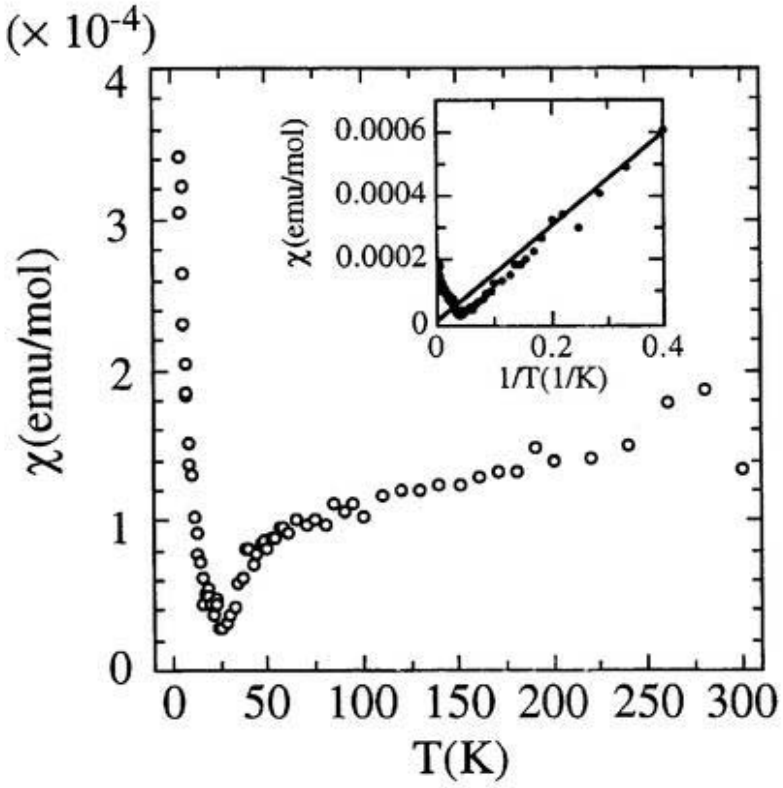

(a)

Fig4.9. Temperature dependences of the magnetic susceptibilities of (a) **1**, (b) **3** and (c) **5**.

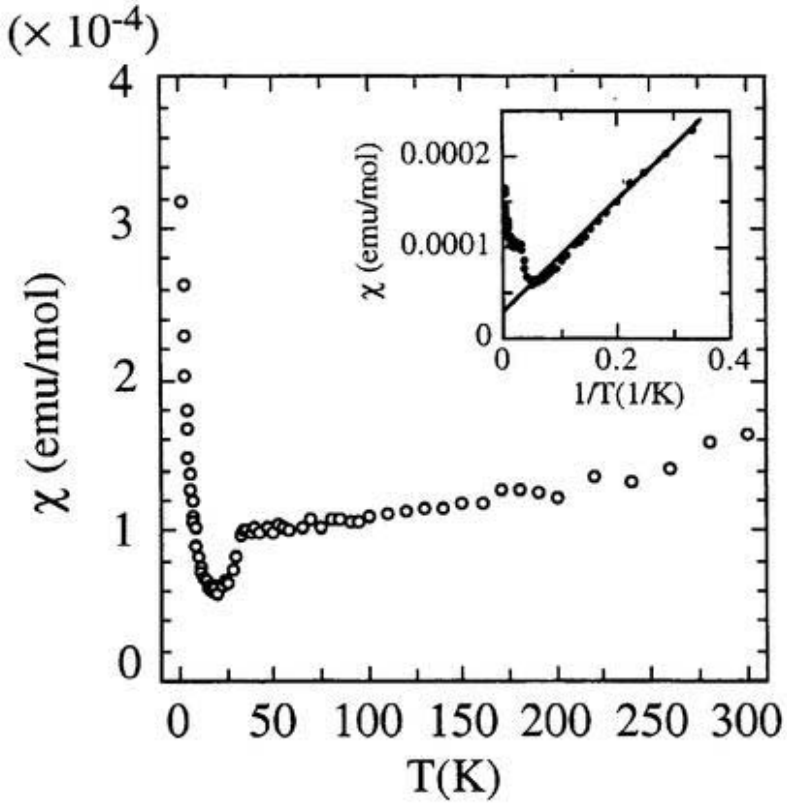

(b)

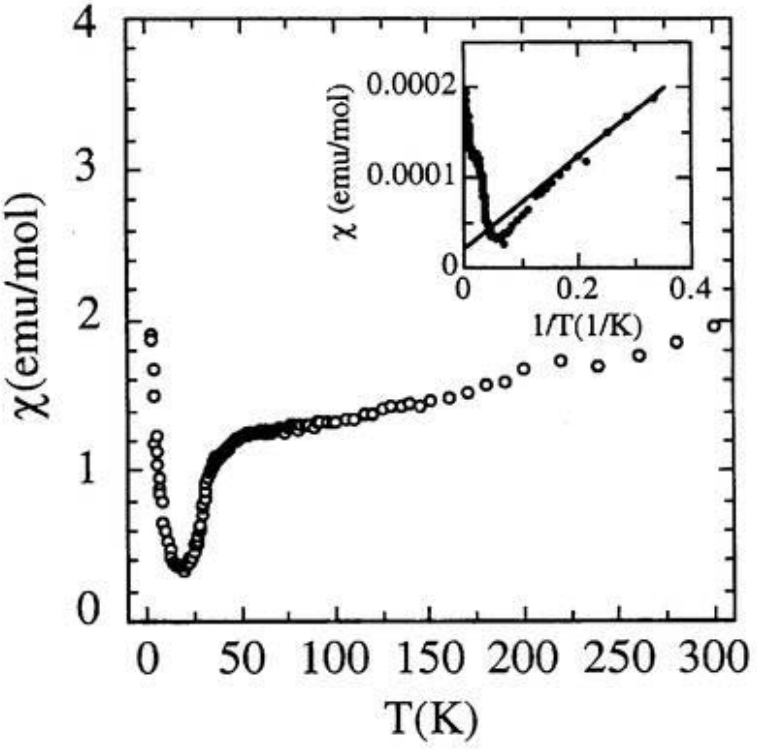

(c)

Fig4.9. Temperature dependences of the magnetic susceptibilities of (a) **1**, (b) **3** and (c) **5**. (continued)

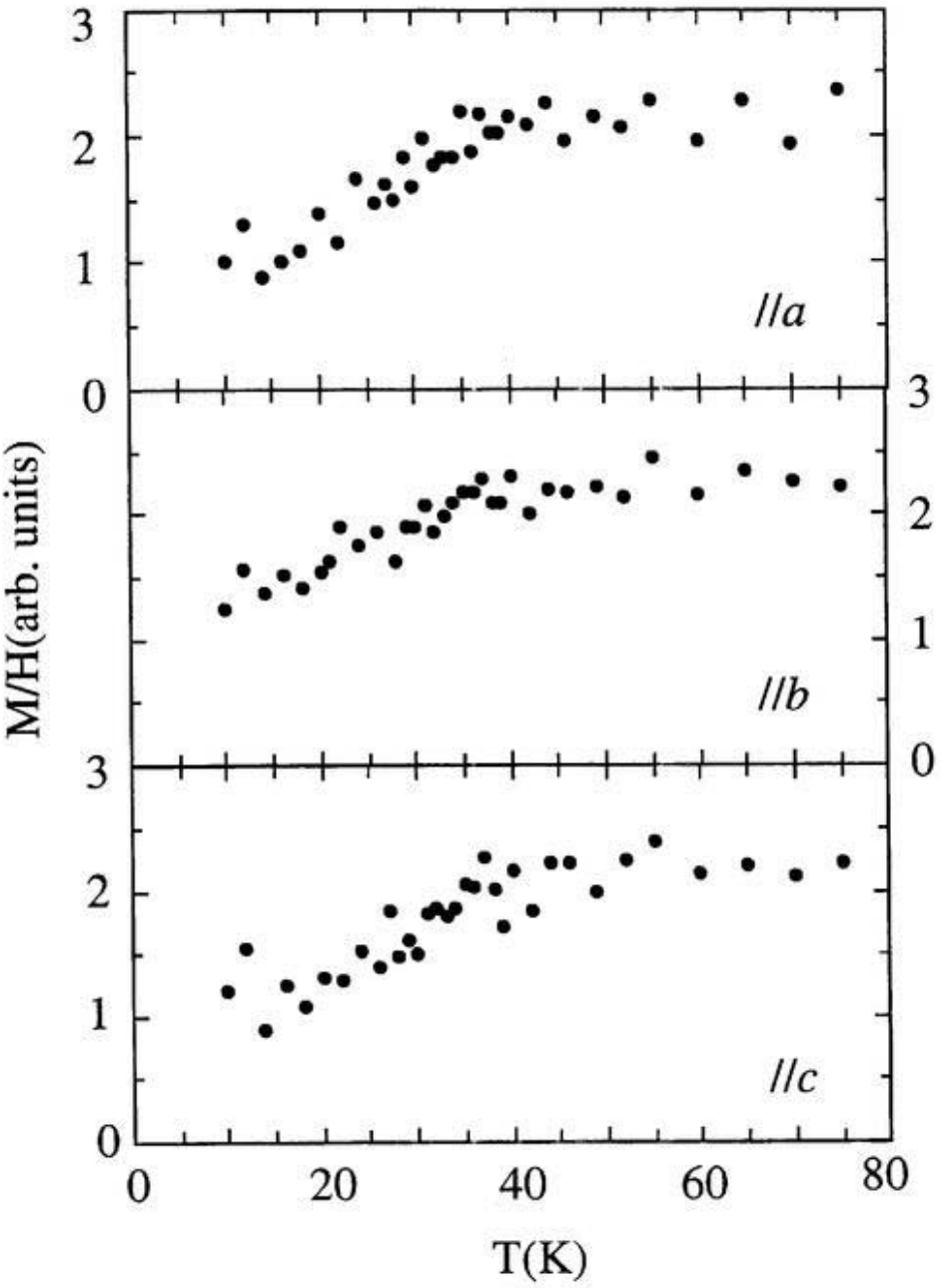

Fig4.10. Anisotropy of temperature dependences of the magnetic susceptibilities of **5**.

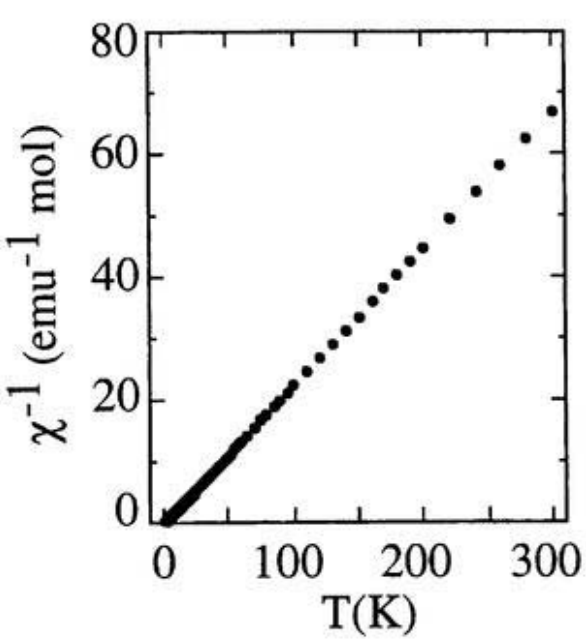

(a)

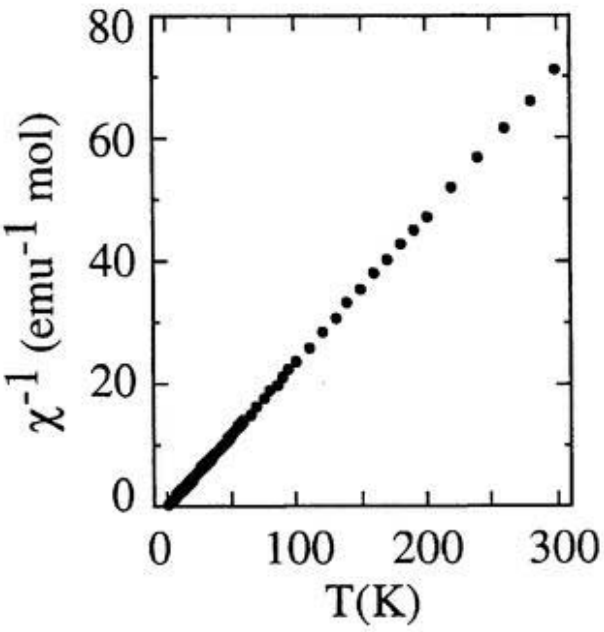

(b)

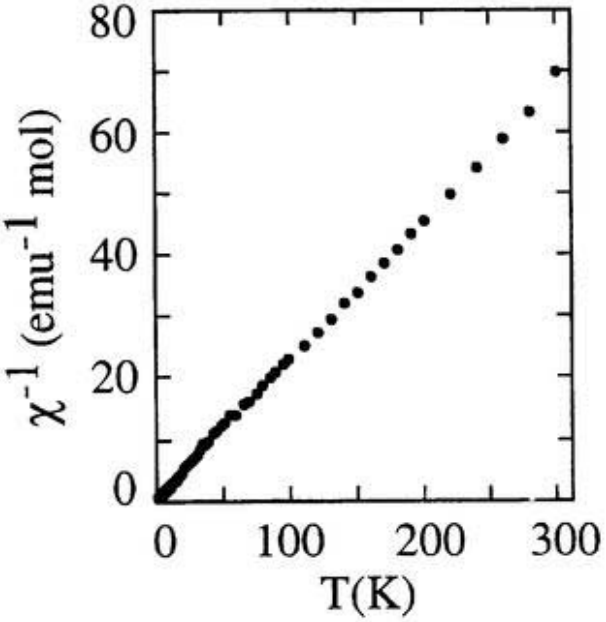

(c)

Fig.4.11. Temperature dependences of the reciprocal value of magnetic susceptibilities of (a) **2**, (b) **4** and (c) **6**.

4.4.3 X-ray oscillation photographs and crystal structures at low temperature

X-ray oscillation photograph of **1** at room temperature was compared with that of below 50 K (see Fig.4.12(a)). Below 50 K, new diffuse reflections appeared between the layers of main Bragg reflections indicating doubling of the lattice constant along the donor stacking direction (parallel to the *c*-axis)(or the four-folded modulation of molecular stacking structure). The X-ray oscillation photographs of **2** also showed the two-folded satellite diffraction spots. Similar X-ray photographs of **1** and **2** suggest that the lattice modulation is originated from the π-electron systems.

X-Ray diffuse scattering experiments were also carried out for **3** and **5**, in order to obtain the information on the origin of the resistivity increase at low temperature. However, no distinct extra spots appeared on the oscillation photographs for both of **3** and **5** below 40 K (see Fig.4.12(b)). Therefore the distortion of crystal lattice will be very small even if it develops below 40 K. Temperature dependences of the lattice constants of **3** were measured. Roughly speaking, temperature dependence of each axis was linear but the lattice constants could not be determined accurately enough to detect the possible anomaly around 40 K. Thermal expansion coefficients (α) are : $\alpha_a = 9.59 \times 10^{-5}$ K^{-1}, $\alpha_b = 1.73 \times 10^{-5}$ K^{-1}, $\alpha_c = 2.71 \times 10^{-5}$ K^{-1}, $\alpha_V = 1.46 \times 10^{-5}$ K^{-1} (see Fig.4.13).

Crystal structures of **3** and **5** were determined at 17 K and 7 K, respectively. Space groups of both structures belonged to $P2_1/m$, which was the same at room temperature. The bond lengths and angles of **3** and **5** determined at the low temperature are in good agreement with the corresponding room-temperature values. The intermolecular distances are 3.46 and 3.47 Å in **3** at 17 K and 3.51 and 3.69 Å in **5** at 7 K. No significant change was observed on the overlapping modes in both **3** and **5**.

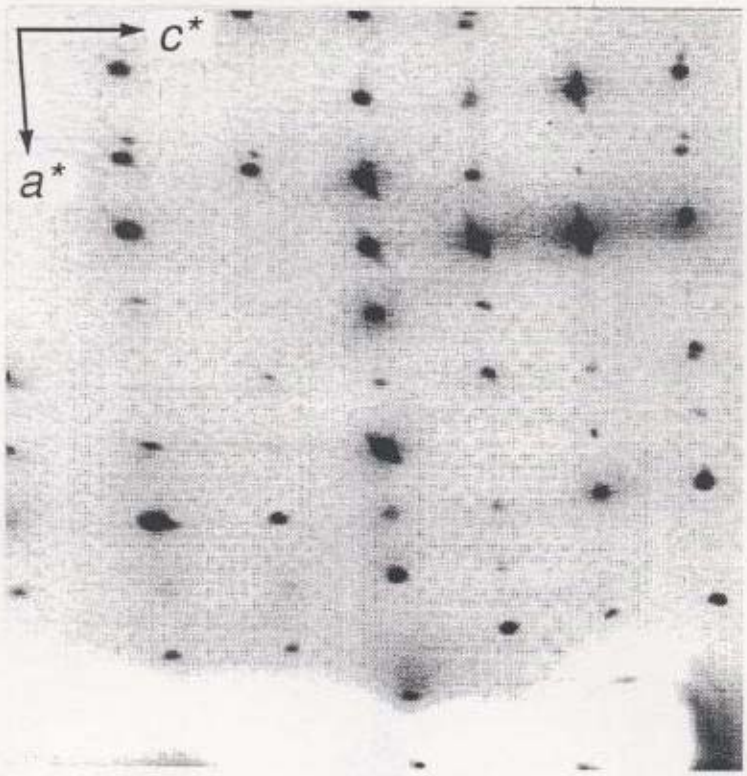

room temperature

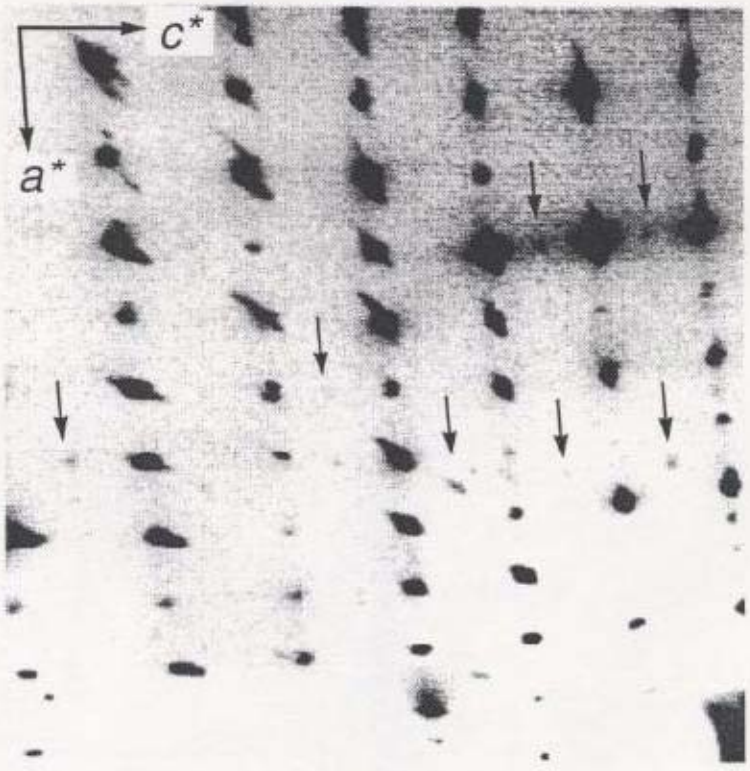

7 K

(a)

Fig.4.12. X-ray oscillation photographs of (a) **1** and (b) **5**.

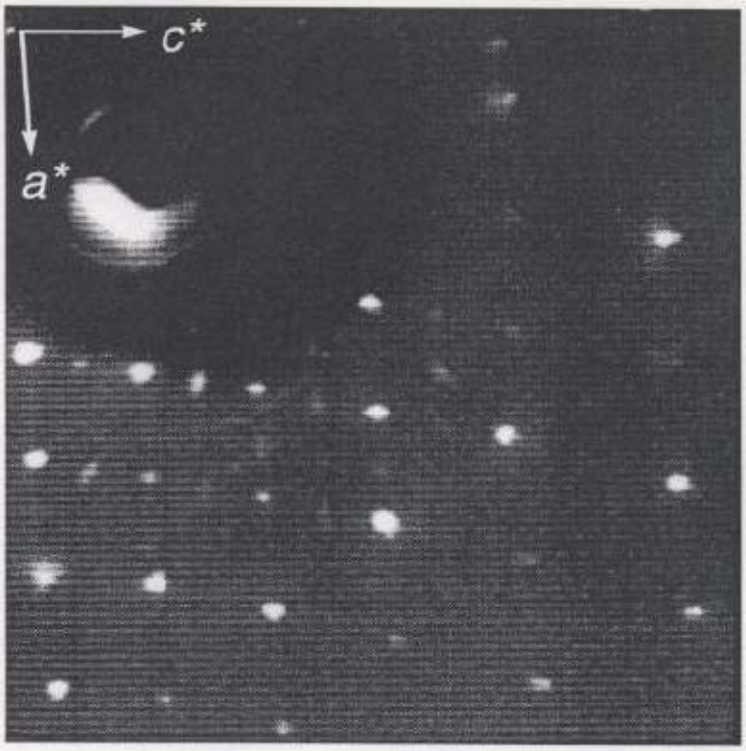

room temperature

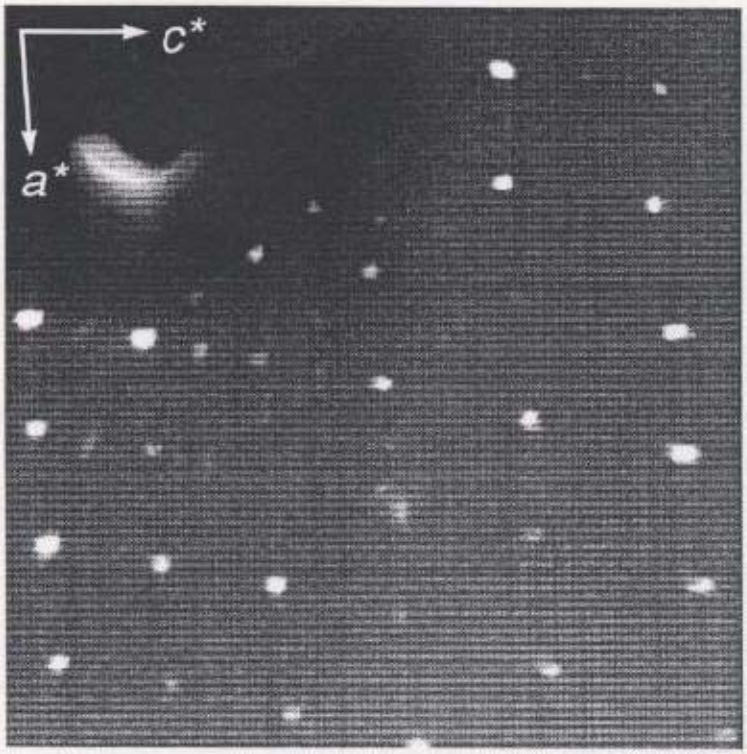

7 K

(b)

Fig.4.12. X-ray oscillation photographs of (a) **1** and (b) **5**. (continued)

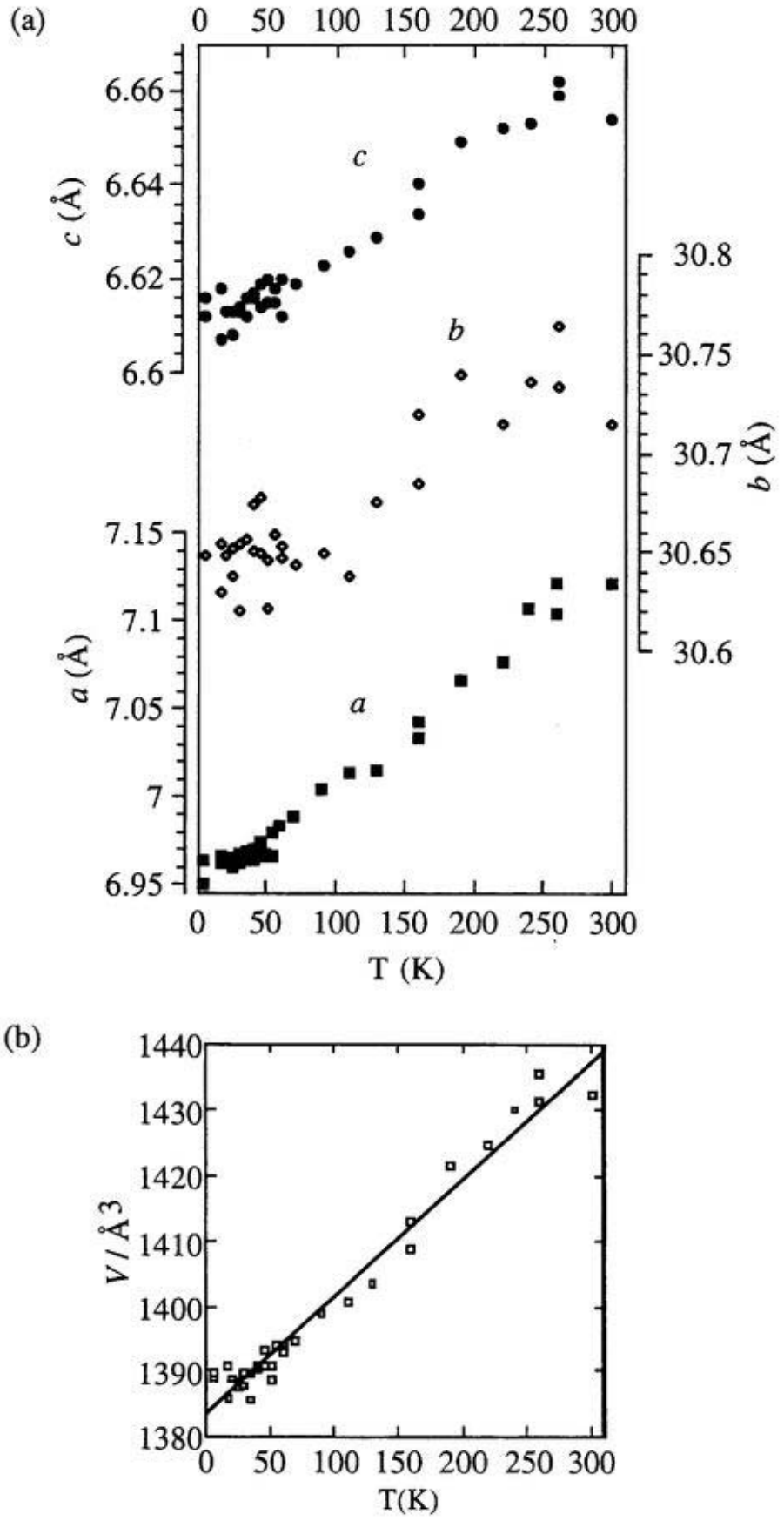

Fig.4.13. Temperature dependences of the lattice constants of **3**.

4.5 *Ground state*

The extended Hückel band structure calculations suggested the EDT-TTF salts (**1** and **2**) to be quasi 1D metals. However, the semiconducting behavior of these salts shows the calculated 1D Fermi surfaces to be artificial. This discrepancy is considered to be originated from the effect of large Coulombic repulsion (U), which makes the system to be an insulator when $U >> t$ (transfer integral). It is well known that the difference between the first and second oxidation potential ($\Delta E = E^2_{1/2} - E^1_{1/2}$) of donor molecule can be regarded as a measure of U. The cyclic voltammograms of EDT-TTF, EDST and EDTS were examined. The obtained ΔE was : EDT-TTF 0.42 eV, EDST 0.35 eV, EDTS 0.37 eV. As shown in Table 4.7, the intermolecular overlap integrals a and b of EDT-TTF salt were much smaller than those of EDST and EDTS salts. This indicates the existence of so-called Mott-Hubbard gap in EDT-TTF conductors **1** and **2**, where the π electrons tend to be localized. The small paramagnetic susceptibility indicates the antiferromagnetic interaction between localized π electrons. It is well known that the one-dimensional antiferromagnetic Heisenberg chain tends to transform to non-magnetic ground state accompanied with periodic lattice distortion (spin-Peierls transition). The sharp decrease of the susceptibility and development of the X-ray reflection spots of **1** below 50 K suggest the spin-Peierls transition. Similar transition will be expected in **2**. The lack of the spin-Peierls behavior in the magnetic susceptibility of **2** is consistent with the high-spin state of Fe ions, which makes the contribution of π electrons inconspicuous in the total magnetic susceptibility.

In the systems of **3-6**, the temperature dependence of the resistivity suggest the MI transition around 40 K. However the periodic lattice modulations were not observed below T_{MI} and the magnetic susceptibility tends to be constant at low temperature. One plausible reason why X-ray diffraction experiments of **3-6** could not detect the extra reflections, might be the incomplete nesting of Fermi surfaces, which is unfavorable for the development of the large periodic lattice distortion (or development of extra X-ray reflection). Thus, the systems of **3-6** are considered to be in the semimetallic state at the low temperature.

Similar to TM systems, the crystal structures of EDT-TTF family have diadic columns

and quasi-1D electronic structures. Moreover, two of EDT-TTF salts (**1** and **2**) have the spin-Peierls ground state, which is reminiscent of $(TMTTF)_2PF_6$. As mentioned before, in a series of TMs conductors, the ground state of the system takes spin-Peierls insulating state, SDW insulating state, SC state and metallic state with increasing (chemical) pressure. However, in a series of EDTs family, there seems to be no system exhibiting SDW transition. Therefore, it may be said that the EDT-TTF series has a different "generalized phase diagram". Compared with the TMs family, EDTs family has small U: ΔE(eV)=0.48 (TMTTF), 0.39 (TMTSF), 0.42 (EDT-TTF), 0.35 (EDST), 0.37 (EDTS). This indicates that the value of t/U is relatively large in EDTS and EDST conductors. Then the electron-lattice interaction will become more important. In addition, the calculated Fermi surfaces of EDST and EDTS salts seem to be more roundish than those of $(TMTSF)_2X$ salts. It is considered that the enhancement of dimensionality in the EDTs system prevents the complete nesting of Fermi surface, and the two of selenium-substituted analogues, EDST and EDTS salts, will take the semimetallic state at low temperature.

4.6 *Summary*

Crystal structure determinations and the resistivity and magnetic susceptibility measurements of **1-6** were carried out. All the crystals were isostructural to each other. The donor molecules stacked almost regularly and the tetrahalide ions located on the mirror planes. The temperature dependences of the resistivity of **1** and **2** were semiconductive. The temperature dependence of the paramagnetic susceptibility of **1** decreases gradually with lowering temperature and then sharply to zero below 50 K. The satellite X-ray reflections showing the doubling the lattice constants along the donor stacks (// the *c*-axis) were observed below 50 K, which indicates the spin-Peierls ground state. The magnetic susceptibility of **2** exhibited the Curie's law. The X-ray oscillation photographs showed the doubling of the lattice periodicity *c* below 50 K. The π-spins and the *d*-spins of Fe^{3+} ions seemed to be almost independent in **2**. Probably π electron system is in spin-Peierls state. In **3**, **4**, **5** and **6**, the temperature dependences of the resistivity were metallic down to *ca.* 40 K, below which the resistivity increased gradually. Magnetic susceptibilities of **3** and **5** decreased gradually down to *ca.* 40 K and then sharply below it, however it was not shown that the system of **3-6** took a non-magnetic state at low temperature. No extra X-ray spots was observed on the X-ray oscillation photographs of **3** and **5**. The crystal structure analyses also indicated no structural change down to the low temperature.

References

[1] D. Jérome, A. Mazaud, M. Ribault and K. Bechgaad, *J. Phys. Lett. (Paris)*, **41**, L-95 (1980).

[2] D. Jérome, H. Schulz, *Adv. Phys.*, **31**(4), 299 (1982).

[3] *Organic conductors, Fundamentals and applications*, ed by J.-P. Farges, New York, Basel, Hong Kong (1994).

[4] (a) R. Kato, H. Kobayashi and A. Kobayashi, *Chem. Lett.*, **1989**, 781. (b) A. Kobayashi, R. Kato and H. Kobayashi, *The Physics and Chemistry of Organic Superconductors*, ed. G.Saito and S. Kagoshima, *Springer Proceedings in Physics*, **51**, 302 (1990).

[5] (a) R. Kato, H. Kobayashi, A. Kobayashi, T. Naito, M. Tamura, H. Tajima and H. Kuroda, *Chem. Lett.*, **1989**, 1839. (b) H. Tajima, M. Inokuchi, A. Kobayashi, T. Ohta, R. Kato, H. Kobayashi and H. Kuroda, *Chem. Lett.*, **1993**, 1235. (c) H. Tajima, M. Inokuchi, S. Ikeda, M. Arifuku, T. Naito, M. Tamura, T. Ohta, A. Kobayashi, R. Kato, H. Kobayashi and H. Kuroda, *Synth. Met.*, **70**, 1035 (1995). (d) M. Inokuchi, H. Tajima, T. Ohta, H. Kuroda, A. Kobayashi, A. Sato, T. Naito and H. Kobayashi, *J. Phys. Soc. Jpn*, **65**(2), 538 (1996). (e) H. Tajima, A. Kobayashi, Y. Ootuka, A. Sato, T. Naito and H Kobayashi, *Synth. Met*, **79**, 141 (1996). (f) H. Tajima, M. Inokuchi, A. Kobayashi, A. Sato, T. Naio, H. Kobayashi and H. Kuroda, *Synth. Met.*, **85**, 1585 (1997). (g) B. Garreau, B. Pomarede, C. Faulmann, J. -M. Fabre, P. Cassoux and J. -P. Legros, *C. R. Acad. Sci. Paris*, **313**(2), 509 (1991). (h) A. Kobayashi, A. Sato, K. Kawano, T. Naito, H. Kobayashi and T. Watanabe, *J. Mater. Chem.*, **5**(10), 1971 (1995).

[6] (a) T. Naito, A. Sato, K. Kawano, A. Tateno, H. Kobayashi and A. Kobayashi, *J. Chem. Soc., Chem. Commun.*, **1995**, 351. (b) A. Kobayashi, T. Naito, A. Sato and H. Kobayashi, *Sysnth. Met.*, **86**, 1841 (1997).

[7] A. Kobayashi, Private communication (1995).

[8] (a) A. Terzis, A. Hountas, A. E. Underhill, A. Clark, B. Kaye, B. Hilti, C. Mayer, J.

Pfeiffer, S. Y. Yiannopoulos, G. Mousdis and G. C. Papavassiliou, *Synth Met.*, **27**, B97 (1988). (b) G. V. Papavassiliou, G. A. Mousdis, J. S. Zambounis, A. Terzis, A. Hountas, B. Hilti, C. W. Mayer and J. Pfeiffer, *Synth. Met.*, **27**, B379 (1988).

[9] T. Mori, Y. Maruyama and H. Inokuchi, *Solid State Commun.*, **88**(6), 411 (1993).

Chapter 5

Temperature-composition phase diagram of λ-(BETS)$_2$(Fe$_x$Ga$_{1-x}$)Cl$_4$

The major part of this work has been published in; (1) Hayao Kobayashi, Akane Sato, Emiko Ojima, Hiroki Akutsu, Akiko Kobayashi, Patrick Cassoux, *J. Am. Chem. Soc.*, **119**(50), 12392 (1997). (2) Akane Sato, Emiko Ojima, Hiroki Akutsu, Hayao Kobayashi, Akiko Kobayashi, Patrick Cassoux, *Chem. Lett.*, **1998**, 673. (3) Hayao Kobayashi, Akane Sato, Hisashi Tanaka, Akiko Kobayashi, Patrick Cassoux, *Coord. Chem. Rev.*, in press.

5.1 Introduction

Recently an increasing attention is being focused on the role of the magnetic ions such as Fe^{3+} and Cu^{2+} incorporated in the organic metals. Since the interaction between the π conduction electrons in the metal band of molecular orbitals of organic molecules and the localized 3d magnetic moments of the counter ions is considered to be weak, the π-d interactions can be expected to become important only at low temperatures. Therefore, the development of stable organic metals with the magnetic anions is required to study the role of π-d interactions in organic conductors. The first stable metallic conductor having the localized moments is (BEDT-TTF)$_3$CuCl$_4$•H$_2$O [1]. The ESR *g*-value and line width of (BEDT-TTF)$_3$CuCl$_4$•H$_2$O gave no evidence of interaction between the conduction electrons and localized spin system, and the magnetic susceptibility at low temperature suggested that there was a weak short-range spin correlation of a probably intradimer type among the $CuCl_4^-$ anions [2]. In 1995, an organic superconductor with the localized d-spin of Fe^{3+}, (BEDT-TTF)$_4$[(H$_2$O)Fe(C$_2$O$_4$)$_3$]•C$_6$H$_5$CN was reported [3]. This superconductor has attracted a considerable interest because it contains Fe^{3+} ions in the high spin state. However, no

significant interaction was observed between π-electrons and magnetic moments.

BETS [bis(ethylenedithio)tetraselenafulvalene] is a BEDT-TTF-analog with four Se atoms. The systematic examination of structural and electrical properties of a series of BETS conductors has revealed that BETS compounds have a strong tendency to give stable metallic states with two dimensional molecular arrangements such as κ- and θ-type structures [4]. In other word, the BETS system enables us to study the role of the π-d interaction in organic metals at low temperature.

BETS compounds with tetrahedral anion, $(BETS)_2MX_4$ (M= Ga, Fe, In; X= Cl, Br) are polymorphic [4-5]. They have two main modifications with κ- and λ-type molecular arrangements. While the plate crystal of κ-type compounds have the metallic ground state, the needle-like crystal of λ-type compounds have the superconductor (M=Ga, X=Cl) or insulator (M=Fe, X=Cl) ground state. The crystals of λ-$(BETS)_2MX_4$ belong to the triclinic system with four-fold quasi-stacking structure of BETS molecules along the *a*-axis. The simple tight-binding band structure of λ-type compound resembles that of two-dimensional κ-type compound in spite that the difference in their molecular arrangements.

Interesting feature of λ-BETS conductors is that their electronic properties are controllable by exchanging the metal atoms of the tetrahedral anions. Non-magnetic $GaCl_4^-$ anions of λ-$(BETS)_2GaCl_4$ can be replaced by the magnetic $FeCl_4^-$ anions without significant changes in the crystal and band structures. The crystal data of λ-$(BETS)_2MCl_4$ (M= Ga, Fe) are as follows [3] : λ-$(BETS)_2GaCl_4$, triclinic system (P $\bar{1}$), a= 16.141(3) Å, b= 18.580(3) Å, c= 6.580(3) Å, α= 98.37(1) °, β= 96.77(1) °, γ= 112.55(1) °, V= 1774.0(5) Å^3; λ-$(BETS)_2FeCl_4$, triclinic system (P $\bar{1}$), a= 16.164(3) Å, b= 18.538(3) Å, c= 6.593(1) Å, α= 98.40(1) °, β= 96.67(1) °, γ= 112.52(1) °, V= 1773.0(5) Å^3.

While λ-$(BETS)_2GaCl_4$ has a superconducting ground state, λ-$(BETS)_2FeCl_4$ undergoes a metal-insulator (MI) transition [5,6]. This difference in the ground state between these salts is undoubtedly originated from the difference in their magnetic nature of the anions. In λ-$(BETS)_2FeCl_4$, the metal-insulator (MI) and antiferromagnetic (AF) transitions take place cooperatively at 8.5 K [7,8]. The magnitude of paramagnetic susceptibility of λ-$(BETS)_2FeCl_4$ above T_{MI} shows that Fe^{3+} is in the high spin state (S= 5/2), and the system transforms into the

AF state where the spin-flop field is about 1 T [9].

In the present study, the magnetic properties of the organic alloy with magnetic and non-magnetic anions, λ-$(BETS)_2(Fe_xGa_{1-x})Cl_4$ were investigated. In this chapter, the details of the electronic property, magnetic property and the temperature-composition phase diagram of λ-$(BETS)_2(Fe_xGa_{1-x})Cl_4$ will be described.

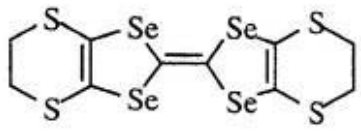

BETS

5.2 *Experimental*

5.2.1 *Preparation of λ-(BETS)$_2$(Fe$_x$Ga$_{1-x}$)Cl$_4$*

The crystals of λ-(BETS)$_2$(Fe$_x$Ga$_{1-x}$)Cl$_4$ were obtained electrochemically. BETS (8-10 mg) and the mixed supporting electrolytes of [(C$_2$H$_5$)$_4$N]FeCl$_4$ and [(C$_2$H$_5$)$_4$N]GaCl$_4$ with suitable mixing ratio (*ca.* 50-60 mg in total) were dissolved in 20 ml of 10 % ethanol-containing chlorobenzene solution. After over-night standing, a constant voltage of 3.1-3.3 V was applied for 12-31 days at 20 °C (see Table 5.1). The thin needle crystals of λ-type were obtained together with the plate crystals of κ-type. Electrolytic conditions are given in Table 5.1.

The ratio of Fe^{3+} to Ga^{3+} in the crystals were determined by EPMA (electron probe microanalysis). Three or four single crystals selected from each batch were attached on a carbon tape and several points on each single crystals were examined by Scanning Electron Microscope, S-450 (Hitachi, Co. Ltd.). Data were accumulated for 200 seconds with the time constants of 12 microseconds. Data collections and analyses were controlled by the Delta Class Analyzer (Kevex). The concentration of Fe^{3+} (x) were also calculated from the magnitude of the magnetic susceptibility at 15 K.

Table 5.1 Electrolytic conditions for preparation of λ-(BETS)$_2$(Fe$_x$Ga$_{1-x}$)Cl$_4$.[a]

Product	BETS (mg)	FeCl$_4$ (mg)	GaCl$_4$ (mg)	voltage (V)	time (days)
Ga	5.1	0	106.7	3.3	31
	5.5	0	87.3	3.3	31
Fe$_{0.02}$Ga$_{0.98}$	6.1	0.1	70.4	3.3	14
	5.3	0.2	71.1	3.3	14
Fe$_{0.11}$Ga$_{0.89}$	5.3	1.1	57.1	3.3	17
Fe$_{0.20}$Ga$_{0.80}$	6.2	8.0	34.1	3.1	20
Fe$_{0.27}$Ga$_{0.73}$	5.4	3.3	51.3	3.2	40
Fe$_{0.36}$Ga$_{0.64}$	5.4	3.3	51.3	3.2	40

Table 5.1 Electrolytic conditions for preparation of λ-$(BETS)_2(Fe_xGa_{1-x})Cl_4$.[a] (continued)

Product	BETS (mg)	$FeCl_4$ (mg)	$GaCl_4$ (mg)	voltage (V)	time (days)
$Fe_{0.42}Ga_{0.58}$	5.1	15.0	31.2	3.3	12
$Fe_{0.47}Ga_{0.53}$	6.5	24.5	32.0	3.3	31
$Fe_{0.50}Ga_{0.50}$	5.6	23.0	36.0	3.3	7
$Fe_{0.55}Ga_{0.45}$	5.0	20.9	20.9	3.1	24
$Fe_{0.63}Ga_{0.37}$	6.4	24.0	11.9	3.1	14
$Fe_{0.68}Ga_{0.32}$	5.9	43.3	18.6	3.3	14
$Fe_{0.74}Ga_{0.26}$	5.3	40.6	7.7	3.1	14
$Fe_{0.88}Ga_{0.12}$	5.0	57.8	3.3	3.3	12
$Fe_{0.95}Ga_{0.05}$	5.0	57.8	3.3	3.3	12
Fe	8.0	56.9	0	3.5	20
	9.4	55.6	0	3.5	18

a Abbreviations in Table. 5.1 are: $FeCl_4$= $[(C_2H_5)_4N]FeCl_4$, $GaCl_4$= $[(C_2H_5)_4N]GaCl_4$, Ga= λ-$(BETS)_2GaCl_4$, Fe_xGa_{1-x}= corresponding the concentration (x) of Fe^{3+} to λ-$(BETS)_2(Fe_xGa_{1-x})Cl_4$, Fe= λ-$(BETS)_2FeCl_4$.

5.2.2 Magnetic susceptibility measurements

Anisotropic magnetic properties

Since the physical properties of λ-$(BETS)_2(Fe_xGa_{1-x})Cl_4$ are very sensitive to even small pressure produced by freezing of grease used to keep the crystals in the glass capillaries, the preparation of oriented thin needle crystals was made very carefully according to the following procedure. The use of grease was avoided. 0.4-1 mg of crystals of λ-$(BETS)_2(Fe_xGa_{1-x})Cl_4$ oriented along the needle direction (//c-axis) were put in a quartz capillary (inner diameter : 0.5-0.7 mmϕ; length: *ca.* 4mm). This quartz capillary containing the crystals was wrapped by a 5 mm^2 aluminum foil packet. The magnetic fields were applied to parallel (//c) or perpendicular ($\perp c$) to the c-axis.

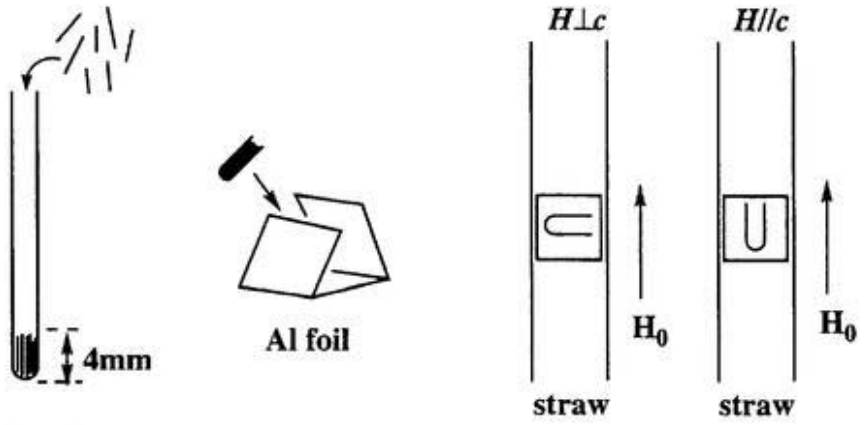

Fig.5.1. Illustration of the sample preparation and setting for the magnetic susceptibility measurements.

The DC susceptibilities of λ-$(BETS)_2(Fe_xGa_{1-x})Cl_4$ (x= 0, 0.27, 0.43, 0.47, 0.55, 0.70 and 1) were measured in the temperature range of 2-15 K. The field dependence of the magnetization (M-H curve) was measured at 2 K up to 7 T. Magnetic susceptibility of λ-$(BETS)_2(Fe_{0.47}Ga_{0.53})Cl_4$ was measured under an AC field of 0.1 Oe amplitude and zero or several Oe of DC field.

Weiss temperature

The Weiss temperatures were obtained from the Curie-Weiss fitting of the susceptibilities of the unoriented polycrystalline samples. 1-2 mg of λ-$(BETS)_2(Fe_xGa_{1-x})Cl_4$ (x= 0, 0.02, 0.11, 0.2, 0.36, 0.43, 0.5, 0.55, 0.63, 0.74, 0.88 and 1) were wrapped in the pieces of aluminum foils and their susceptibilities were measured in the temperature range of 2-300 K under 5-10 kOe.

Magnetic susceptibilities were corrected by subtracting the Pascal's diamagnetic contribution [9].

5.3 EPMA Analyses of λ-$(BETS)_2(Fe_xGa_{1-x})Cl_4$

As mentioned before, the crystals of $(BETS)_2MCl_4$ (M= Ga, Fe) are polymorphic [4,5]. In most cases, κ-phase was a major product and λ-phase was a miner one. Crystal growth of λ-$(BETS)_2(Fe_xGa_{1-x})Cl_4$ was depend sensitively on the amount of the supporting electrolytes and the applied voltage. Usually 5-7 mg of BETS was used (8.7-12.2 mmol). The best conditions for the growth of λ-type crystals were as follows: the amount of sum of two supporting electrolytes, $[(C_2H_5)_4N]FeCl_4$ and $[(C_2H_5)_4N]GaCl_4$ and the applied voltage were about 40 mg and 3.1 V or about 60 mg and 3.3 V where 20 ml of the mixed solution of chlorobenzene and ethanol (9:1, v/v) were used. Length of the standing hours of the electrolytic cell before starting the electrocrystallization was also an important factor for obtaining good crystalline samples. The interval of 12 hours gave good results. Electrolyses in other conditions gave frequently almost only κ-type crystals or small amount of λ-type crystals.

The close similarity of the lattice constants of λ-$(BETS)_2FeCl_4$ and λ-$(BETS)_2GaCl_4$ suggests that $FeCl_4^-$ and $GaCl_4^-$ ions can be readily replaced by each other. In the cases of λ-$(BETS)_2GaBr_xCl_{1-x}$ and λ-$(BETS)_2FeBr_xCl_{1-x}$, the x-value (Br-content) can be estimated from the unit cell volume [12,13]. But it was difficult to determine the composition of Fe/Ga from the lattice parameters, because the atomic radii of Fe and Ga resemble to each other. The Fe/Ga composition was tried to determine by the atomic population refinements in X-ray structure analyses, but it was not so successful. Therefore the composition was determined by EPMA.

Figure 5.1 shows the relation between the mixing ratio of $[(C_2H_5)_4N]FeCl_4$ to $[(C_2H_5)_4N]GaCl_4$ in the solution (x_{sol}) and the x-value of the crystal (x_{cryst}). The x_{sol}-value was in good agreement with x_{cryst} around $0.4<x<0.6$. But Fe^{3+} ions tended to be included preferentially in the small-x region ($x<0.3$) and Ga^{3+} ions tended to be included somewhat preferentially in the large-x region ($x>0.7$). The Fe^{3+}/Ga^{3+} ratio tends to be scattered for crystal to crystal in the large-x ($x>0.9$) and small-x ($x<0.1$) regions. However, the results of EPMA measurements indicates that crystals of λ-$(BETS)_2(Fe_xGa_{1-x})Cl_4$ can be regarded as fairly homogeneous organic conductors.

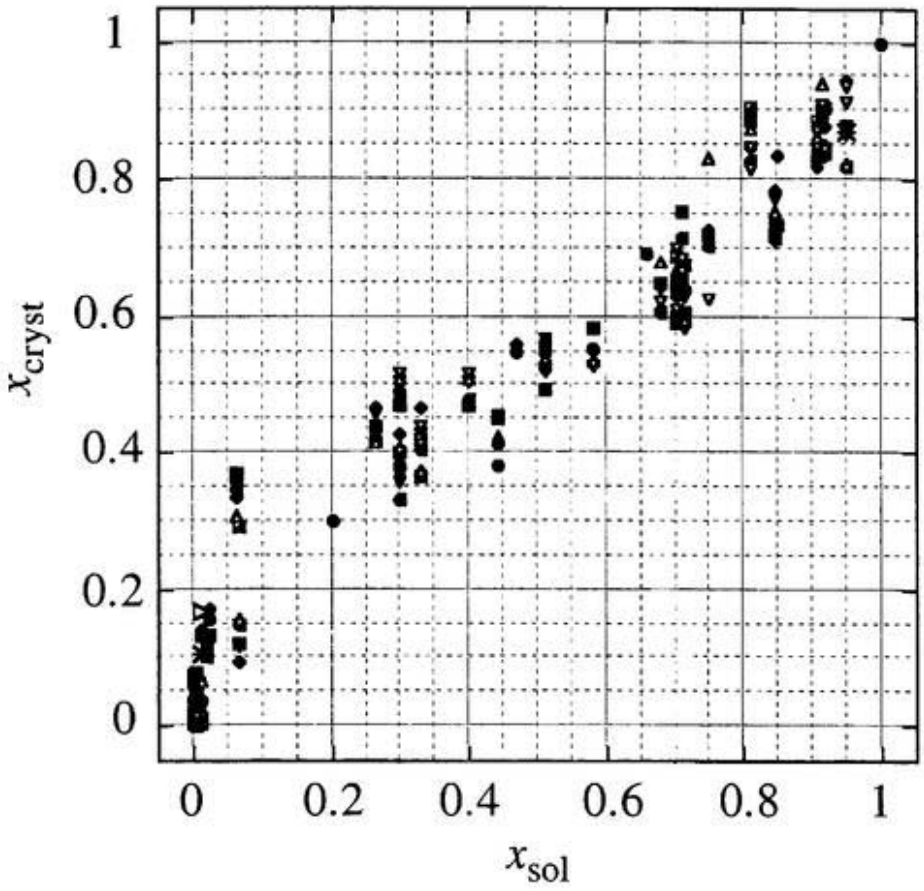

Fig. 5.1. The relation between x of the crystal (x_{cryst}) determined by EPMA and the mixing ratio of $[(C_2H_5)_4N]FeCl_4$ and $[(C_2H_5)_4N]GaCl_4$ in the solution (x_{sol}), from which the crystals were grown.

5.4 *Electrical properties*

Several years ago, it was reported that λ-$(BETS)_2(Fe_xGa_{1-x})Cl_4$ ($x \approx 0.5$) exhibited a superconducting transition around 4.5 K [14]. At that time, the systematic examinations of the resistivities of λ-$(BETS)_2(Fe_xGa_{1-x})Cl_4$ ($0 < x < 1$) were made down to 4.2 K and many interesting resistivity behaviors observed. Nevertheless, any definite results could not be obtained mainly due to the insufficient quality of the crystals (large sample dependence) and the limitation of the lowest experimental temperature of 4.2 K, which did not permit us to disclose a new transport phenomena hidden just below 4.2 K. Recently, an unprecedented superconductor-to-insulator transition was discovered in our laboratory. In this chapter, the resistivity behavior of λ-$(BETS)_2(Fe_xGa_{1-x})Cl_4$ is described to make clear the meaning of the susceptibility studies to be described below.

Temperature dependences of the electrical resistivities of λ-$(BETS)_2(Fe_xGa_{1-x})Cl_4$ (x= 0, 0.13, 0.55, 0.74 and 1) are shown in Fig.5.2. The values of the electrical resistivity of the λ-$(BETS)_2(Fe_xGa_{1-x})Cl_4$ were approximately independent on x ($\rho_{RT} \approx 30$ S cm^{-1}). The temperature dependence of the resistivity above 10 K was essentially the same for all the crystals. The resistivity increases gradually with reducing temperature down to *ca.* 90 K. Below 90 K, the resistivity decreased fairly rapidly down to about 10 K and below 10 K, the resistivity behavior changed systematically with x. At $x < 0.35$, the system underwent a superconducting transition. Superconductor transition temperature (T_c) gradually increased with decreasing x. At $x > 0.5$, the system showed the metal-insulator (MI) transition. The MI transition temperature (T_{MI}) was reduced from 8.5 K (x= 1) to about 4.5 K ($x \approx 0.55$) with decreasing in x. T_c and T_{MI} are listed in Table 5.2. The on-set temperature of the resistivity drop was dependent on the sample. But the on-set temperature (the temperature, where the resistivity reduces sharply to zero) exhibited a systematic x-dependence. Therefore, the off-set temperatures were taken.

Table 5.2. Critical temperatures (T_c, and T_{MI} or $T_{SC\text{-}I}$) of λ-$(BETS)_2(Fe_xGa_{1-x})Cl_4$.

Compounds	T_c (K)	T_{MI} or $T_{SC\text{-}I}$ (K)
λ-$(BETS)_2GaCl_4$	6	
λ-$(BETS)_2(Fe_{0.13}Ga_{0.87})Cl_4$	5.4	
λ-$(BETS)_2(Fe_{0.35}Ga_{0.65})Cl_4$	4.8	
λ-$(BETS)_2(Fe_{0.45}Ga_{0.55})Cl_4$	4.2	3.1
λ-$(BETS)_2(Fe_{0.55}Ga_{0.45})Cl_4$		4.5
λ-$(BETS)_2(Fe_{0.63}Ga_{0.37})Cl_4$		5.8
λ-$(BETS)_2(Fe_{0.74}Ga_{0.26})Cl_4$		6.2
λ-$(BETS)_2FeCl_4$		8.5

As shown in Fig.5.3, the resistivity of λ-$(BETS)_2(Fe_{0.43}Ga_{0.57})Cl_4$ showed a superconducting transition at 4.0-4.5 K and a subsequent superconductor-to-insulator (SC-I) transition at 3.0-3.6 K. λ-$(BETS)_2(Fe_{0.55}Ga_{0.45})Cl_4$ showed the MI transition at 4.5 ± 0.5 K at ambient pressure but exhibited a SC-I transition at 1 kbar (Fig.5.4(b)). The resistivity of λ-$(BETS)_2(Fe_{0.35}Ga_{0.65})Cl_4$ showed a superconducting transition at 4.7 K but no indication of SC-I transition was obtained down to 0.5 K (Fig.5.5). Therefore it is considered that the crystal with $x < 0.35$ has a superconducting ground state.

According to these resistivity data, the temperature *versus* x phase diagram was obtained (Fig.5.6). T_{MI} of λ-$(BETS)_2(Fe_xGa_{1-x})Cl_4$ decreases from 8.5 K (x= 1) to 4.5 K (x= 0.5) with decreasing in x. In the region of x<0.5 the superconducting phase was appeared. T_c decreases gradually from 6 K (x= 0) to 4.2 K (x= 0.42) with increasing x. At $0.35 < x < 0.5$, SC-I transition was observed.

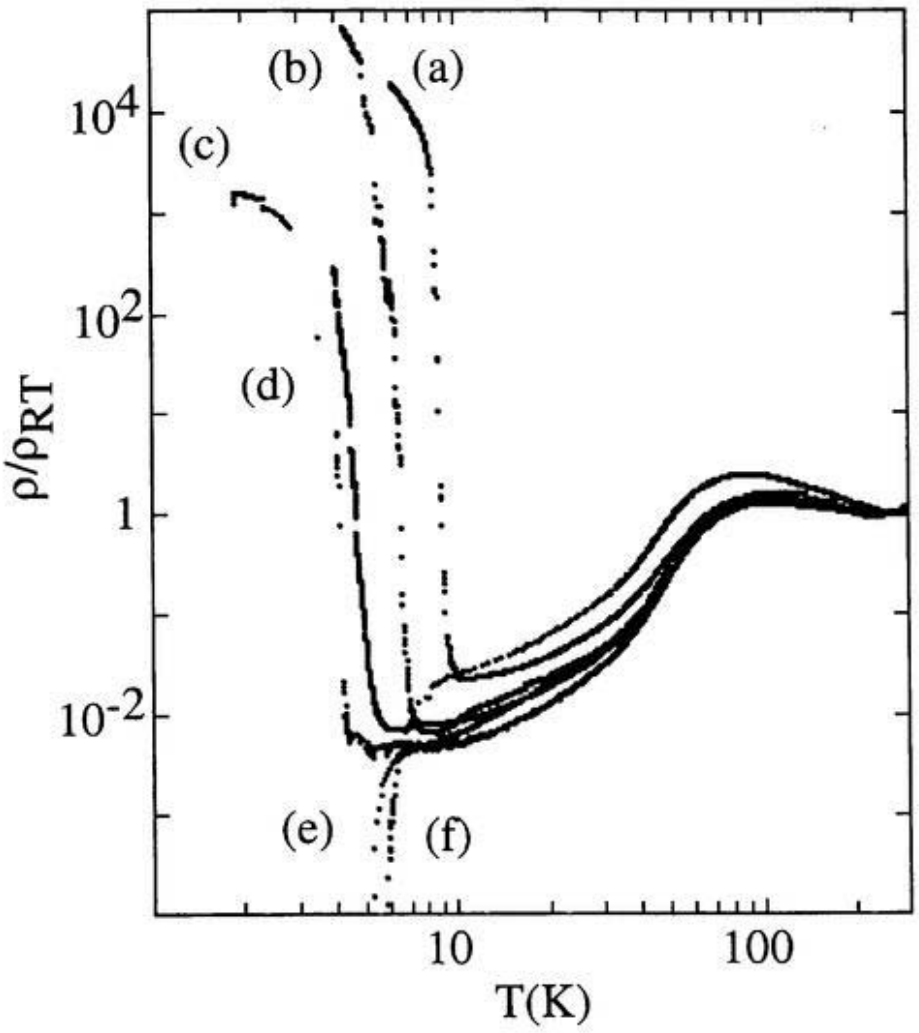

Fig.5.2. Temperature dependences of the electrical resistivities of λ-$(BETS)_2(Fe_xGa_{1-x})Cl_4$. (a) x= 1, (b) x= 0.74, (c) x= 0.63, (d) x= 0.55, (e) x= 0.13, (f) x= 0.

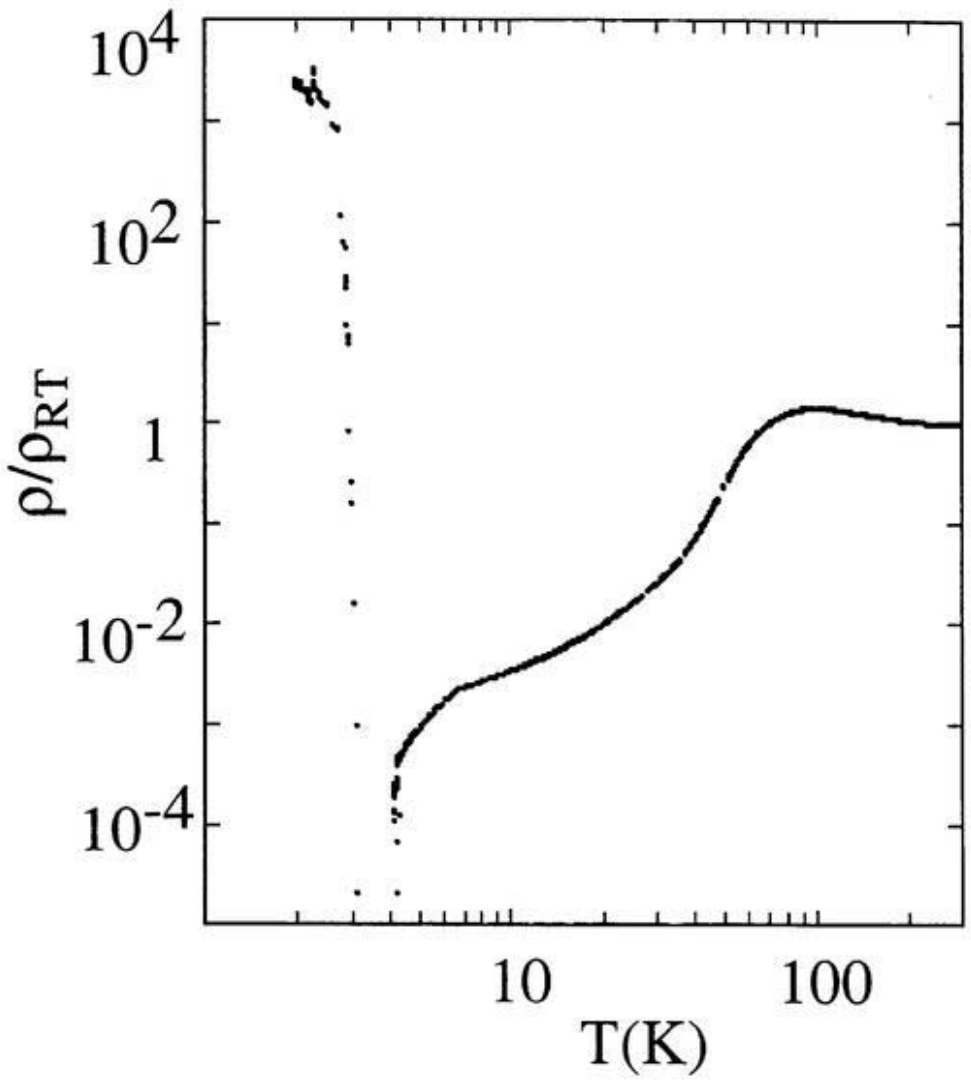

Fig.5.3. Temperature dependence of the electrical resistivity of λ-$(BETS)_2(Fe_{0.43}Ga_{0.57})Cl_4$.

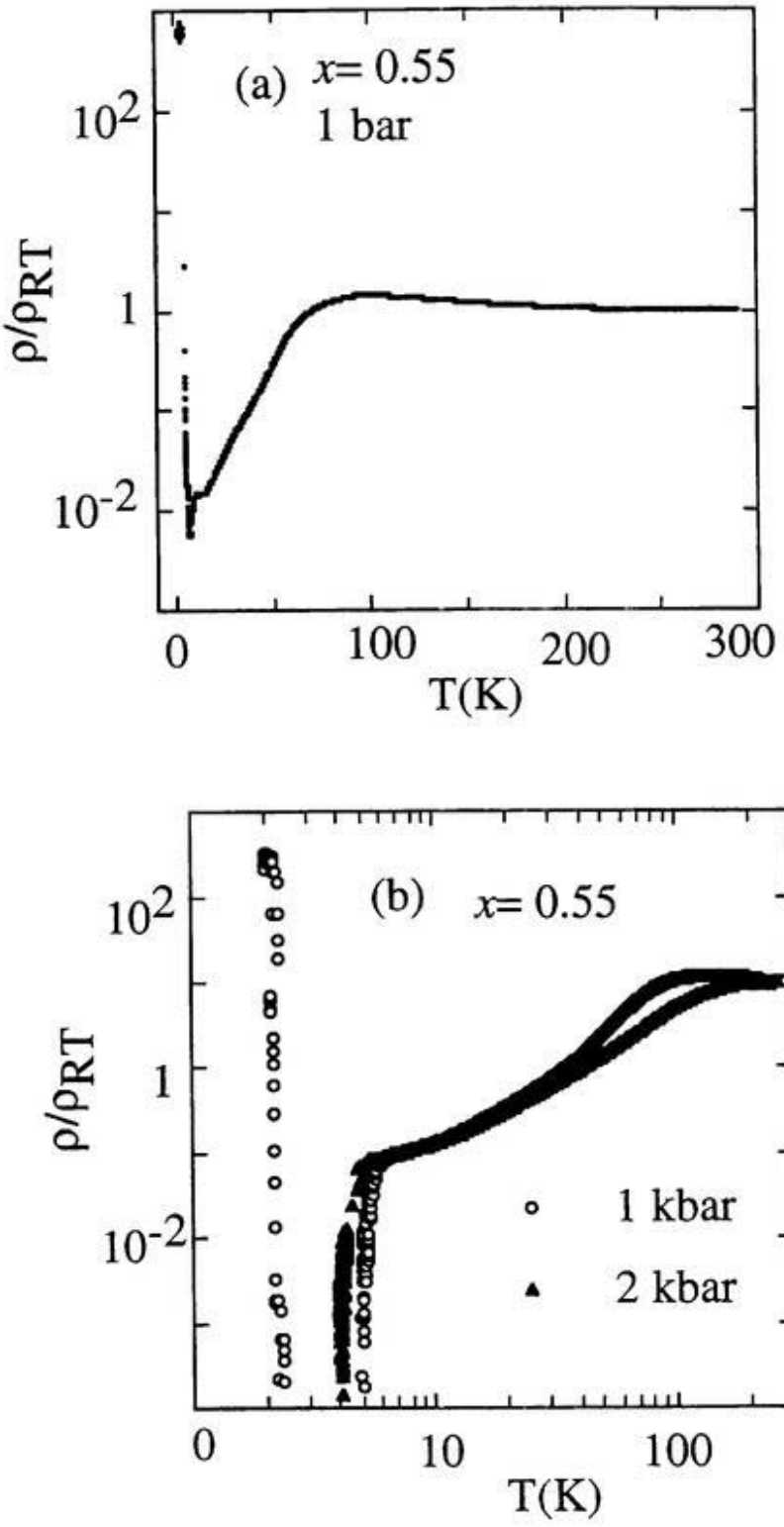

Fig.5.4. Temperature dependence of the resistivities of λ-$(BETS)_2(Fe_{0.55}Ga_{0.45})Cl_4$ (a) at ambient pressure. A small dip was observed. (b) under 1 kbar and 2 kbar.

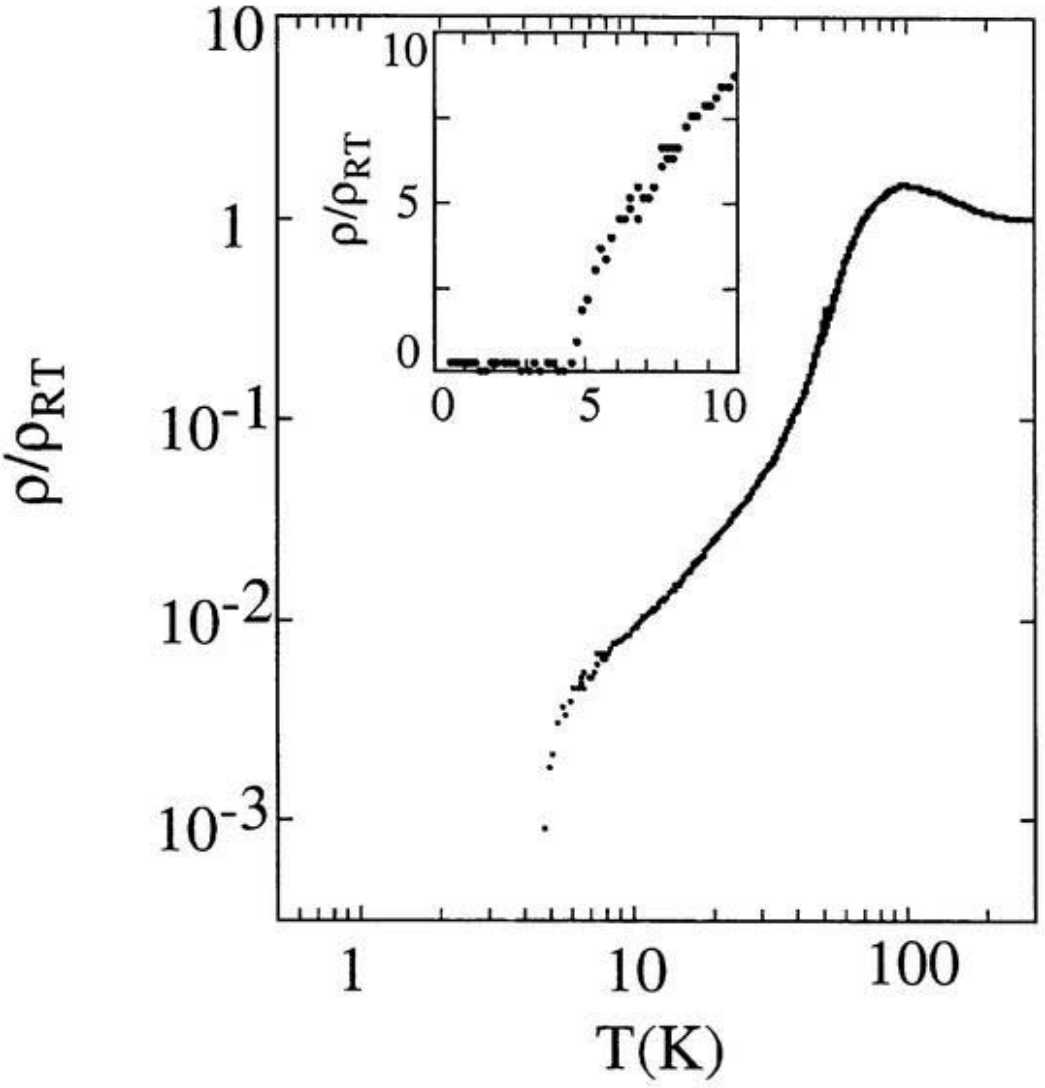

Fig.5.5. Temperature dependence of the resistivity of λ-$(BETS)_2(Fe_{0.36}Ga_{0.64})Cl_4$.

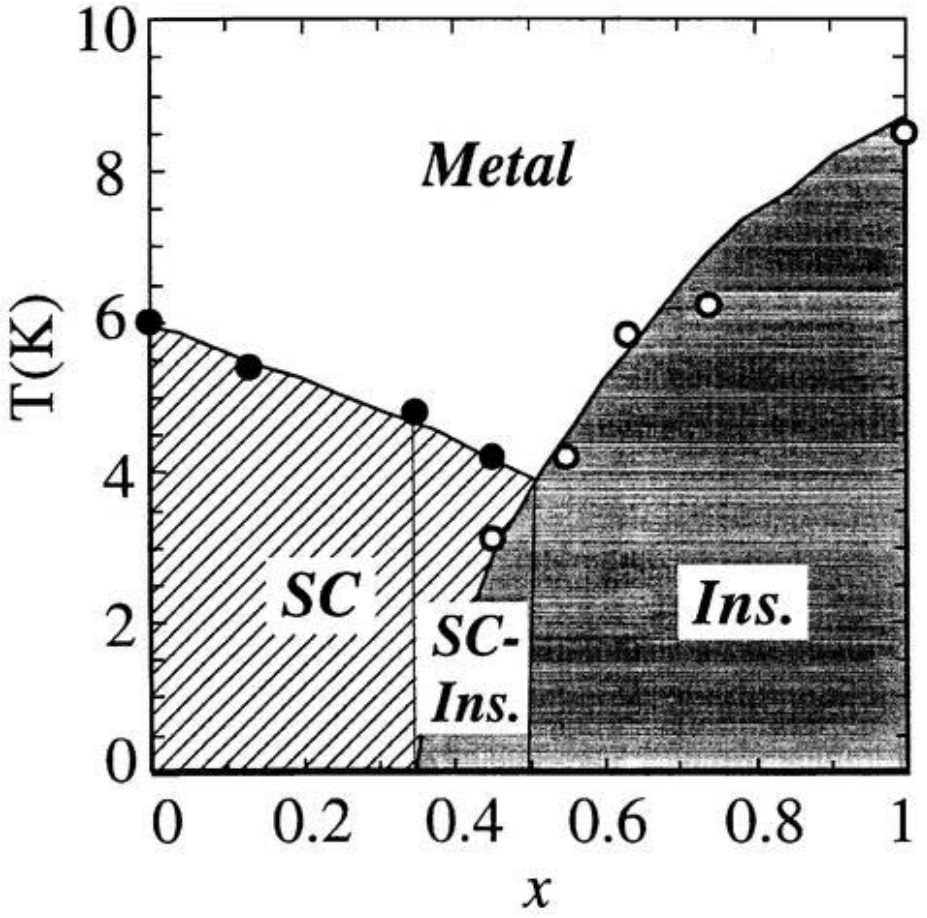

Fig.5.6. Temperature versus composition, x phase diagram of λ-$(BETS)_2(Fe_xGa_{1-x})Cl_4$. The superconductor-to-insulator (SC-I) transition is seen at $0.35<x<0.5$.

5.5 *Magnetic properties*

5.5.1 Anisotropy of the magnetic susceptibility

Superconducting phase

In the course of the systematic studies on the λ-type BETS superconductors performed under the collaboration with H. Tanaka and A. Kobayashi (The University of Tokyo), the magnetic susceptibilities of λ-$(BETS)_2GaCl_4$ were examined. Fig.5.7 shows the temperature dependence of the magnetic susceptibility of λ-$(BETS)_2GaCl_4$ at 2 Oe. Diamagnetic susceptibility was saturated when the magnetic field was applied to perpendicular to the *c*-axis ($H \perp c$). The saturation value of -57 emu/mol was 1.15 times as large as the complete diamagnetic value due to a large magnetizing effect in the present geometry. This value suggests the full Meissner volume fraction of λ-$(BETS)_2GaCl_4$. The magnetic behavior for $H \perp c$ was somewhat sluggish because the susceptibility for $H \perp c$ was regarded to be the average of the susceptibility for H//(conduction plane (//*a*)) and that for $H \perp$(conduction plane (//*b*)). On the other hand, the susceptibility value of H//c was 35% of the perfect Meissner value (χ= -50 emu/mol). These susceptibilities suggest that the superconducting state of λ-$(BETS)_2GaCl_4$ was strongly anisotropic. Magnetization curves of λ-$(BETS)_2GaCl_4$ at 2 K are shown in Fig.5.8. These magnetization curves shows that λ-$(BETS)_2GaCl_4$ is a typical Type-II superconductor, where the lower critical field (H_{c1}) seems to be lower than 11 Oe for $H \perp c$.

Similar to λ-$(BETS)_2GaCl_4$, the magnitude of diamagnetic susceptibility of the superconducting state of λ-$(BETS)_2(Fe_xGa_{1-x})Cl_4$ suggested the full Meissner state. The magnetic susceptibilities of λ-$(BETS)_2(Fe_{0.27}Ga_{0.73})Cl_4$ under the magnetic field range of 1 Oe - 10 kOe are shown in Fig.5.9. The susceptibility for $H \perp c$ was almost saturated under the magnetic field of 1 Oe and its value was about -62 emu/mol, while that for H//c was about -21 emu/mol. These values are a little larger than those of λ-$(BETS)_2GaCl_4$. By increasing the magnetic field, the magnetic state was changed from the superconducting state to the paramagnetic state. Figure 5.10 shows the *M-H* curves for the field parallel and perpendicular to the *c*-axis.

The susceptibility measurements were carried out also for the two samples, λ-

$(BETS)_2(Fe_{0.43}Ga_{0.57})Cl_4$ and λ-$(BETS)_2(Fe_{0.47}Ga_{0.53})Cl_4$ exhibiting the SC-I transition. Both samples gave essentially the same result. Fig.5.11(a) shows the AC susceptibility of $H\perp c$ of λ-$(BETS)_2(Fe_{0.47}Ga_{0.53})Cl_4$ which was measured under an AC field of 0.1 Oe in an amplitude and the zero or several Oe of DC field. A large drop associated with the SC transition was observed around 4 K and the recovery of susceptibility corresponding to the SC-I transition was observed around 3 K. The Meisnner volume fraction was estimated to be *ca.* 75 %. Considering very small temperature range of the superconducting state (3.5 - 4 K), this value was unexpectedly large and can be regarded as the first clear evidence that the SC-I transition is a bulk transition. The magnetization curve of $H\perp c$ at 4 K was shown in Fig.5.11(b). The superconducting state of $H\perp c$ was kept up to *ca.* 60 Oe.

Insulating phase

Figure 5.12 shows the susceptibility of λ-$(BETS)_2(Fe_{0.43}Ga_{0.57})Cl_4$ in the magnetic field range of 50-1000 Oe. The susceptibility drop at 50-100 Oe for $H\perp c$ around 3.5 K reflects the effect of the superconducting transition. The susceptibility drop based on the superconducting transition was almost disappeared above 200 Oe. The susceptibility becomes field-independent at 500-1000 Oe, where the fairly sharp drop of the susceptibility was observed at $T_{SC\text{-}I}$ for $H//c$.

It is reported that similar susceptibility drop (ΔM) was also observed for $H//c$ at T_{MI} in λ-$(BETS)_2FeCl_4$ system [8,11]. The magnitude of $\Delta M/H$ is more than 20 times larger than the paramagnetic susceptibility of λ-$(BETS)_2GaCl_4$. And the ratio of ΔM to total magnetization M ($\Delta M/M$) is 0.07-0.08, which is roughly equal to the ratio of the paramagnetic susceptibility of localized π spins with (S=1/2) to that of Fe^{3+} spins with S=5/2 ($(\mu_\pi)^2/(\mu_d)^2 = 0.085$). Based on these facts, a π-d coupled AF insulating structure was proposed in λ-$(BETS)_2GaCl_4$.

In the case of λ-$(BETS)_2(Fe_{0.43}Ga_{0.57})Cl_4$, ΔM and $\Delta M/M$ were estimated to be 0.04 emu/mol, and 0.15 at 3.5 K respectively (see Table 5.3). Considering the magnitude of total susceptibility of the paramagnetic state is approximately proportional to Fe-concentration of the system, the magnitude of susceptibility of λ-$(BETS)_2(Fe_{0.43}Ga_{0.57})Cl_4$ is considered to be

about 43 % of λ-$(BETS)_2FeCl_4$, which was consistent with the experimental values at 15 K Therefore, the susceptibility drop of λ-$(BETS)_2(Fe_{0.43}Ga_{0.57})Cl_4$ ($\Delta M/M$ = 0.15) will correspond to 6.5 % of M in the Fe-100 % system (0.15 × 0.43 = 0.065), which is roughly equal of the 7-8 % drop of M in λ-$(BETS)_2FeCl_4$. Thus, similar to λ-$(BETS)_2FeCl_4$, λ-$(BETS)_2(Fe_{0.43}Ga_{0.57})Cl_4$ will have a π-d coupled AF spin structure below T_{SC-I}.

Magnetic susceptibilities of λ-$(BETS)_2(Fe_{0.55}Ga_{0.45})Cl_4$ under the magnetic field of 10-1000 Oe were shown in Fig.5.13. A small drop of susceptibility observed in the $H\perp c$ around 3.5 K for the magnetic field of 10 Oe is considered to be connected to the partial superconducting behavior frequently observed in the resistivity measurements (Fig.5.4(a)). The small drop of susceptibility for $H\perp c$ almost disappeared above 50 Oe, and the susceptibilities at 500-1000 Oe showed a sharp drop for $H//c$ indicating the π-d coupled AF phase similar to those of λ-$(BETS)_2(Fe_{0.43}Ga_{0.57})Cl_4$ and λ-$(BETS)_2FeCl_4$ [8]. ΔM and $\Delta M/M$ were estimated to be 0.038 emu/mol, and 0.12 at 4 K. The 12 % drop of M of this system corresponds to 6.6 % drop in the Fe-100 % system (0.12 × 0.55 = 0.66), which is again roughly equal to the magnitude of susceptibility drop in λ-$(BETS)_2FeCl_4$.

Similar susceptibility behavior was also observed in λ-$(BETS)_2(Fe_{0.7}Ga_{0.3})Cl_4$ (Fig.5.14). ΔM and $\Delta M/M$ were estimated to be 0.02 emu/mol, and 0.092 at 4 K. The 9.2 % drop of M of this system corresponds to 6.6 % drop of M in Fe-100 % system (0.092 × 0.70 = 0.64), which is roughly equal to 7-8 % drop of M in λ-$(BETS)_2FeCl_4$.

These facts suggest that the π-d coupled AF spin structure develops in the insulating ground state of λ-$(BETS)_2(Fe_xGa_{1-x})Cl_4$ ($x > 0.35$).

Table 5.3. Susceptibility drops (ΔM) and decreasing ratios ($\Delta M/M$) of λ-$(BETS)_2(Fe_xGa_{1-x})Cl_4$.

Compounds	ΔM (emu/mol)	$\Delta M/M$	H_f (kOe)
λ-$(BETS)_2(Fe_{0.43}Ga_{0.57})Cl_4$	0.04 (4 K)	0.15	6
λ-$(BETS)_2(Fe_{0.55}Ga_{0.45})Cl_4$	0.038 (4 K)	0.12	7
λ-$(BETS)_2(Fe_{0.7}Ga_{0.3})Cl_4$	0.02 (6 K)	0.092	7.5
λ-$(BETS)_2FeCl_4$	0.012 (8.25 K)	0.07-0.08 [11]10	

Magnetization curves of λ-$(BETS)_2(Fe_xGa_{1-x})Cl_4$ (x= 0.47, 0.7 and 1) at 2 K are shown in Fig.5.15. The spin flop transitions were observed for $H//c$. The spin-flop field (H_f) decreases almost linearly with decreasing in x (Fig.5.16).

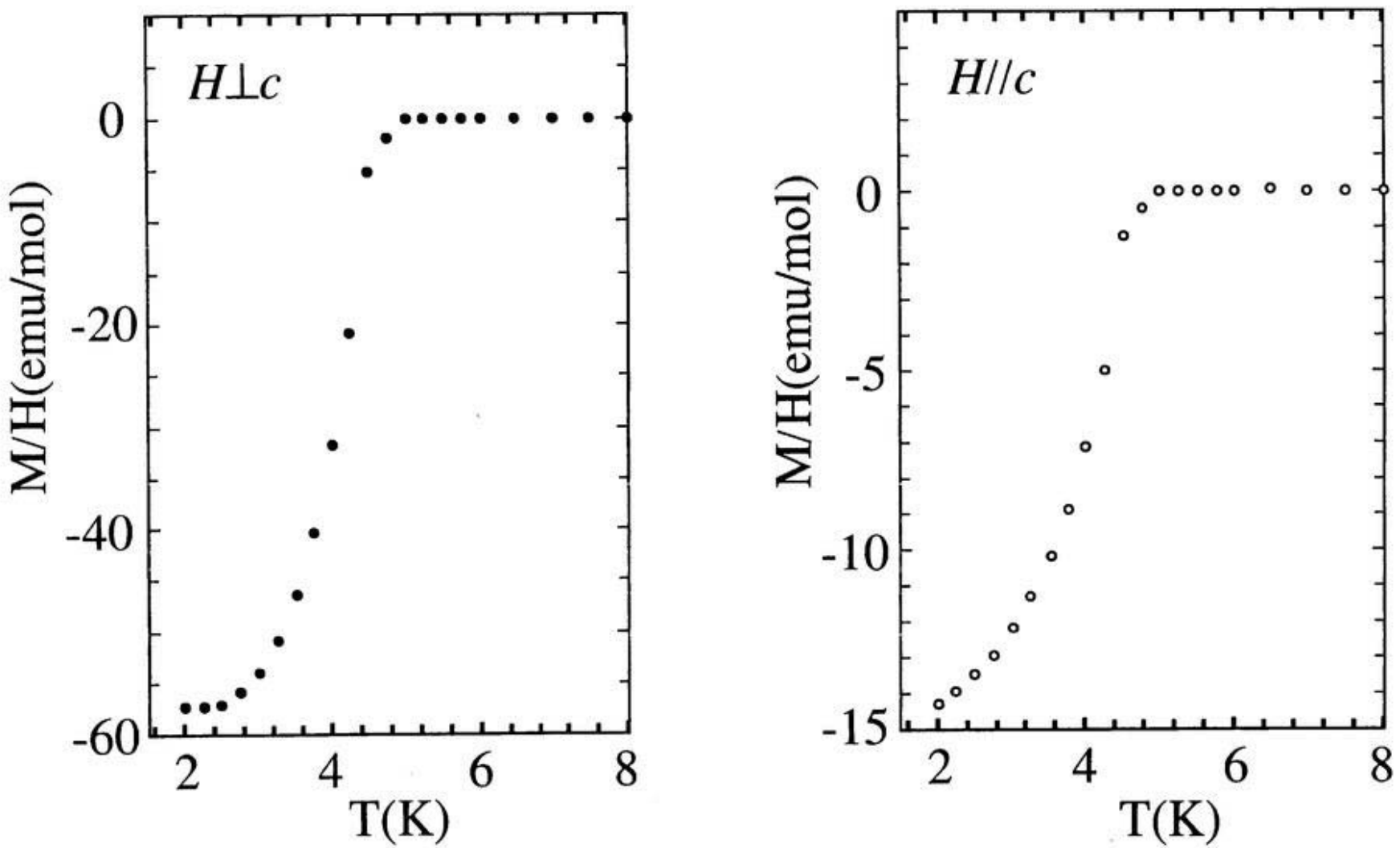

Fig.5.7. Magnetic susceptibility of λ-$(BETS)_2GaCl_4$. Applied magnetic field is 2 Oe.

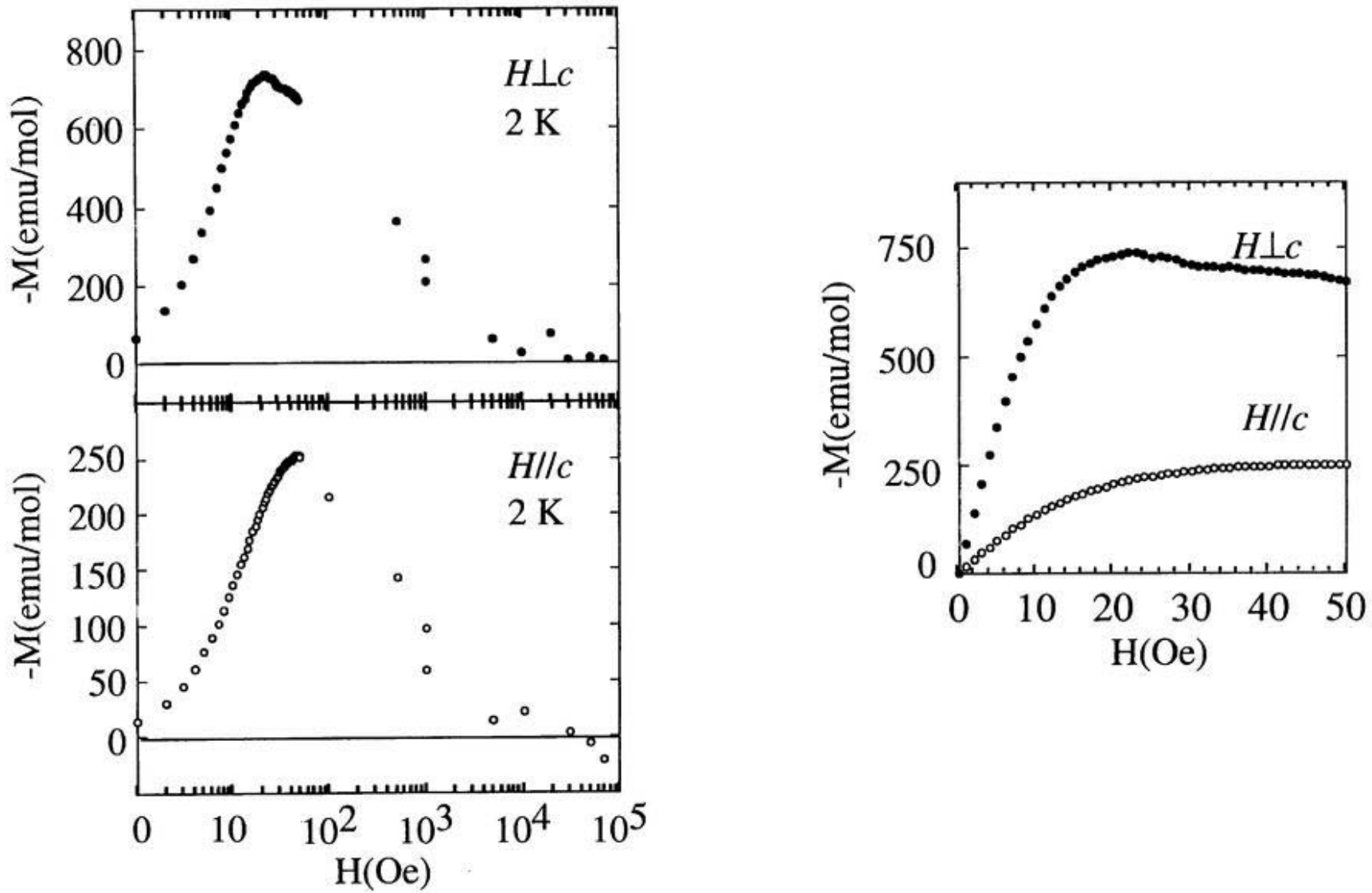

Fig.5.8. Magnetization curves at 2 K of λ-$(BETS)_2GaCl_4$.

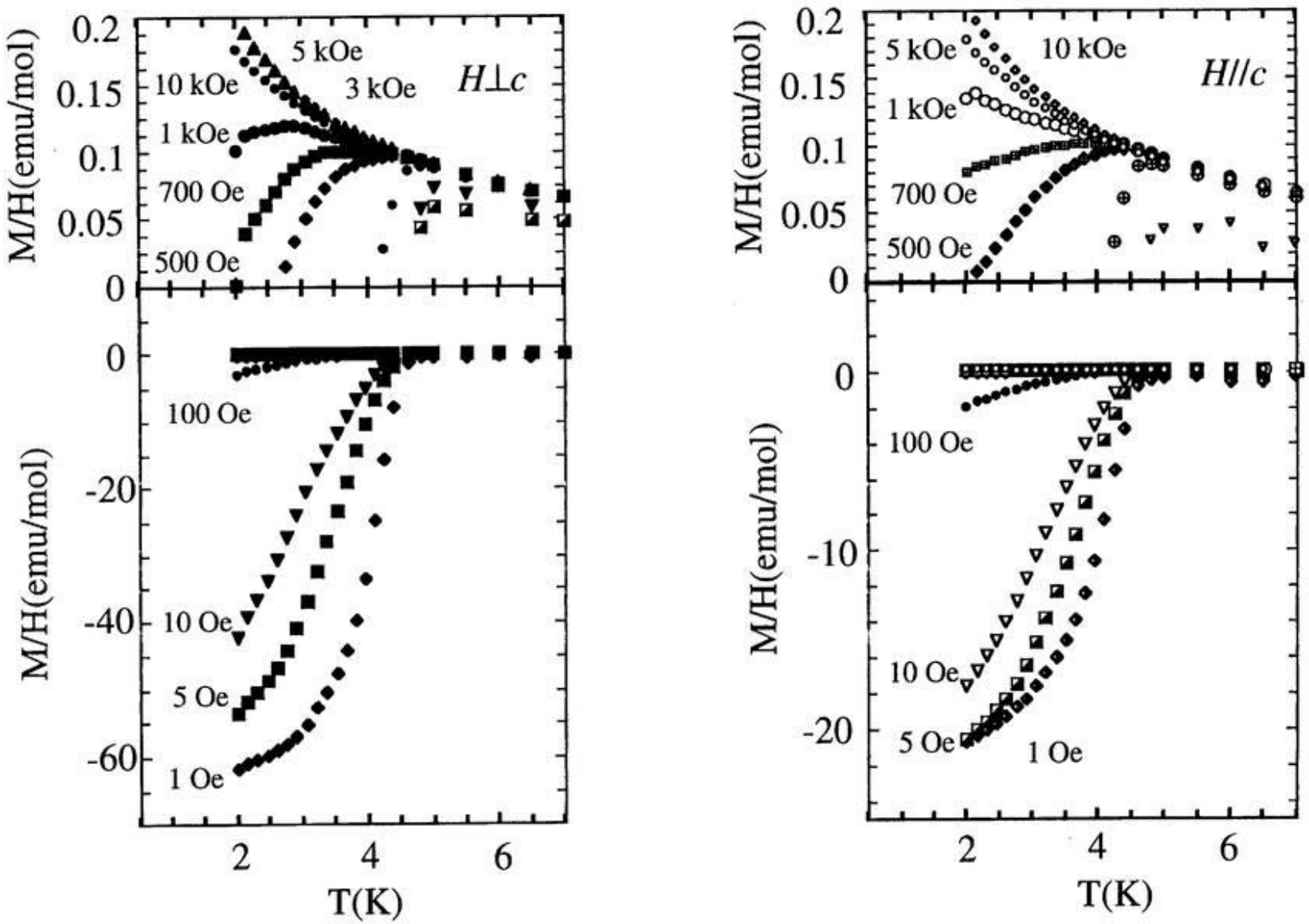

Fig.5.9. Magnetic susceptibilities of λ-$(BETS)_2(Fe_{0.27}Ga_{0.73})Cl_4$.

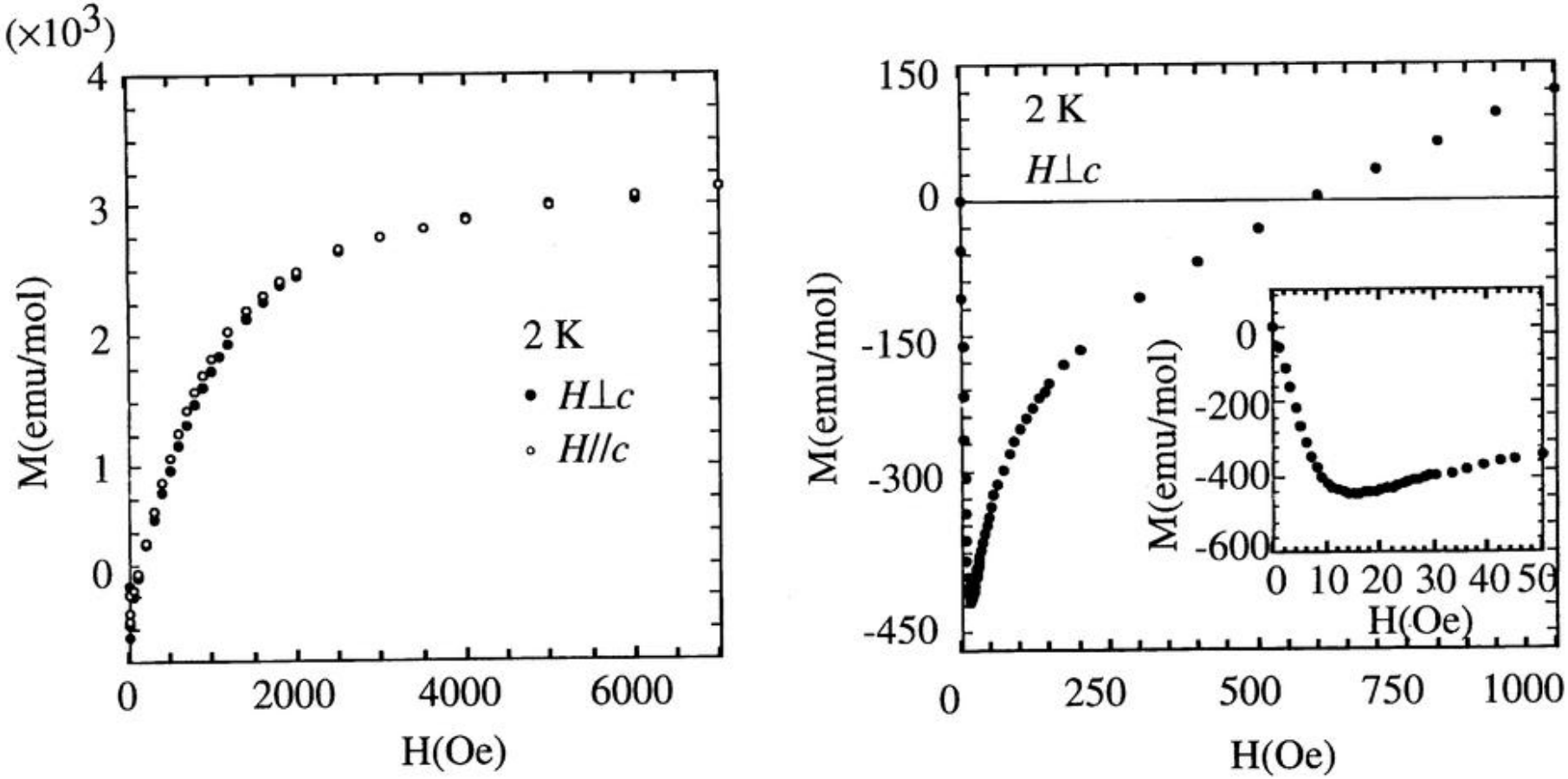

Fig.5.10. Magnetization curves of H⊥c at 2 K of λ-$(BETS)_2(Fe_{0.27}Ga_{0.73})Cl_4$.

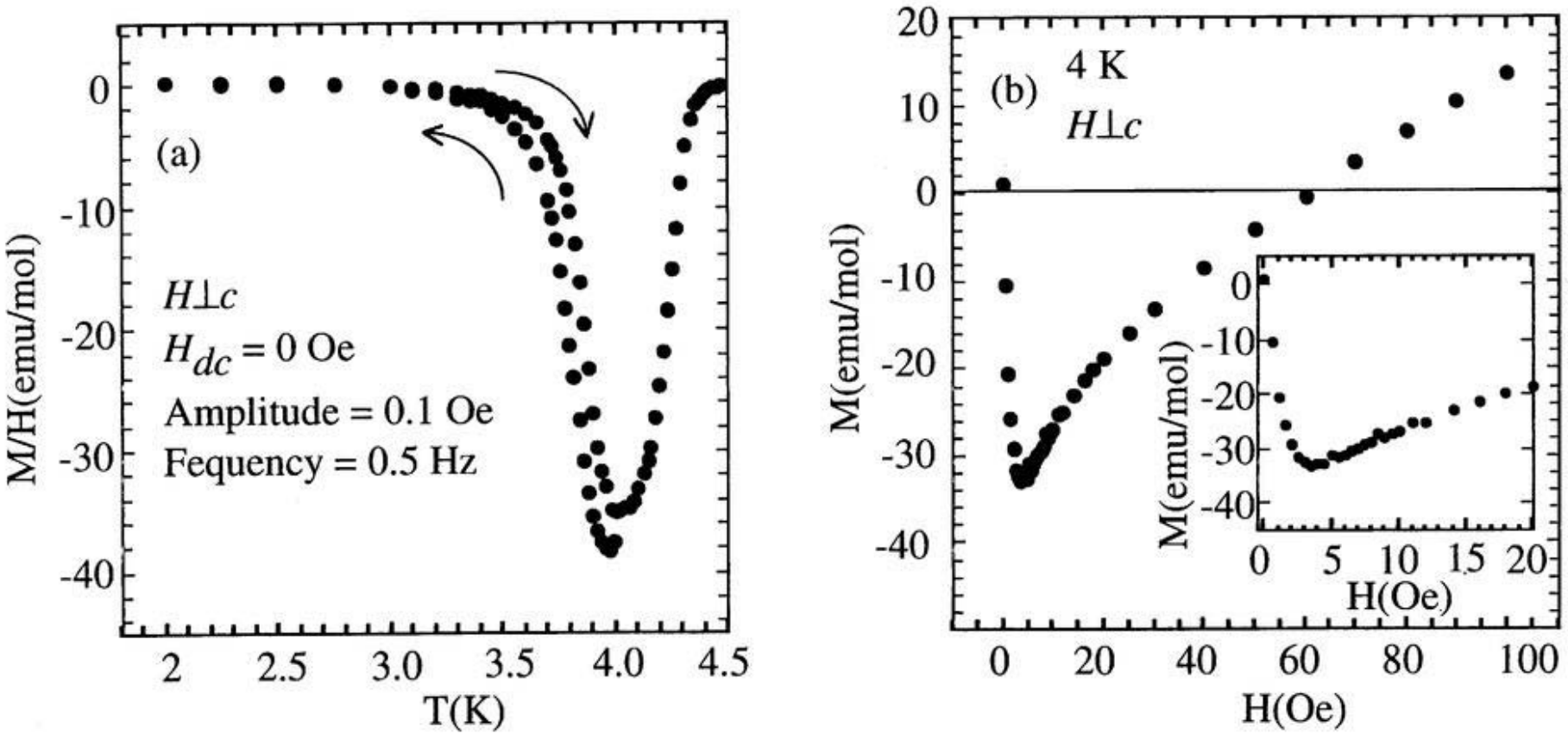

Fig.5.11. (a) *AC* susceptibility and (b) the magnetization curve of $H\perp c$ at 2 K of λ-$(BETS)_2(Fe_{0.47}Ga_{0.53})Cl_4$.

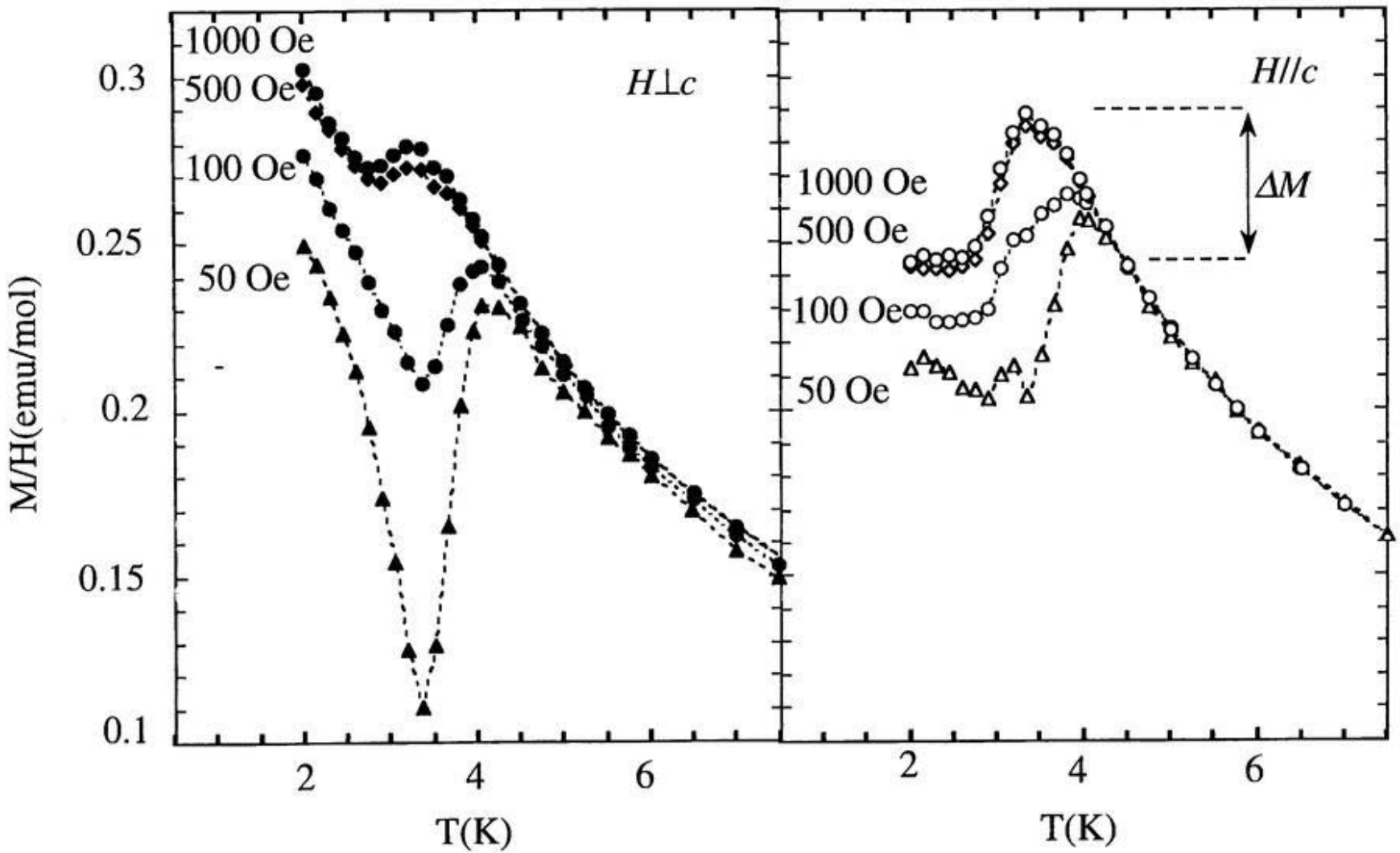

Fig.5.12. Magnetic susceptibility of λ-$(BETS)_2(Fe_{0.43}Ga_{0.57})Cl_4$

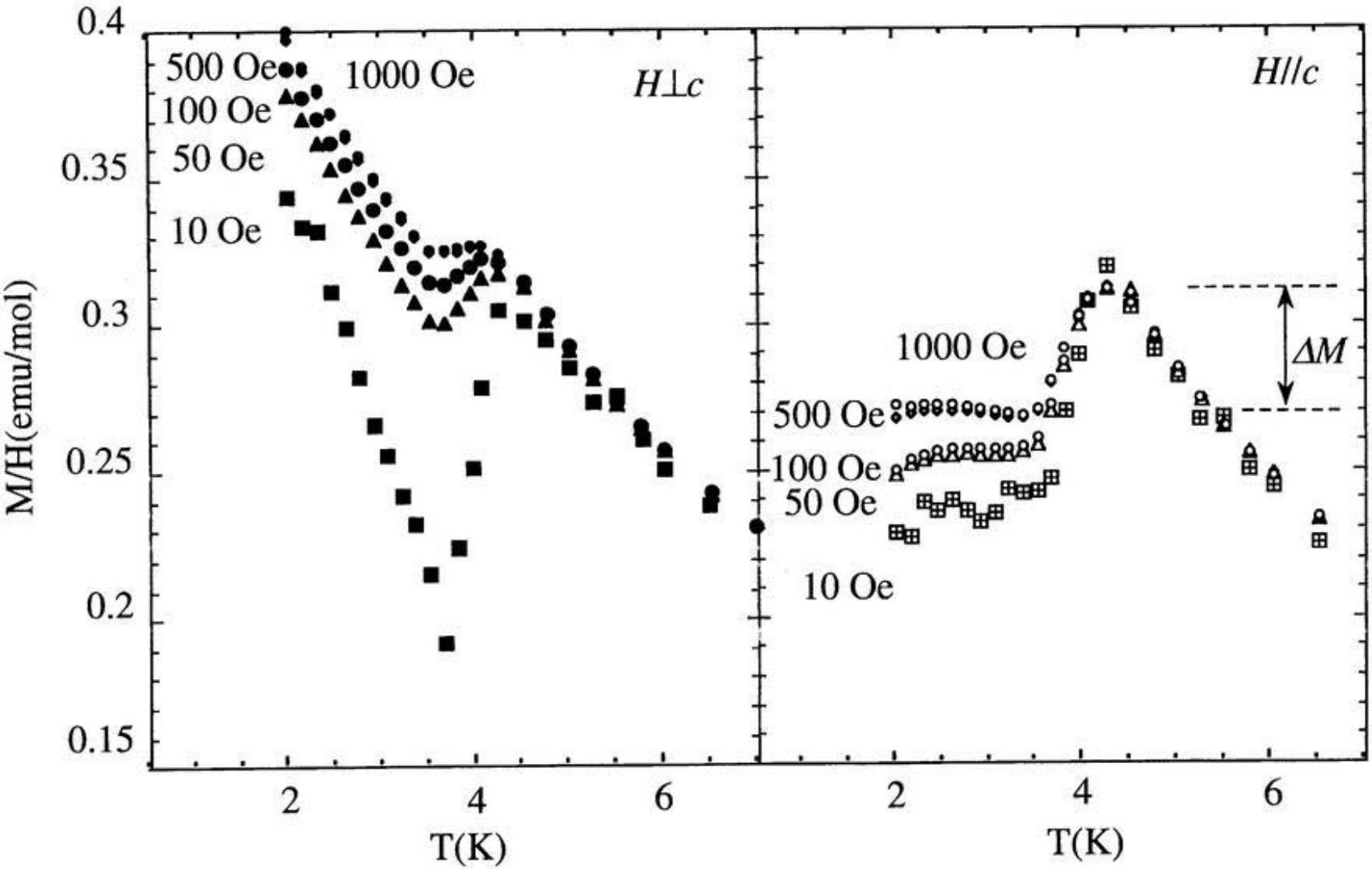

Fig.5.13. Magnetic susceptibility of λ-$(BETS)_2(Fe_{0.55}Ga_{0.45})Cl_4$

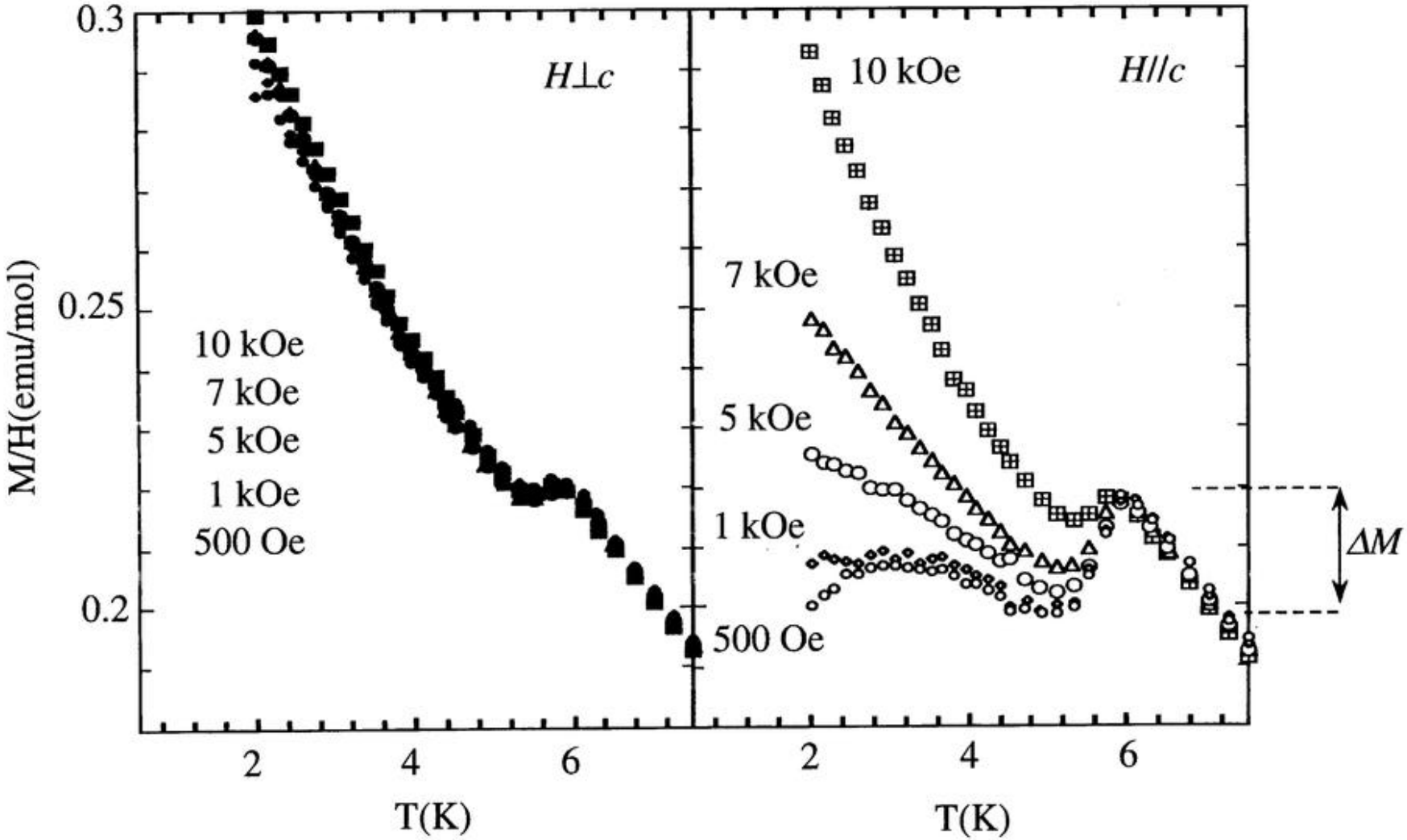

Fig.5.14. Magnetic susceptibility of λ-$(BETS)_2(Fe_{0.7}Ga_{0.3})Cl_4$

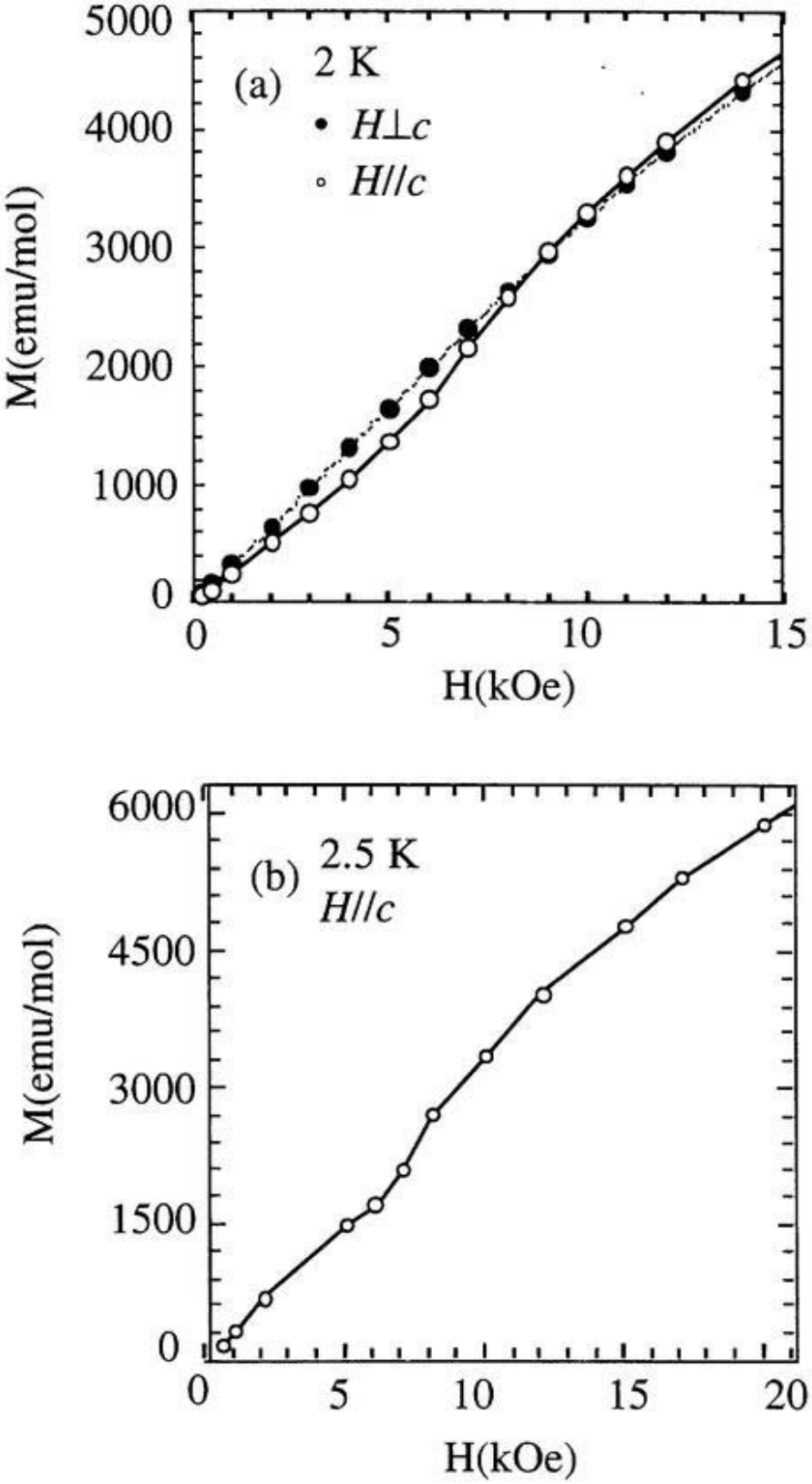

Fig.5.15. Magnetization curves at 2 K of (a) λ-$(BETS)_2(Fe_{0.47}Ga_{0.53})Cl_4$, (b) λ-$(BETS)_2(Fe_{0.47}Ga_{0.53})Cl_4$, (c) λ-$(BETS)_2(Fe_{0.7}Ga_{0.3})Cl_4$ and (e) λ-$(BETS)_2FeCl_4$.

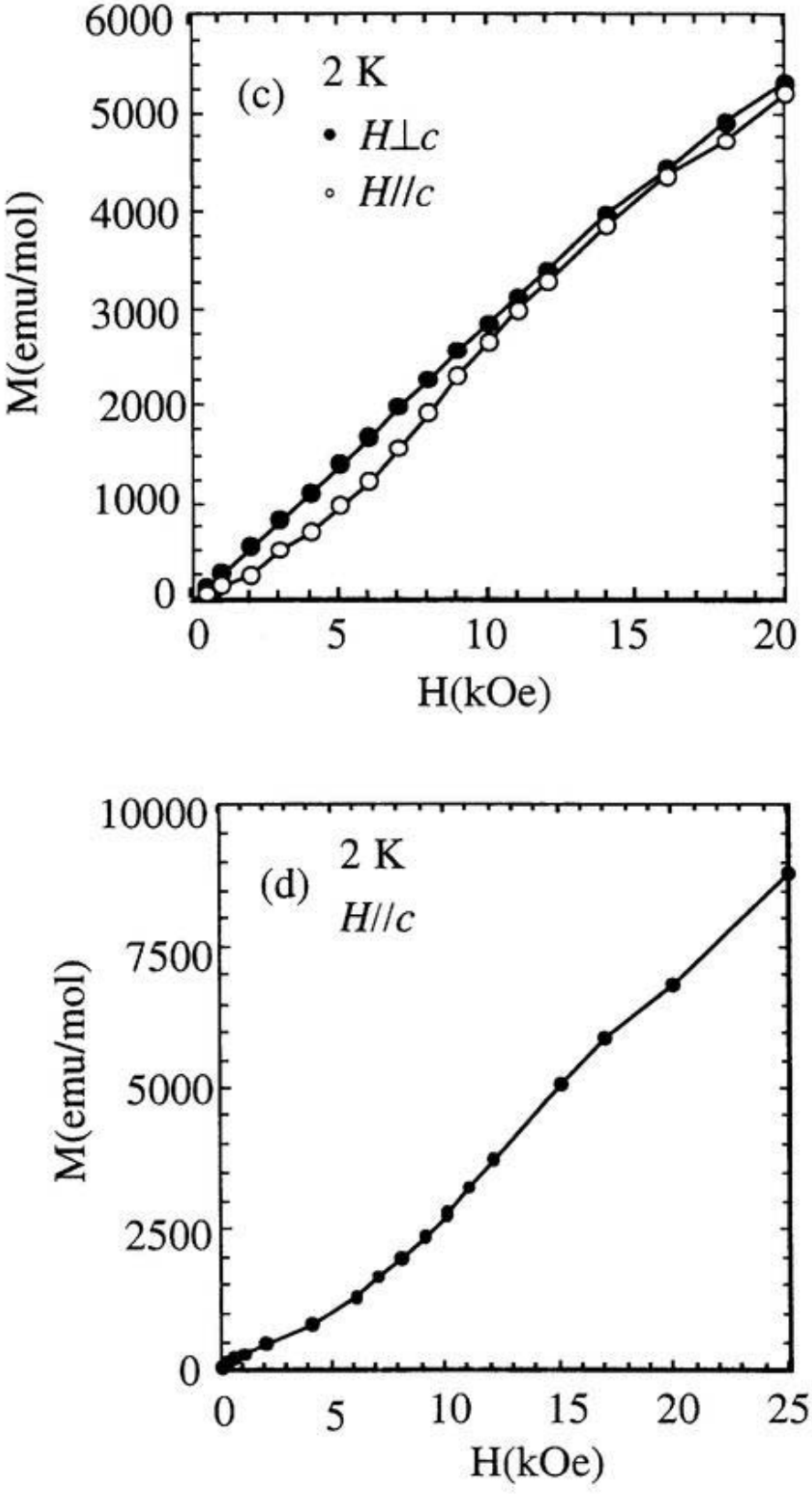

Fig.5.15. Magnetization curves at 2 K of (a) λ-$(BETS)_2(Fe_{0.47}Ga_{0.53})Cl_4$, (b) λ-$(BETS)_2(Fe_{0.47}Ga_{0.53})Cl_4$, (c) λ-$(BETS)_2(Fe_{0.7}Ga_{0.3})Cl_4$ and (e) λ-$(BETS)_2FeCl_4$.(continued)

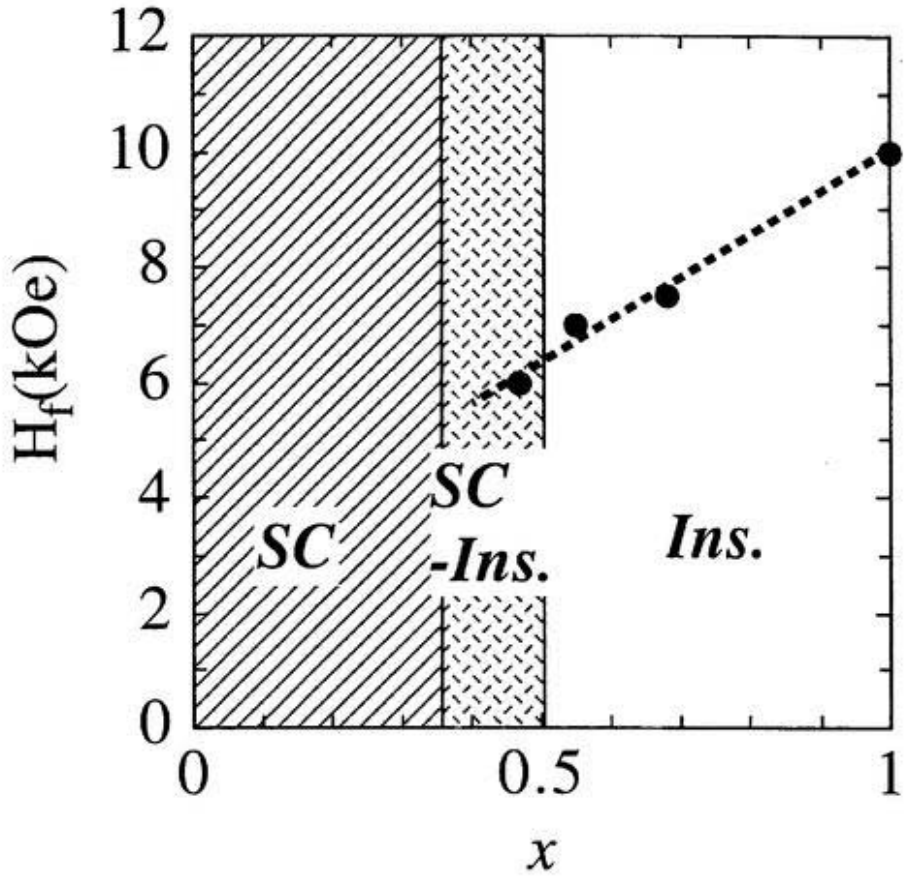

Fig.5.16. The spin flop field, H_f versus composition, x phase diagram of λ-$(BETS)_2(Fe_xGa_{1-x})Cl_4$.

5.5.2 *Weiss temperature*

Weiss temperatures (θ) represents the magnitude of the interaction between Fe^{3+} ions. Relation between θ and the Fe^{3+} concentration x in λ-$(BETS)_2(Fe_xGa_{1-x})Cl_4$ is shown in Fig.5.18. Weiss temperatures estimated by the Curie-Weiss fitting to the susceptibilities are listed in Table 5.3. Weiss temperature of λ-$(BETS)_2FeCl_4$ previously determined mainly from ESR data was reported to be -15 K [8,14]. However, the re-examination of susceptibilities gave a smaller value of -8 K. In spite of wide scattering of data points, it is clear that θ decreases with decreasing x in the range of $x < 0.35$ and tends to be constant in the range of $x < 0.35$ ($\theta = -1.8$ K) (Fig.5.17). It may be natural that θ decreases with decreasing x, but the constant θ in the small-x region was unexpected result, especially in very small x-region. Since the shortest Fe···Fe distance is longer than 6 Å, the AF interaction between Fe ions must be mediated by π electrons of BETS molecules. Therefore, the constant θ in the lower x-region will be explained in terms of the magnetic interaction of diluted spins mediated by π electrons.

Considering that the π-d coupled AF insulating state is realized in the x-region ($x > 0.35$), where θ decreases with decreasing x, T_{MI} seems to have a strong correlation with θ in the range of $x>0.35$. The π-d coupling will become too weak to induce the π-d coupled AF spin structure at $x<0.35$ and the system behaves as a simple organic superconductor with independent diluted magnetic ions in this region.

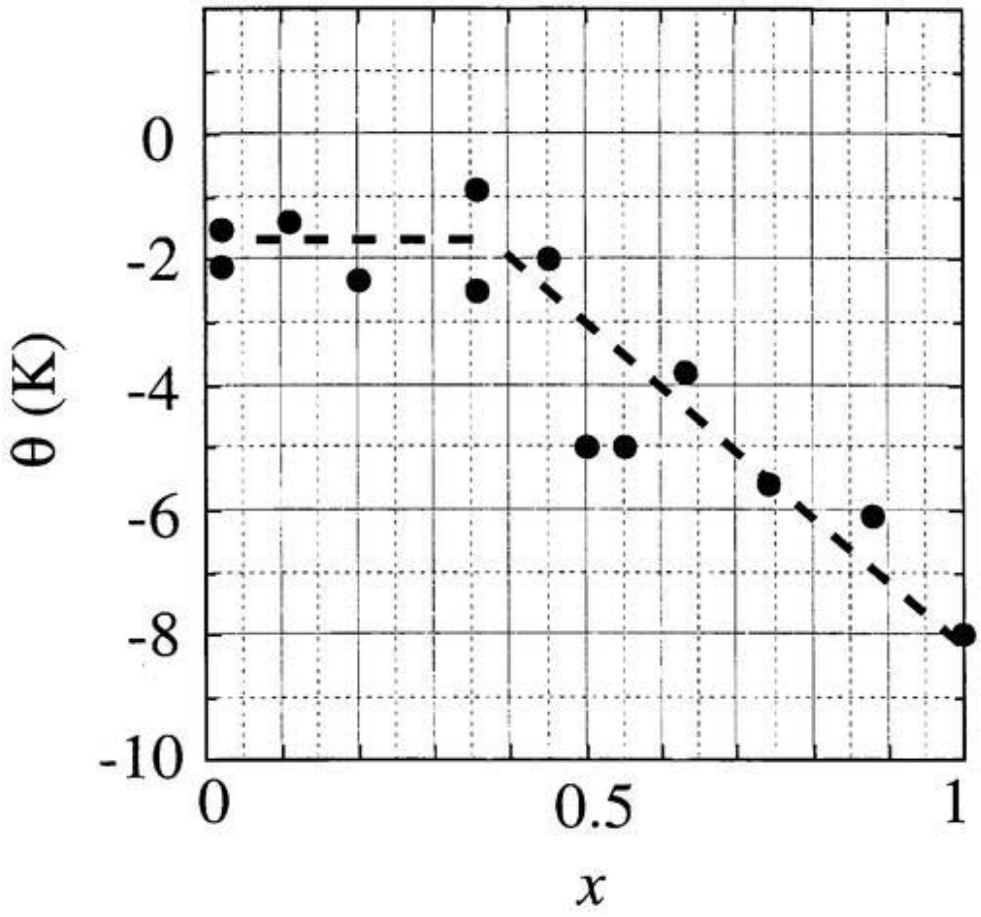

Fig.5.17. The Weiss temperature versus composition, x phase diagram of λ-$(BETS)_2(Fe_xGa_{1-x})Cl_4$.

5.6 *Summary*

Organic alloy systems with mixed the magnetic and non-magnetic anions, $FeCl_4^-$ and $GaCl_4^-$, of λ-$(BETS)_2(Fe_xGa_{1-x})Cl_4$ were synthesized. The general feature of the temperature-composition (x) phase diagram was determined by the resistivity measurements. λ-$(BETS)_2(Fe_xGa_{1-x})Cl_4$ may be the first organic alloy whose ground state can be controlled continuously from a superconducting state to an antiferromagnetic insulating state by changing the mixing ratio of the non-magnetic ($GaCl_4^-$) to magnetic ($FeCl_4^-$) anions. The crystals with $x > 0.5$ exhibited the MI transition. The superconducting transition was observed at $x < 0.5$. In the region of $0.35 < x < 0.5$, the system exhibited the unprecedented SC-I transition never observed even in inorganic superconductors. The *ac* susceptibility of λ-$(BETS)_2(Fe_xGa_{1-x})Cl_4$ ($x = 0.47$) indicated the Meissner volume fraction to be about 75 % at 4 K, which is the first clear evidence for the bulk nature of the SC-I transition. The magnetic susceptibility experiments revealed that the π-d coupled AF insulating ground state develops at $x>0.35$. The x-dependence of Weiss temperature (θ) of λ-$(BETS)_2(Fe_xGa_{1-x})Cl_4$ indicating Fe···Fe AF interaction in the metallic state was determined. θ diminished with decreasing in x in the range of $x>0.35$ and was independent of x in the range of $x < 0.35$.

References

[1] (a) L. I. Bravov, A. V. Gudenko, V. B. Ginodman, A. V. Zavarykina, V. E. Korotkov, N. D. Kushch, L. P. rozenberg, A. G. Khomenko, R. P. Shibaeva, E. B. Yagubskii, *Izv. Akad. Nauk, SSP, Ser. Khim. N1*, 206 (1990). (b) P. Day, M. Kurmoo, T. Mallah, I.R. Marsden, R.H. Friend, F.L. Pratt, W. Hayes, D. Chasseau, J. Gaultier, G. Bravic, L. Ducasse, *J. Am. Chem. Soc.*, **114**, 10722 (1992).

[2] M. Kurmoo, A.W. Graham, P. Day, S.J. Coles, M.B. Hursthouse, J.L. Caulfield, J. Singleton, F.L. Pratt, W. Hayes, L. Ducasse, P. Guionneau, *J. Am. Chem. Soc.*, **117**, 12209 (1995).

[3] (a) R. Kato, A. Kobayashi, A. Miyamoto, H. Kobayashi, *Chem. Lett.*, **1991**, 1045. (b) T. Naito, A. Miyamoto, H. Kobayashi, R. Kato, A. Kobayashi, *Chem. Lett.*, **1991**, 1945. (c) A. Kobayashi, R. Kato, T. Naito, H. Kobayashi, *Synth. Met.*, **55-57**, 2078 (1993).

[4] (a) H. Kobayashi, T. Udagawa, H. Tomita, K. Bun, T. Naito, A. Kobayashi, *Chem. Lett.*, **1993**, 1559. (b) L. K. Montogomery, T. Burgin, T, Miebach, D. Dunham, J.C. Huffmann, J.E. Schirber, *Mol. Cryst. Liq. Cryst.*, **284**, 73 (1996).

[5] A. Kobayashi, T. Udagawa, H. Tomita, T. Naito, H. Kobayashi, *Chem. Lett.*, **1993**, 2179.

[6] H. Kobayashi, H. Tomita, T. Naito, A. Kobayashi, F. Sakai, T. Watanabe, and P. Cassoux, *J. Am. Chem. Soc.*, **118**, 368 (1996).

[7] L. Brossard, R. Clerac, C. Coulon, M. Tokumoto, T. Ziman, D. K. Petrov, V. N. Laukhin, M. J. Naughton, A. Audouard, F. Goze, A. Kobayashi, H. Kobayashi, and P. Cassoux, *Euro. Phys. J. B*, **1**, 439 (1998).

[8] M. Tokumoto, T. Naito, H. Kobayashi, A. Kobayashi, V.N. Laukhin, L. Brossard, P. Cassoux, *Synth Met.*, **86**, 2161 (1997).

[9] "Landolt-Börnstein", Neue Serie II/11, Springer-Verlag (1981).

[10] The susceptibility of the H⊥c of λ-(BETS)$_2$($Fe_{0.43}Ga_{0.57}$)Cl_4 which was reported for the first time in the refelence of H. Kobayashi, A. Sato, E. Ojima, H. Akutsu, A.

Kobayashi, P. Cassoux, *J. Am. Chem. Soc.*, **119**(50), 12392 (1997), is incorrect, because partially effective pressure was happened to be created by the freezing of a small amount of grease used to keep the crystals in the capillary.

[11] H. Akutsu, E. Arai, H. Kobayashi, H. Tanaka, A. Kobayashi, P. Cassoux, *A. Am. Chem. Soc.*, **119**, 12681 (1997).

[12] H. Tanaka, A. Kobayashi, T. Saito, K. Kawano, T. Naito, H. Kobayashi, *Adv. Mater.*, **8**, 812 (1996).

[13] H. Akustu, K. Kato, E. Ojima, H. Kobayashi, H. Tanaka, A. Kobayashi, P. Cassoux, *Phys. Rev. B*, **58**(14), 9294 (1998).

[14] H. Kobayashi et al., unpublished data.

Chapter 6

Concluding remarks

In the present study, the developments of new molecular conductors and their characterizations were made on the systems composed of multi-chalcogen π molecules, such as $M(dmise)_2$ conductors, $(EDT)_2MCl_4$ (M= Ga, Fe) and λ-$(BETS)_2(Fe_xGa_{1-x})Cl_4$. In order to investigate the electronic and magnetic states of these materials, the crystal structure determinations, the electrical resistivity measurements and the magnetic susceptibility measurements were carried out.

In Chapter 3, the investigation on the $M(dmise)_2$ (M= Ni, Pd) compounds were described. The single crystals were prepared by the standard electrochemical oxidation method. The electrical resistivity of $[(CH_3)_3HN][Ni(dmise)_2]_2$ was metallic around room temperature at ambient pressure. The tight-binding band calculation by the extended Hückel methods indicated that $[(CH_3)_3HN][Ni(dmise)_2]_2$ and $[(CH_3)_2H_2N][Ni(dmise)_2]_2$ have even stronger intermolecular interactions along the long molecular axis than in the transverse direction due to a close distance between the selone groups. The band calculations also indicated that the Fermi surfaces of $[(CH_3)_3HN][Ni(dmise)_2]_2$ and $[(CH_3)_2H_2N][Ni(dmise)_2]_2$ were quasi three dimensional. $Cs[Pd(dmise)_2]_2$ was found for the first time to exhibit a metallic behavior down to low temperature among the $M(dmise)_2$ systems, though the crystal structure could not be determined due to its poor crystal quality. The crystal structure of the second stable metallic $M(dmise)_2$ conductor, (N,N-dimethylpiperidinium)$[Ni(dmise)_2]_2$, was determined. The electrical resistivity has a small anomaly at 250 K and the crystal structure transformed to the five-folded superstructure at the same temperature. The magnetic susceptibility, in contrast to the resistivity and crystal structure, showed no distinct anomaly at 250 K. The unexpectedly large paramagnetic susceptibility and its temperature dependence seem to be inconsistent with the simple metal model of this system.

In Chapter 4, the electrical, structural and magnetic investigation on the low dimensional

conductors of EDT-TTF salts with MCl_4^- anions (M=Fe, Ga) and its selenium-substituted analogues (EDTs series) were descried. Crystals were prepared by the electrical oxidation method. Six crystals of D_2MCl_4 (D= EDT-TTF, EDST, EDTS; M= Ga, Fe) were found to be isostructural with each other. The tight-binding electronic band structure examinations suggested that their band structures were quasi one-dimensional. Ground states of π electron systems of $(EDT\text{-}TTF)_2MCl_4$ (M= Ga, Fe) were considered to be the spin-Peierls state. The magnetic susceptibilities of $(EDST)_2GaCl_4$ and $(EDTS)_2GaCl_4$ decreased gradually down to T_{MI} and the sharp decreases of susceptibilities were observed isotropically below it. However the susceptibilities of those two salts seemed to have the constant values at low temperature and their X-ray diffraction experiments could not detect the lattice distortion at "metal-insulator" transition around 40 K. Thus the ground states of $(EDST)_2MCl_4$ and $(EDTS)_2MCl_4$ are considered to be the semimetallic state.

In Chapter 5, the magnetic investigation on the organic alloy system with mixed magnetic and non-magnetic anions, λ-$(BETS)_2(Fe_xGa_{1-x})Cl_4$ were described. The preparation condition of the crystals is presented. The electrical resistivities indicate that the system showed the superconducting (SC) transition at $x<0.5$ and the metal-insulating (MI) transition at $x > 0.5$. In the region of $0.35 < x < 0.5$, the system exhibited the SC-I transition which is the unprecedented behavior among the organic conductors. The magnetic susceptibility dropped largely at T_c and its recovered at $T_{SC\text{-}I}$. The Meissner volume fraction at $x\approx0.45$ showed that the SC-I transition is a bulk transition. Similar to the pure $FeCl_4$ system (x= 1), the small drop of susceptibility at T_{MI} and spin flop behavior were observed when the field was applied to parallel to the c-axis at $x > 0.35$. This indicates that the insulating state at $x > 0.35$ takes the π-d coupled antiferromagnetic spin structure with easy axis parallel to the c-axis.

List of publications

Chapter 3

(1) Enhancement of the Dimensionality of Molecular π Conductors by the Selone Substitution of M(dmit)$_2$ (M= Ni, Pd) Systems: Newly Synthesized dmise Compounds [Me$_x$H$_{4-x}$N][Ni(dmise)$_2$]$_2$ (x= 1-3) and Cs[Pd(dmise)$_2$]$_2$ (dmise= 4,5-Dimercapto-1,3-dithiole-2-selone)

Akane Sato, Hayao Kobayashi, Toshio Naito, Fumiko Sakai and Akiko Kobayashi

Inorg. Chem., **36**(23), 5262-5269 (1997).

(2) A New Ni(dmise)$_2$ Complex N,N-dimethylpiperidinium[Ni(dmise)$_2$]$_2$, with Stable Metallic State

Akane Sato, Hayao Kobayashi and Akiko Kobayashi

Chem. Lett., **1997**, 1275-1276.

Chapter 5

Temperature-Composition Phase Diagram of the Organic Alloys, λ-BETS$_2$(Fe$_x$Ga$_{1-x}$)Cl$_4$, with Mixed Magnetic and Non-Magnetic Anions

Akane Sato, Emiko Ojima, Hiroki Akutsu, Hayao Kobayashi, Akiko Kobayashi and Patrick Cassoux

Chem. Lett., **1998**, 673-674.

Other publications

Chapter 3

(1) Pressure-Temperature Phase Diagram of a Molecular Superconductor α-EDT-TTF[Ni(dmit)$_2$]

Hiroyuki Tajima, Makoto Inokuchi, Haruo Kuroda, Akiko Kobayashi, Akane Sato, Toshio Naito, Hayao Kobayashi

Rev. High Pressure. Dci. Technol., **7**, 532-534 (1998).

(2) Electrical and Structural Properties and Phase Diagram of a Molecular Superconductor β-$[(CH_3)_4N][Pd(dmit)_2]_2$

Akiko Kobayashi, Akihito Miyamoto, Reizo Kato, Akane Sato and Hayao Kobayashi

Bull. Chem. Soc. Jpn., **71**, 997-1006 (1998)

(3) Electrical Conductivity and Upper Critical Magnetic Field of the Molecular Superconductor α-EDT-TTF[Ni(dmit)$_2$]

Makoto Inokuchi, Hiroyuki Tajima, Toshiaki Ohta, Akiko Kobayashi, Haruo Kuroda, Toshio Naito, Akane Sato and Hayao Kobayashi

Advanced Materials for Optics and Electronics, **6**, 367-370 (1996)

(4) Magnetic and transport properties of an ambient-pressure superconductor α-EDT-TTF[Ni(dmit)$_2$]

Hiroyuki Tajima, Makoto Inokuchi, Akiko Kobayashi, Akane Sato, Toshio Naito and Hayao Kobayashi and Haruo Kuroda

Synth. Met., **85**, 1585-1586 (1997).

(5) Development and low-temperature crystal structures of M(dmiX)$_2$ (X= S, Se) conductors

Akiko Kobayashi, Toshio Naito, Akane Sato and Hayao Kobayashi

Synth. Met., **86**, 1841-1842 (1997).

(6) Meissner and diamagnetic shielding effects of α-EDT-TTF[Ni(dmit)$_2$]

Hiroyuki Tajima, Akiko Kobayashi, Youiti Ootsuka, Akane Sato, Toshio Naito and Hayao Kobayashi

Synth. Met., **79**(2), 141-143 (1996).

(7) Electrical resistivity under high pressure and upper critical magnetic field of the molecular superconductor α-(EDT-TTF)[Ni(dmit)$_2$]

Makoto Inokuchi, Hiroyuki Tajima, Toshiaki Ohta, Haruo Kuroda, Akiko Kobayashi, Akane Sato, Toshio Naito and Hayao Kobayashi

J. Phys. Soc. Jpn., **65**(2), 538-544 (1996).

(8) Origin of the resistivity anomalies of (EDT-TTF)[M(dmit)$_2$] (M= Ni, Pd)

Akiko Kobayashi, Akane Sato, Kiyoshi Kawano, Toshio Naito, Hayao Kobayashi and Tokuko Watanabe

J. Mater. Chem., **5**(10), 1671-1679 (1995).

(9) The new synthetic metals of M(dmise)$_2$: [Me$_3$HN][Ni(dmise)$_2$]$_2$ and (EDT-TTF)[Ni(dmise)$_2$]

Toshio Naito, Akane Sato, Kouich Kawano, Akiko Tateno, Hayao Kobayashi and Akiko Kobayashi

J. Chem. Soc., Chem. Commun. **1995**, 351-352.

Chapter 4

A. Sato, H. Akutsu, E. Ojima, H. Kobayashi and A. Kobayashi, to be submitted.

Chapter 5

(1) Superconductor-to-Insulator Transition in an Organic Metal Incorporating Magnetic Anions: λ-(BETS)$_2$(Fe$_x$Ga$_{1-x}$)Cl$_4$ [BETS= bis(ethylenedithio)tetraselenafuluvalene; x≈0.55 and 0.43)

Hayao Kobayashi, Akane Sato, Emiko Arai, Hiroki Akutsu, Akiko Kobayashi and Patrick Cassoux

J. Am. Chem. Soc., **119**(50), 12392-12393 (1997).

(2) New BETS Conductors with Magnetic Anions and Metals with Tetrahedral non-magnetic and magnetic anions (BETS= bis(ethylenedithio)tetraselenafulvalene)

Hayao Kobayashi, Toshio Naito, Akane Sato, Koichi Kawano, Akiko Kobayashi, Hisashi Tanaka, Taro Saito, Madoka Tokumoto, Luc Brossard and Patrick Cassoux

Mol. Cryst. Liq. Cryst., **284**, 61-72 (1996).

(3) Structural and electrical properties of BETS compounds with transition metal complex anions

Hayao Kobayashi, Emiko Arai, Akane Sato, Toshio Naito, Hisashi Tanaka, Akiko Kobayashi, Taro Saito and Patrick Cassoux

Synth. Met., **85**, 1595-1596 (1997).

(4) Hayao Kobayashi, Akane Sato, Hisashi Tanaka, Akiko Kobayashi, Patrick Cassoux, *Coord. Chem. Rev.*, in press.